Doctoral Dissertation

Chiroptical Activity of Nanorod-DNA Polyion-Complexes

（ナノロッド−DNA ポリイオン複合体のカイロプティック活性）

Yali Shi

Graduate School of Life Science, Hokkaido University

2024 December

Contents

Chapter 1

General Introduction

1.1 Chirality

1.1.1 Molecular Chirality

Chirality, the property whereby an object's geometric orientation cannot be superimposed onto its mirror image, exists from individual molecules to supramolecular systems in nature.[1] For the chiral molecules, the typical conformation is that its tetrahedral carbon centers are attached to four different atoms or groups, resulting in non-superimposable mirror images.[2], as shown in **Figure 1.1**. A chiral molecule is one that contains an asymmetric carbon atom, resulting in two non-superimposable mirror-image isomers known as enantiomers. Although these enantiomers have the same chemical composition and bonding, their spatial arrangement differs, leading to distinct biological activities when interacting with other chiral environments, such as enzymes or receptors. So far, it is known that the basic substances that make up living organisms all have chirality. For example, amino acids in living organisms are almost exclusively L-enantiomers, while sugars are typically D-enantiomers.[3] This selectivity is a fundamental aspect of the complexity of biological systems.[4]

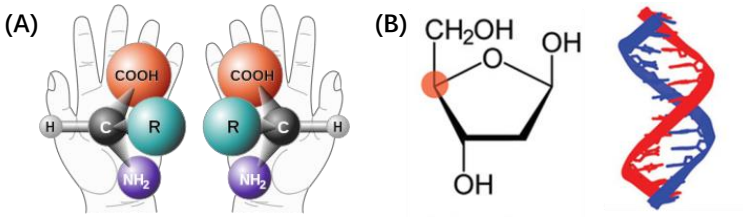

Figure 1.1 (A) Mirror structures of chiral molecules (left- and right-handed). (B) Chirality in biomolecules of DNA.D-deoxyribose and right-handed helix of DNA.[3]

The importance of chiral molecules extends beyond fundamental research to industrial applications, such as in pharmaceuticals, agrochemicals, and flavors. In biological systems, many molecules are chiral, and macromolecules like enzymes and receptors are often chiral as well. The interactions between chiral molecules and these biological macromolecules are typically stereoselective, meaning that only one enantiomer binds effectively and triggers a specific biological response.[5] Furthermore, many drugs are chiral, and different enantiomers can have different effects in the body.[6] For instance, one enantiomer might be therapeutically

effective, while the other could be ineffective or cause adverse side effects. Therefore, pharmaceutical companies aim to develop drugs with high enantiomeric purity.[7]

Circular Dichroism (CD) is a valuable spectroscopic technique used to study the chiral properties of molecules, particularly in the analysis of the secondary structure and conformational changes of biomolecules such as proteins and nucleic acids.[8] CD refers to the phenomenon where chiral molecules absorb left- and right-handed circularly polarized light to different extents. This differential absorption leads to a distinct signal in the absorption spectrum at certain wavelengths, known as the CD spectrum **(Figure 1.2).**[9] The origin of this effect lies in the chiral structure of the molecule, and it provides insights into the conformation, secondary structure, and other properties of the molecule across different wavelength ranges. However, a major obstacle in practical applications is the weak chiral response of natural chiral molecules.[10] For most chiral molecules, their CD bands are located in the ultraviolet spectral region, and the corresponding asymmetry factor used to characterize the optical chirality signal is very small. Even concentrated solutions can only rotate the light polarization by a few millidegrees, making sensitive detection and analysis of small numbers of chiral molecules difficult to achieve.[11]

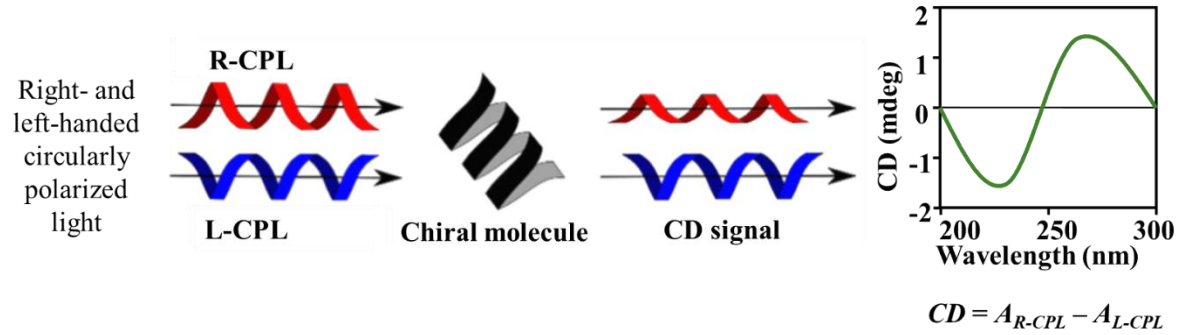

Figure 1.2 Right- and left-handed circularly polarized light (R-CPL and L-CPL) transmitted through a chiral object can differ in speed as well as their wavelength and the extent to which they are absorbed. Circular dichroism is the difference (CD = $A_{R\text{-}CPL} - A_{L\text{-}CPL}$).[12]

1.1.2 Plasmonic Chirality

Plasmonic CD, arising from complexes of molecules and nanoparticles complex, is one of the important directions in chiral materials research in recent years. Through the design and

regulation of nanostructures, significant chiral optical responses can be achieved in the visible (Vis-) and near-infrared (NIR-) light regions. The emergence of plasmonic CD has greatly expanded the limitations of traditional molecular CD in the UV region, providing a powerful tool for analyzing chiral molecules, designing new chiral optical materials, and detecting biological chiral molecules.[13]

1.1.2.1 Localized Surface Plasmon Resonance

Gold is one of the most chemically stable elements in nature, but nanoscale gold particles have special physical and chemical properties.[14] This is because when the size of gold nanoparticles (AuNPs) is small enough, it causes the gold nanoparticles to transform into insulators and form standing electron waves of different energy levels. When electromagnetic waves radiate to spherical metal nanoparticles whose particle size is much smaller than the excitation wavelength, their free electrons will collectively oscillate in local areas on the surface of the metal nanoparticles. If the frequency of the incident light is equivalent to the collective oscillation frequency of free electrons, resonance will occur, which is called localized surface plasmon resonance (LSPR) **(Figure 1.3B, D)**.[15]

Among a variety of AuNPs, gold nanorods (AuNRs) offers several key advantages to assemble chiro-plasmonic nanostructures, particularly in the fields of plasmonics and chiral nanotechnology.[16] One of the most significant advantages of AuNRs is their highly tunable LSPR. Unlike spherical nanoparticles, AuNRs exhibit two distinct plasmon resonance modes, transverse mode corresponding to oscillations across the short axis of the nanorod (T-LSPR) and longitudinal mode, corresponding to oscillations along the long axis (L-LSPR). The L-LSPR of AuNRs can be easily tuned across the visible to NIR regions by simply varying the aspect ratio (length-to-width ratio). This tunability allows for the optimization of plasmonic responses for specific chiral applications, enabling stronger and more controllable optical activity in the chiro-plasmonic nanostructures **(Figure 1.3B, D)**.[17] The second one is the efficient assembly into complex chiral architectures. At least four AuNPs are required to construct chiral structures, while only two tilted AuNRs can form asymmetric nanostructures with chiroptical activity.[18] They can be assembled into helical, twisted, or other chiral

arrangements through various strategies. The third is the enhanced and the tunable of chiral optical activity. The anisotropic nature of AuNRs enables them to produce stronger electromagnetic field enhancements at their tips when excited by light. When assembled into chiral geometries, this local field enhancement amplifies the interaction between light and chiral molecules, leading to stronger CD signals compared to isotropic particles like spheres.[19] And it is difficult to tune the chiroptical responses in pyramidal or helical NP structures, because it is limited to control the interparticle distances. Conversely, the chiroptical activity of two NRs can be regulated simply by controlling their tilting. For example, Meng et al. achieved dynamic chiral regulation of NR assemblies by changing the temperature or pH.[20] This enhanced chiral optical activity is beneficial for sensitive detection of chirality, which is critical in applications like biosensing and enantioselective catalysis.

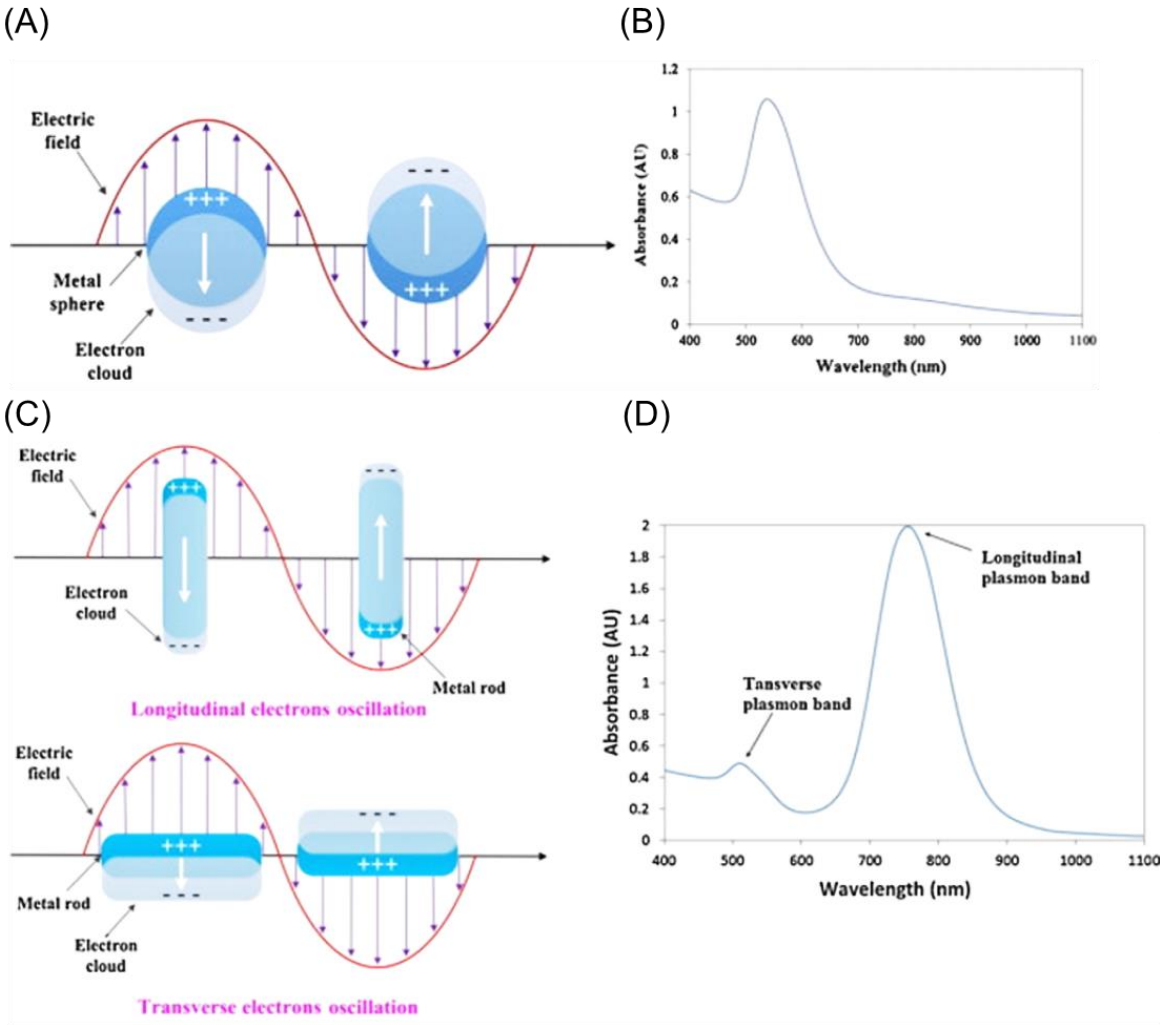

Figure 1.3 Schematic illustration of LSPR excitation for AuNPs (A) and AuNRs (C). A typical LSPR absorption band of AuNPs (B) and AuNRs (D).[21]

1.1.2.2 Mechanism of Plasmonic CD

In the study of plasmonic CD, three different mechanisms may lead to the generation of chiroptical signals.[16, 22] The first mechanism is the coupling of NPs with chiral molecules **(Fig. 1.4A)**. When a chiral molecule is placed between two NPs, the enhanced electromagnetic field (hot spot) can significantly enhance the Coulomb interaction between the chiral molecule dipole and the NPs, thereby transferring the chirality of the molecule to the NPs. This coupling effect induces a chiroptical response in the surface plasmon resonance absorption region of NPs and further amplifies the chiral signal due to the enhancement of the hot spot.[23, 24] The second mechanism is the chiral arrangement of NPs **(Fig. 1.4B)**. Structural chirality can be achieved by arranging NPs in a chiral manner. Such as, NPs are modified on the surface of polymers to form a tetrahedral structure or helical structure, and AuNRs are used as assembly units to construct twisted structure. These arranged structures can effectively induce and enhance the chiroptical response of plasmon[25, 26] The third mechanism is the formation of chiral shapes in single NPs **(Fig. 1.4C)**. Chiral molecules are introduced into the growth process to control the growth path of the seeds, thereby preparing large-sized chiral helical NPs. The presence of high Miller-index surfaces and functional groups in the chiral molecules creates enantioselective interactions at the interfaces, driving asymmetric growth and resulting in helical morphologies composed of chiral elements.[27-30]

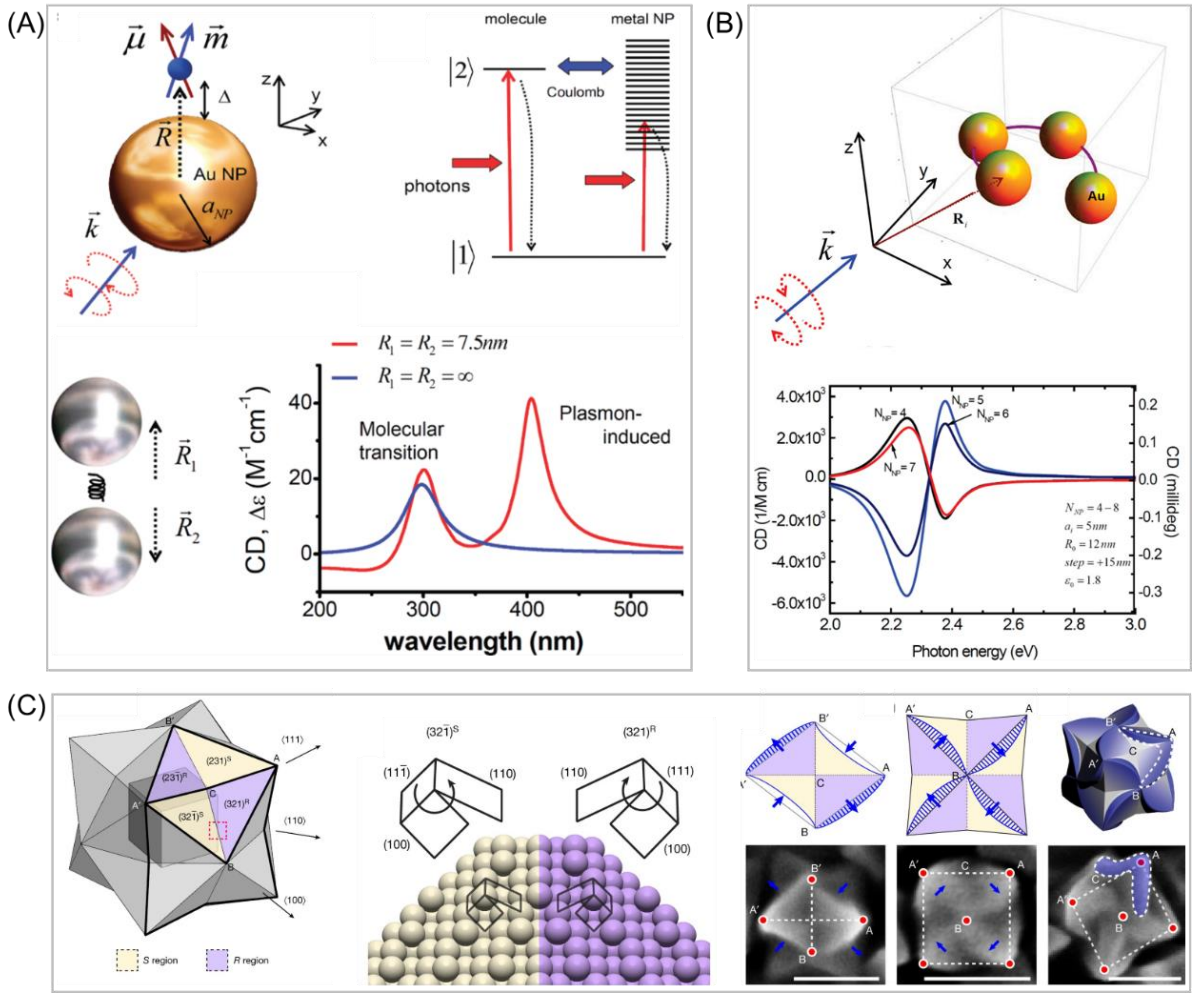

Figure 1.4 Mechanism of Plasmonic CD. (A) The new plasmonic CD was induced by a complex composed of NPs and chiral molecules when they coupled via Coulombic interaction.[31] (B) Helical NP structures show the strongest plasmonic CD signals and its sign was changed with the number of NPs.[32] (C) Chirality evolution in a single NP caused by an interaction between molecular enantioselectivity and asymmetric growth on a high-Miller-index surface.[30]

1.1.3 Fabrication of Chiral Plasmonic

There are three main ways to construct chiral plasmonic nanomaterials at the nanoscale. First, the top-down physical approach is a straightforward way to construct chiral metal nanostructures. Researchers have used techniques such as focused ion beam,[33] electron beam lithography **(Figure 1.5A)**[34] and multi-photon laser direct writing[35] to try to construct chiral shaped nanostructures. Using these methods, photonic metamaterials, broadband circularly polarizing devices, optically active achiral structures can be obtained, and trace detection of chiral biomolecules can be achieved.[36] However, there are still drawbacks such as poor crystal quality, limited material selection, and high-cost method.[37] The second method is a lower-cost bottom-up chemical synthesis. This approach enables the fabrication of chiroptical nanostructures with excellent tunability, precise nanoscale control and scalable production. So far, optically active nanoparticles can be synthesized using different chiral molecules. For example, Nam et al. successfully synthesis single AuNPs with chiral helices by adding amino acids, peptides, or adenine-based ssDNA molecules during the growth of NPs **(Figure 1.5B)**.[30, 38, 39] Although some progress has been made in this field recently, the unclear mechanism of the method and the limited availability of molecules capable of synthesizing such chiral NPs have hindered further development in this area.[37] The third approach involves utilizing templates such as DNA,[40, 41] peptides, [42, 43] liquid crystals[44, 45] and organic soft materials[46, 47] to assemble achiral NPs into chiral structures. The complexes formed by mental NPs and molecules show a strong plasmonic CD response due to the stronger Coulomb and electromagnetic interactions Furthermore, the plasmonic CD in NPs-molecules complexes can be easily tuned through changing the types or size of NPs.[48] This assembly method usually includes the following two ways: (1) modifying NPs with molecules to induce optical activity**(Figure 1.5C)**;[40] (2) arranging metal NPs into chiral structures, like helix using template molecules, for example DNA origami **(Figure 1.5D)**.[41]

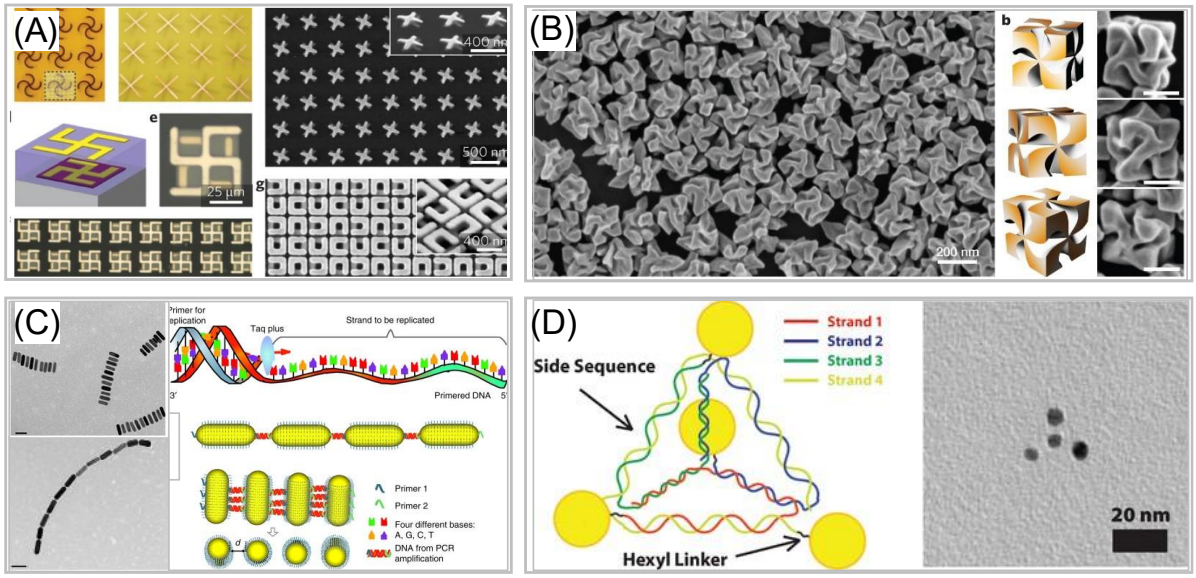

Figure 1.5 Fabrication methods of chiral plasmonic. (A) 3D chiral metamaterials fabricated by electron-beam lithography.[34] (B) 3D chiral metamaterials fabricated by bottom-up chemical synthesis.[30] (C) PCR-based chiral AuNRs assemblies.[40] (D) DNA-nanocrystal pyramids.[41]

1.2 Applications of Chiral Plasmonic

In contrast to small biomolecules that normally exhibit weak CD signal in UV regions, NPs can be easily synthesized with tunable optical activity, offering the possibility to extend CD from UV to visible and NIR regions, and the CD signal is significantly enhanced. Therefore, this unique optical activity of chiral nanomaterials has been providing many new application opportunities **(Figure 1.6)**.

1.2.1 Biomolecule Identification and Drug Screening

Many biologically significant molecules, such as amino acids, proteins, and DNA, are inherently chiral. Chiral plasmonic materials, through their enhanced CD signals, can be employed to detect and identify these molecules with high sensitivity.[40] For example, in protein structure analysis, chiral plasmonics can be used to detect conformational changes in proteins by interacting with their chiral nature. When proteins bind to the surface of plasmonic nanoparticles, the optical response changes, allowing researchers to infer structural information about the proteins.[44] Unlike traditional methods, which often rely on chemical labeling, chiral plasmonics offers label-free detection, eliminating the need for complex chemical

modifications of biomolecules. This greatly simplifies the workflow and reduces interference in biomolecule analysis. For example, Kadodwala and co-workers reported chiral plasmonic nanostructures can be used to distinguish proteins, because different amino acid compositions in proteins can induce changes in the chiral surface charge distribution.[49] In addition, drug molecules often exist as chiral isomers, and these isomers can have vastly different biological activities and toxicities. By detecting the interactions between chiral drug molecules and chiral plasmonic nanostructures, researchers can quickly assess the chiral behavior and activity of drugs in biological environments. For example, the chiral plasmonic shurikens with SERS active silver nanoclusters for enantio-selective sensing **(Figure 1.6A)**.[50] On the other hand, Lu et al. designed a drug screening technology using NRs with long-range order under the illumination of light. NRs can sense the pancreatic cancer biomarker, peptide hIAPP, at a critical concentration of 3.0 μM, and form helical assemblies with hIAPP, showing chiral spectra in the NIR region.[43]

1.2.2 Chemical and Biochemical Nano-sensors

The emergence of chiral plasmonic nanostructures has greatly promoted the development of chemical and biochemical sensing fields. Since chiral plasmonic sensors are able to amplify optical signals and selectively interact with chiral molecules, they provide a powerful platform for the detection and analysis of various chemical and biochemical species with high sensitivity and specificity. For instance, Kotov et al. prepared side-by-side AuNRs assemblies, which were used for detecting oligonucleotides at the attomolar level.[40] Via T-Hg^{2+}-T interactions, Zhu et al. reported the application of gold nanorods ladder assemblies as chiroptical sensors for detecting Hg^{2+} **(Figure 1.6B)**.[51] Zhang et al. also demonstrated the detection concentration of Hg^{2+} ranging from 1 to 500pg/ml using pyramidal gold nanoparticle/DNA framework.[52] Xu et al. demonstrated the sensing capability of special DNA-modified AuNRs toward microRNA-21 by self-assembling into dimers with chiroptical activity in living cells.[53] Zhu et al. demonstrated the enantioselective analysis of Cysteine and Glutathione based on the strong CD signals caused by Cysteine and Glutathione-induced end-to-end self-assembly of AuNRs.[54]

1.2.3 Bioimaging and Disease Diagnosis

With the rapid progress in fabricating chiral plasmonic nanostructures, chiral plasmonic nanomaterials have emerged as a groundbreaking tool in bioimaging and disease diagnosis due to their unique optical properties. Traditional imaging methods, such as fluorescence and magnetic resonance imaging (MRI), often require labels or contrast agents that can alter the behavior of the biological system. Chiral plasmonic nanostructures offer a label-free approach to bioimaging, allowing for real-time and non-invasive imaging of chiral biomolecules. In addition, many diseases, including cancer, neurodegenerative disorders, and infectious diseases, are associated with changes in the structure or expression of chiral biomolecules, such as proteins or nucleic acids. By detecting these changes, chiral plasmonic sensors can provide early diagnostic information and monitor disease progression. Xu et al. prepared chiroptical shell-satellite nanostructures with the ability to generate reactive oxygen species under CPL irradiation, which has a very high phototherapy effect on cancer cells especially in the irradiation of R-CPL irradiation. So, it can be performed simultaneously in tumors by X-ray computed tomography and photoacoustic imaging.[55] Furthermore, this group also reported that DNA-bridged chiroptical assemblies of AuNPs can intertwine with the cytoskeletal fibers of cells, significantly accelerating the differentiation of neural stem cells under CPL **(Figure 1.6C)**. When they were transplanted into the hippocampus of an Alzheimer's disease mouse model and exposed to CPL, amyloid plaque formation was reduced by over 70%.[56]

1.2.4 Catalysis

While chiral plasmonic structures have found applications in sensing, bioimaging, and diagnostics, their use in catalysis represents a particularly exciting frontier. The combination of chirality with plasmon-enhanced catalysis opens new avenues for designing highly efficient and selective catalytic processes, particularly in the field of asymmetric catalysis. It has been reported that plasmonic nanomaterials can be used for chiral catalysis. For example, Xu et al. prepared chiroptical nano-gapped Au–Ag nanostructures, which showed higher catalytic activity than AuNPs and Au@Ag core-shell NPs under CPL irradiation the greater numbers of hot electrons.[57] In addition, Ding et al. demonstrated that DNA-covered AuNPs can selectively

catalyze glucose as a glucose oxidase mimic due to the environmentally responsive chiral ligand of DNA **(Figure 1.6D)**. AuNPs were covered with random curling of DNA and structural DNA showed higher activity towards L-glucose and D-glucose, respectively.[58]

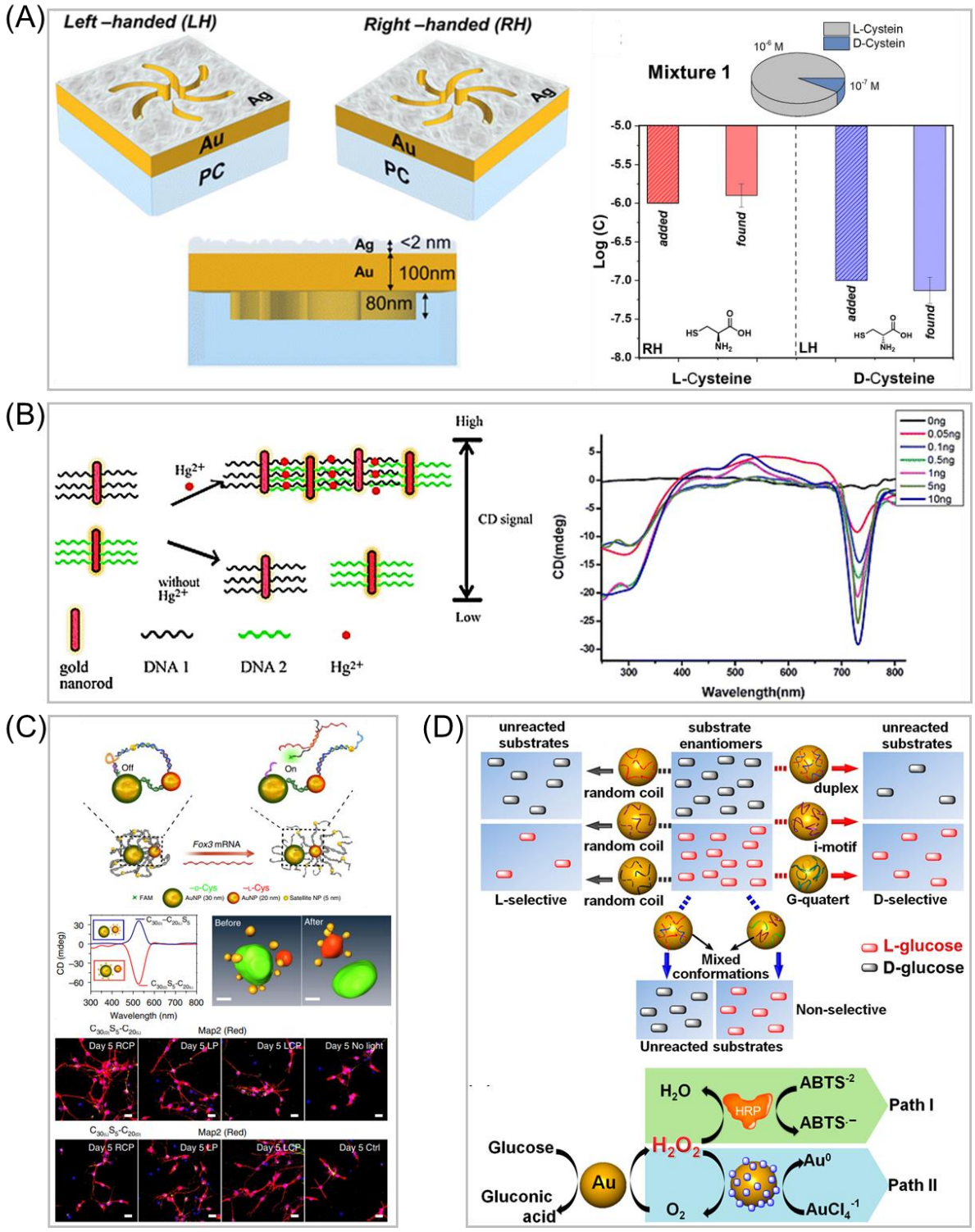

Figure 1.6 (A) The enantio-selective discrimination for L/D cysteine using SERS-substrates formed by chiroptical shurikens and silver nanoclusters.[50] (B) AuNRs assembly-based chirality sensors for detection of Hg^{2+}.[51] (C) CPL transduced by DNA-bridged chiroptical assemblies of AuNPssignificantly accelerates the differentiation of neural stem cells.[56] (D) DNA-covered AuNPs as a glucose oxidase mimic for selective catalysis of glucose.[58]

1.3 Chiral Templates Mediated Chiral Plasmonic

1.3.1 DNA-Mediated Chiral Plasmonic

DNA, as a chiral biopolymer, naturally forms a right-handed double-helix with well-defined molecular geometry and possesses unique flexibility, designability, and programmability. These properties of DNA can be harnessed to guide the assembly of metallic nanoparticles into chiral structures. In recent works, many chiral plasmonic nanostructures have been constructed using DNA to mediate the assembly. Among these works, four main approaches have been developed for DNA-mediated chiral plasmonic. First, DNA can be a template for NPs attaching at specific locations along the DNA helix.[28] By arranging multiple nanoparticles along the DNA backbone, a helical or twisted configuration is formed. The plasmonic coupling between adjacent nanoparticles generates strong chiral optical responses. The second one is the hybridization-mediated assembly. In this method, complementary DNA strands attached to plasmonic nanoparticles can be designed to hybridize, bringing the nanoparticles into a well-defined, chiral arrangement. The hybridization process occurs spontaneously due to the sequence-specific binding of the complementary DNA strands, forming nanostructures such as dimers, trimers, and higher-order assemblies with chiral geometry.[40] The resulting structure exhibits plasmonic coupling between the nanoparticles, leading to enhanced CD signals.[41] For example, Wang et al. reported that individual NRs didn't show any CD signals, but the dimer structure of NPs existed bisignate CD signals.[59] The third approach is the DNA origami-based assembly. DNA origami is a technique where DNA strands are folded into complex 2D and 3D structures with nanometer precision. Using this method, DNA can be folded into intricate geometries that serve as scaffolds for precisely positioning plasmonic nanoparticles. DNA origami allows for the creation of highly customizable and well-ordered chiral plasmonic arrays, such as helices or other chiral motifs.[26] So far, many plasmonic chiral structures have been acquired, uch as Au nanoparticle tetramers[60], bipyramids[61], toroids[62], helices[63, 64], AuNR dimers[18, 65] helices[66, 67] and so on. This approach provides programmable control over the distance and orientation of the nanoparticles, which directly influences their

optical properties. The last approach is DNA-mediated chemical synthesis of chiral nanoparticles. For example, Nam's group introduced adenine oligomers to interact with high-Miller-index surfaces during the growth process to synthesize single NPs with chiroptical activity.[39] Although experiments had shown that plasmonic chirality was affected by oligomer length and CTAB concentration, the exact mechanism of plasmonic chirality induced by the interaction between molecules and Au still needs further exploration.

1.3.2 Amino Acids, Peptides and Proteins Mediated Chiral Plasmonic

Amino acids, peptides, and proteins are naturally chiral molecules. Most amino acids (except glycine) have asymmetric carbon centers, leading to the existence of left-handed (L) and right-handed (D) enantiomers. In the case of peptides and proteins, chirality stems from their sequence of amino acids and the formation of secondary structures like alpha-helices and beta-sheets, which also exhibit chirality. When these chiral biomolecules interact with plasmonic nanoparticles, they induce chiral arrangements or modify the local environment of the nanoparticles, leading to chiroptical properties in the plasmonic structures. Among many recent works, two main approaches have been developed for amino acids, peptides and proteins mediated chiral plasmonic. On the one hand, peptides and proteins can be employed to construct assemblies. Tang's group reported the end-to-end AuNR assemblies combined by cysteine, which not only displayed plasmonic CD signals in the visible-NIR light region, but also tuned the intensity and wavelength of the plasmonic CD by changing the aspect ratio of AuNRs.[68] Amino acids, peptides, or proteins can also directly adsorb onto the surface of plasmonic nanoparticles via electrostatic interaction. For example, Shinmori et al. prepared chiroptical complex formed by AuNRs and proteins though electrostatic interactions.[42] And the AuNPs helices could also be prepared via the accurate distribution of Au nanoparticles on the twisted peptide or protein self-assemblies. Song et al. prepared Au nanoparticles double helices via the accurate distribution of Au nanoparticles on the twisted peptide self-assemblies.[69] Kumar et al. reported that AuNRs can generate strong chiroptical activity after being adsorbed on helical protein fibrils to form a helical arrangement and can be applied to the treatment of Parkinson's disease.[70] The chiral molecular structures of these biomolecules influence the

orientation and assembly of the nanoparticles. This adsorption often leads to a chirality transfer, where the chiral biomolecule imparts its chiral signature to the plasmonic nanostructure, resulting in chiral optical properties. On the other hand, On the other hand, amino acids, peptides, and proteins also play an important role in the chemical preparation of chiroptical NPs. In seed-mediated growth process, achiral NPs are used as seeds to achieve chiral guidance through the adsorption of amino acids, peptides, and proteins. For example, Wu's group used cysteine to regulate the overgrowth of Au and prepared starfruit-shaped AuNPs. These carambola-like AuNPs exhibit significant chiroptical activity, demonstrating the potential of amino acids in inducing chirality in NPs.[71] In addition, the research of Nam's group further expanded the application of amino acids, peptides and proteins in the synthesis of chiral NPs. They successfully prepared AuNPs with three-dimensional chiral morphology, opening up a new way for the chirality control of nanomaterials.[30, 38]

1.3.3 Other Templates Mediated Chiral Plasmonic

Except DNA, amino acids, peptides and proteins, other templates such as polymers, cellulose nanocrystals (CNCs) and silica helices also served as soft templates to construct the chiral plasmonic. For example, Manuel et al. reported that they successfully combined AgNPs with polymers through the interaction between amide groups and AgNPs and prepared chiral dynamic nanomaterials based on the tunability of helical polymers.[72] Jung et al. fabricated NP superstructures with chiroptical activities by controlling the growth of AuNPs on the helical nanofiber template of hydrogel. And the tunability of the diameter of the AuNPs and the length of AuNPs in the helical fibers increased the flexibility of the plasmonic CD wavelength.[73] Xie et al. used chiral mesoporous silica as scaffolds for the growth of anisotropic Ag nanowires. These Ag nanowires inherited the helical morphology of the silica templates and exhibited strong chiral optical responses.[74]

1.4 π–π Stacking Interaction in DNA

As a biomolecule, DNA not only plays a crucial role in biological heredity but is also widely used in nanotechnology, materials science and biomedicine due to its unique structural and functional properties. As shown in **Figure 1.7**, the basic unit of DNA is the nucleotide, each consisting of a phosphate group, deoxyribose, and a nitrogenous base nucleobase. DNA typically shows a right-handed double-helix structure, which is formed by two antiparallel polynucleotide chains connected by hydrogen bonds between the bases. Adenine (A) pairs with thymine (T) through two hydrogen bonds, while guanine (G) pairs with cytosine (C) through three hydrogen bonds, ensuring the stability of the double helix and recognition of target sequences. Furthermore, the helical structure of DNA has inherent chirality and can interact with molecules or nanomaterials to produce unique optical properties.[75]

In addition to hydrogen bonds, π–π stacking interactions between aromatic nitrogenous bases are another important force for stabilizing the DNA double helix.[76] π–π stacking refers to the attractive forces that occur between planar aromatic rings, which have delocalized π-electrons. In DNA, the nitrogenous bases possess aromatic rings, allowing them to interact through their π-electron clouds when stacked on top of one another, causing them to bind more tightly together and thereby enhancing the overall stability of DNA. For instance, in G-quadruplex structures, planar arrangements formed by guanine stacks are further stabilized by π-π interactions and the coordination of ions with guanine oxygens, which is critical in telomeres and gene regulatory regions.[77] The stacking interactions are sequence-dependent, and different base pair combinations exhibit different stacking strengths. Guanine (G) and adenine (A) are known to stack more strongly compared to cytosine (C) and thymine (T), due to the larger π-system in the purine rings. In particular, G-C stacks tend to stabilize the DNA helix more than A-T stacks.

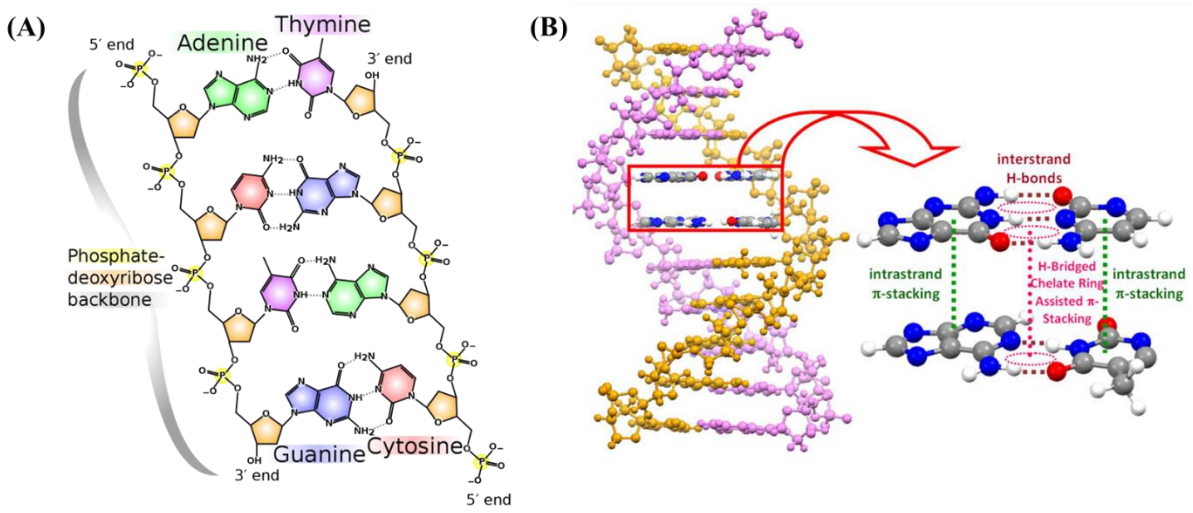

Figure 1.7 (A) Structure of DNA double helix and base pairing. The dotted lines between adenine and thymine and between guanine and cytosine indicate hydrogen bonds. (B) π -π stacking interactions between A-T and G-C base pair shown as green dotted lines.[78]

1.5 Purpose of the Present Study

Chirality, the lack of mirror symmetry, exists from individual molecules to supramolecular systems. Despite the similar chemical and physical properties for a pair of chiral molecules known as enantiomers, they exhibit distinct physiological effects, making the analysis and control of molecular chirality critical, especially in pharmacology. Circular dichroism (CD), the difference in absorption of left- and right-handed circularly polarized light, is often used to characterize molecular chirality. Recently, plasmonic CD, arising from the interaction between chiral molecules and metal nanoparticles, has attracted significant attention as a principle for highly sensitive detection of biomolecules. However, it remains unclear which structural features of the molecule induce the plasmonic CD. DNA forms a right-handed double helix when double-stranded, but even when single-stranded, it can have a variety of secondary structures depending on its base sequence. Examples include the G-quartet of guanine-rich DNA, the i-motif of cytosine-rich DNA, and the single-stranded helical structure of adenine-rich DNA. Due to this programable structural diversity of DNA, DNA-noble metal nanoparticle complexes become an ideal model for discussing the origin of plasmonic CD. Thus, in this study, the author focused on the plasmonic CD of Au nanorods (AuNRs) and DNA polyion complexes.

Chapter 2, the author investigated the plasmonic CD of AuNR–DNA polyion complexes. In particular, the author investigated the effects of AuNR–DNA mixing ratio, base sequence, the presence or absence of duplex formation and mixture of noncomplementary DNA on the plasmonic CD and discussed the structural features of the adsorbate required to induce the plasmonic CD. In addition, the author also showed by cryo-TEM that AuNRs are assembled into twisted ribbons via DNA.

Chapter 3, the author explores the potential of AuNR–DNA polyion complexes in enhancing the chirality of metal-mediated DNA. Specifically, in the absence of metal ions (Hg^{2+}/Ag^{+}), the polyion complexes formed between ssDNA (dT_{22}/dC_{22}) and AuNR did not exhibit any plasmonic CD response. However, in the presence of metal ions (Hg^{2+}/Ag^{+}), the

interactions between T-Hg^{2+}-T or C-Ag^{+}-C base pairs mediate the conversion of ssDNA (dT_{22}/dC_{22}) into dsDNA. This transformation results in significant plasmonic CD when forming polyion complexes with AuNR. Specially, polyion complexes formed by AuNRs and Ag^{+}-mediated DNA exhibited plasmonic circular dichroism (CD) that are up to ~400 times stronger than the molecular CD signal of DNA.

Chapter 4, the author summarized the thesis and discussed the prospective use of this chiroptical AuNR–DNA polyion complexes.

Chapter 2 **Plasmonic circular dichroism of nanorod–DNA polyion complexes: What DNA makes nanorods chiroptically Active?**

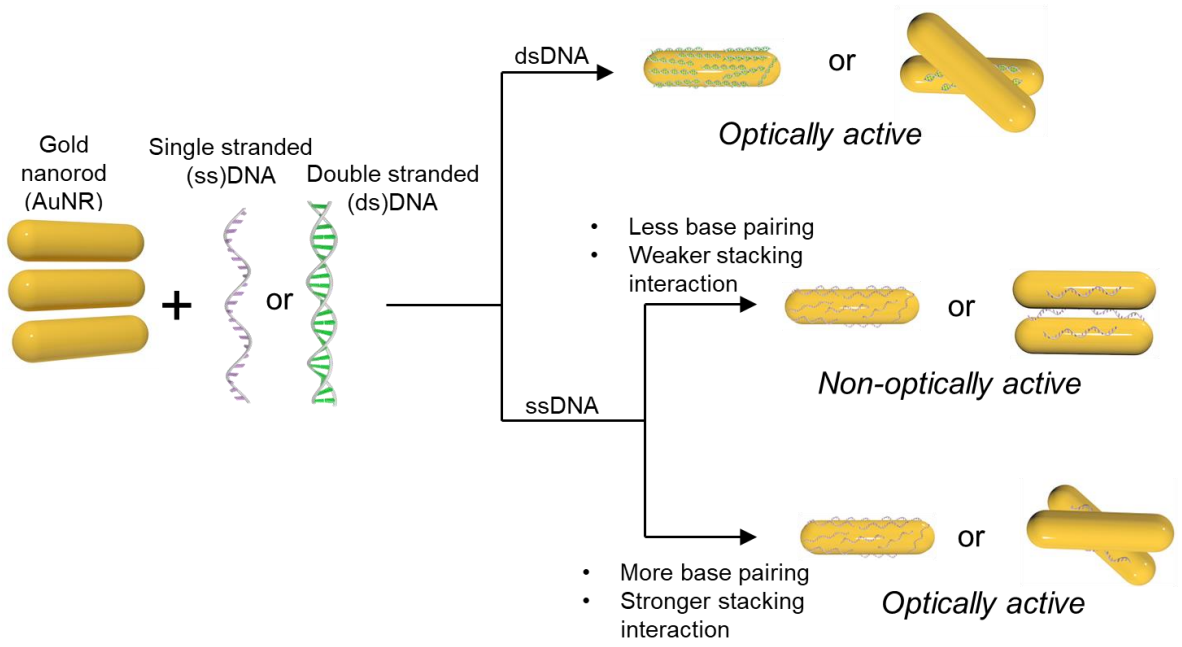

Chapter 3 **Plasmonic circular dichroism-based metal ion detection using gold nanorod–DNA complexes**

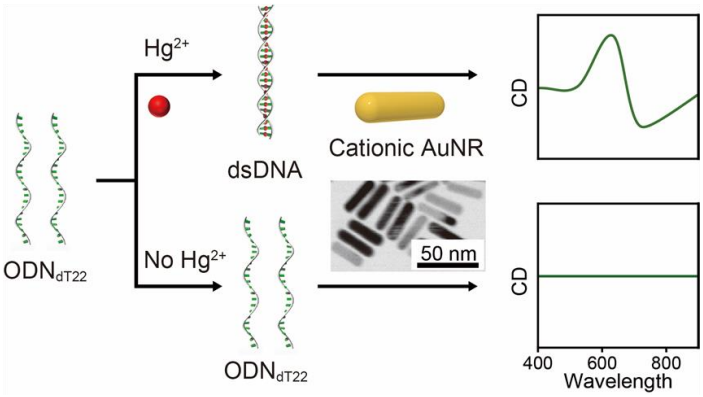

Figure 1.8 Schematic illustration of this doctoral thesis.

Chapter 2

Plasmonic Circular Dichroism of Nanorod–DNA Polyion Complexes: What DNA Makes Nanorods Chiroptically Active?

2.1 Abstract

Chiral nanostructures have gained significant interest due to their unique optical properties, which are promising for applications in sensing and catalysis. However, understanding the chiroptical mechanisms of nanoparticles and molecules remains a challenge. This study aims to investigate the optical chirality of AuNR–DNA polyion complexes and to correlate DNA structural characteristics with their optical activity. I employed a combination of circular dichroism (CD) spectroscopy and cryo-TEM tomography to analyze the chirality of AuNR–DNA complexes. The CD spectra of AuNR–DNA complex showed characteristic chiral optical activity, which was dependent on the structure of DNA. The 3D reconstructions revealed a highly ordered chiral assembly of AuNRs with dihedral angles of 0-10°. This study provides a comprehensive understanding of the chiral assembly of AuNR–DNA complexes, highlighting their potential for applications in chiral sensing. This also provides an understanding of interactions between nanoparticles and molecules on the generation of chirality, though further studies are needed to gain a deeper understanding the mechanisms of chirality induced by AuNR and DNA.

2.2 Introduction

Chirality is a structural property of molecules and materials that is closely related to biological and optical properties. For example, although mirror images of chiral molecules (enantiomers) have the similar chemical and physical properties, they exhibit different physiological effects since most of the biomolecules in living organisms are homochiral (amino acids are L-form and sugars are D-form).[79] Therefore, the analysis and control of molecular chirality is an extremely important issue, especially in the pharmaceutical industry.[80] Chiral molecules also exhibit the difference in absorption of left and right circularly polarized light, i.e., circular dichroism (CD).[81] Since CD reflects the structure of chiral molecules, the CD spectrometer is a powerful tool for structural analysis of biomolecules and macromolecules. The ability to follow changes in two states, such as DNA duplex formation and transition to a higher order conformation, is one of the advantages of CD spectrometry.[82]

Noble metal nanoparticles such as gold and silver are intriguing materials that exhibit localized surface plasmon resonance (LSPR).[83] Recently, methods to make achiral plasmonic nanoparticles chiral optically active have been reported in the context of biosensors and metamaterials. For example, chiral optically active plasmonic nanostructures can be fabricated by simply adsorbing chiral molecules onto the particles.[42] When chiral molecules are present in the electromagnetic field generated near the plasmonic nanoparticle surface, dipole-dipole interactions occur between the particle and the molecule, inducing a plasmonic CD.[31] The use of stronger electromagnetic fields generated between particles in the vicinity, so-called "hot spots", also falls into this category. It is also effective to utilize DNA origami,[13] helical fibers formed by small molecules,[73] peptides,[84] viruses and proteins,[85] and chiral mesoporous silica[86] as a template to assemble particles in a chiral arrangement. In addition, plasmonic nanoparticles bridged by chiral molecules can become optically active. This method has attracted particular attention because it enables highly sensitive detection of biomolecules.[87] However, the origin of the plasmon chirality is still controversial because the particles form chiral aggregates at the same time that the chiral molecules are located at the hot spots. In addition, many questions

remain as to what kind of chiral molecules can induce plasmonic chirality.

Chiral molecular bridging has been achieved by electrostatic interactions with proteins,[42, 85] amino acids,[88] and synthetic polymers,[46] as well as by DNA hybridization.[40] On the other hand, electrostatic interaction with DNA has rarely been exploited.[89-92] However, the polyion complexes of plasmonic nanoparticles and DNA can be an ideal system to discuss the origin of plasmonic chirality, because the structure of DNA has been the subject of intense research due to its biological importance, and much knowledge has already been established. For example, it is well known that π-π stacking interactions between bases stabilize the DNA double helix structure.[75] In addition, the secondary structure adopted by single-stranded (ss)DNA can be programmed by designing the base sequence. Therefore, DNA is suitable for discussing the origin of plasmonic CD in relation to the structure of adsorbates. Another advantage is the availability of L-DNA,[93] a mirror-image isomer of the natural form of D-DNA, thanks to the expansion of DNA synthesis technology. The biorthogonal properties of L-DNA (i.e., the inability to form a duplex with D-DNA) also help to discuss the effect of adsorbate structure on plasmonic CD. More importantly, the detection of specific DNA is an important technique in medical research and diagnostics,[94] the food and pharmaceutical industries,[95, 96] and environmental monitoring.[97] It would be of great benefit if structural information about DNA could be obtained from CD spectra even with small sample volumes.

In this study, I have investigated the plasmonic CD of gold nanorods (AuNRs) and DNA polyion complexes. The preparation of AuNR–DNA polyion complexes is shown in **Scheme 2-1**. In particular, I investigated the effects of AuNR–DNA mixing ratio, base sequence, and the presence or absence of duplex formation on the plasmonic CD, and discussed the structural features of the adsorbate required to induce the plasmonic CD. In addition, I showed by cryo-TEM that AuNRs are assembled into twisted ribbons via DNA. I believe that this study not only proposes a new DNA detection method, but also provides insight into the origin of induced plasmonic CD.

2.3 Experimental Section

2.3.1 Materials and Instruments

20-(11-Mercaptoundecanyloxy)-3, 6, 9, 12, 15, 18-hexaoxaeicosane-1-amine (cationic ligand) was purchased from Dojindo Laboratories (Japan). The single strand(ss) DNA of 22 base were purchased from Thermo Fisher Scientific Inc. (USA). Extinction spectra were measured with a V-770 UV-vis spectrometer (JASCO Corp., Japan). Dynamic light scattering (DLS) profiles were obtained with a Zetasizer Nano ZS (Malvern Panalytical, UK). Circular Dichroism (CD) measurements were conducted with a J-820 spectrometer (JASCO Corp., Japan). The Cryo-Electron Microscopy (Cryo-EM) images were collected using a CRYO ARM™ 300 II (JEM-3300) system (JEOL Corp., Japan). Base sequences of the DNA strands used in the present study as shown below:

Code	Base number Base sequence (5′ → 3′)
ssDNA-1	GTACGAACGCCATCGACTTACG
ssDNA-2	CGTAAGTCGATGGCGTTCGTAC
dA_{22}	AAAAAAAAAAAAAAAAAAAAAA
dT_{22}	TTTTTTTTTTTTTTTTTTTTT
dG_{22}	GGGGGGGGGGGGGGGGGGGGG
dC_{22}	CCCCCCCCCCCCCCCCCCCCC
A_6C_{16}	ACCCCCCCCACCACCAAACCCC
$G_{16}T_6$	GGGGTTTGGTGGTGGGGGGGGT
$A_{11}C_{11}$	ACCAACCCAACCCCCAAAACAA
$G_{11}T_{11}$	TTGTTTTGGGGGTTGGGTTGGT
$A_{16}C_6$	AAAAAACACCCCAAAAAACAAA
G_6T_{16}	TTTGTTTTTTGGGGTGTTTTTT
A_6G_{16}	AGGGAGAGGAGGAGGGGAGGGG
T_6C_6	CCCCTCCCCTCCTCCTCTCCCT
$A_{11}G_{11}$	GAGAGAAAGGGAGGGGAAAAAG

$T_{11}C_{11}$	CTTTTTCCCCTCCCTTTCTCTC
$A_{16}G_6$	GAGAGAAGAGAAAAAGAAAAAA
$T_{16}C_6$	TTTTTTCTTTTTCTCTTCTCTC

2.3.2 Synthesis of gold nanorods (AuNRs)

AuNRs with a diameter of ~10 nm and a length of ~40 nm were synthesized according to the seed growth method.[98] (1) Preparation of seed solution: a gold seed solution was prepared in a 50 mL plastic tube by adding an ice-cold $NaBH_4$ solution (600 μL, 0.01 M) to a mixture of a $HAuCl_4 \cdot 3H_2O$ solution (250 μL, 0.01 M) and a CTAB solution (7.5 mL, 0.1 M) under gentle shaking. The seed solution was then kept in an incubator (30°C) for at least 2 h. (2) Growth reaction: growth solutions were prepared in 100 mL plastic tubes by sequentially adding $HAuCl_4 \cdot 3H_2O$ solution (400 μL, 0.01 M), $AgNO_3$ solution (240 μL, 0.01 M) and an ascorbic solution (64 μL, 0.1 M) to a CTAB solution (40 mL, 0.1 M). The gold seed solutions (96 μL) were injected into the growth solutions (40 mL) while the growth solution was shaken gently. The growth solutions were then left undisturbed in an incubator (30°C) for at least 3 h. (3) Purification: the prepared AuNRs solutions were transferred to 1.5 mL plastic tubes and divided into 1000 mL portions. The AuNRs were sedimented by centrifugation (18,000 g, 20 min, 30°C), and the supernatant (900 μL) was removed. The plastic tubes were then filled with Milli-Q water (900 μL) and vortexed. This centrifugal purification procedure was repeated twice so that all chemicals except for the AuNRs were diluted 100-fold.

2.1.3 Surface modification of AuNRs with cationic ligands

Methanol solutions of the cationic ligand(20-(11-Mercaptoundecanyloxy)-3, 6, 9, 12, 15, 18- hexaoxaeicosane-1-amine, hydrochloride) (10 mM) were prepared. The ligand solution (10 mM, 35 μL) was added to the purified AuNRs solution (1000 μL) in a 1.5 mL plastic tube. The AuNRs solution containing the ligands was vortexed and kept undisturbed at 42°C for at least 12 h. Then, the solution was centrifuged (18 000 g, 20 min, 30°C), the supernatant (900 μL) was removed, and Milli-Q water (900 μL) was added to the residue solution. This centrifugal purification was performed twice to remove free ligands from the AuNRs solution. Finally, the

concentration of the ligand modified AuNRs was adjusted to the desired concentration by centrifugal concentration.

2.3.4 AuNR–DNA Assembly Formation

To facilitate AuNR–ssDNA assembly formation, the AuNRs(16 nM) and ssDNA with a length of 22nt were mixed in 10 mM Tris-HCl (pH 7.7) buffer. To facilitate AuNRs-dsDNA assembly formation, the dsDNA with a length of 22bp was carried out with ssDNA and complementary DNA in 10 mM Tris-HCl (pH 7.7) buffer for 20 min first before mixing AuNRs(16 nM). All experiments were performed at room temperature.

2.3.5 Measurement of Circular Dichroism (CD) Spectroscopy

Each of the samples was transferred to a quartz cuvette with an optical path length of 1 mm. The quartz cuvettes were set in a CD spectrometer, and the CD spectra were collected. The measurement conditions were as follow, scan speed: 200 nm/min, response: 1 msec, bandwidth: 15 nm, and scans: 2. All of the CD spectra were smoothed using a 50-point Savitzky-Golay algorithm.

2.4 Results and Discussion

2.4.1 The formation of AuNR–DNA polyion complexes

First, I investigated the formation of DNA complexes with AuNRs via electrostatic interactions. I prepared cationic AuNRs **(Figure 2-1)** (size: ~40 nm × ~10 nm, zeta potential: +13.8 mV) by the surface exchange of cetyltrimethylammonium bromide (CTAB)-covered AuNRs with primary amine-terminated hexaethylene glycol thiol ligands, to make them both more stable and controllable. Then, the cationic AuNRs were added into the Tris-HCl buffer solution containing DNA to form AuNR–DNA complexes. Dynamic light scattering (DLS) was used to characterize the complexes. The final concentrations of AuNR and Tris-HCl were set at 16 nM and 10 mM, respectively, while the DNA concentration was varied. Unless otherwise noted, the DNA sequences used are 5'-GTACGAACGCCATCGACTTACG-3' (22 nt D-form ssDNA1) and its complementary strand, 5'-CGTAAGTCGATGGCGTTCGTAC-3' (22 nt D-form ssDNA2). Note that ssDNA1 was used in the ssDNA experiments below.

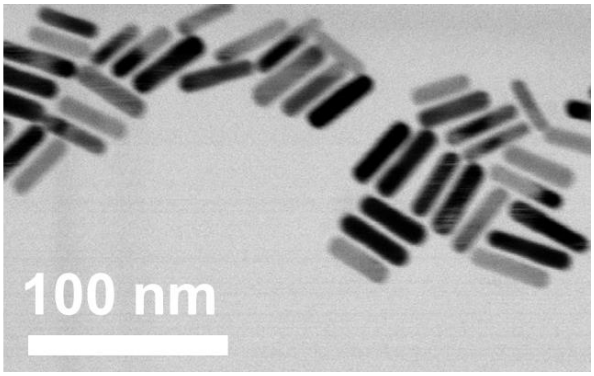

Figure 2-1 AuNRs with length of 40 nm and diameter of 10 nm.

It has already been reported by Link et al that polyion complexes of plasmonic nanoparticles and chiral biomolecules exhibit plasmonic CD signals that depend on conformation of biomolecules.[85] Therefore, I started our work by investigating the aggregation state of AuNR–DNA polyion complexes by dynamic light scattering (DLS) and UV-Vis-NIR spectroscopy **(Figure 2-2 and Table 2-1).** At relatively low DNA concentrations (≤0.6 μM for ssDNA and ≤0.3 μM for dsDNA), the sizes of the AuNR–DNA polyion complexes were

estimated to be ≈106 nm from the DLS profiles **(Figure 2-2A, G and Table 2-1)**, but DLS peaks were also observed in regions much smaller than the size of the NR used. These correspond to the peaks resulting from the rotational motion of individual NRs, suggesting the presence of NRs that are not assembled with each other. This was also supported by their extinction spectra. As shown in Figure 1D, J, a shoulder peak, which is associated with the L-LSPR peak, appeared at ≈776 nm. With the increasing DNA concentration, the shoulder peak increased in intensity while the main peak, located at ≈700 nm, decreased in intensity. The former peak corresponds to aggregated AuNRs and the latter to one non-aggregated AuNRs, indicating that the two states coexist in these DNA concentration ranges. In addition, it was also suggested that side-by-side (SBS) AuNR aggregates mainly occurred, because SBS AuNR aggregates exhibit L-LSPR peak at a shorter wavelength than AuNRs alone.

In the medium DNA concentration ranges (0.6–0.8 μM for ssDNA and 0.3–0.4 μM for dsDNA), the AuNR–DNA polyion complexes with sizes larger than 2300 nm were formed **(Figure 2-2B, H and Table 2-1)** and immediately sedimented at the bottom of a cuvette **(Figure 2-3)**. Therefore, some of the AuNR–DNA polyion complexes fell out of the optical path during the measurement, resulting in an overall decrease in extinction intensity compared to the other conditions **(Figure 2-2E, K)**. In addition, the L-LSPR peak was apparently broadened, indicating the random aggregation of AuNRs.

When the DNA concentration was further increased (≥2 μM for ssDNA and ≥1 μM for dsDNA), the AuNRs were initially covered by the excess DNA and thus did not form large aggregates (estimated sizes were less than ≈91.3 nm, **Table 2-1**), thus maintaining a stable dispersed state in solution **(Figure 2-3)**. At even higher DNA concentrations (≥20 μM for ssDNA and ≥20 μM for dsDNA), the sizes of AuNR–DNA polyion complexes (≈43.8 nm) are almost the same as those of the AuNRs alone (≈37.8 nm) **(Figure 2-2C, I and Table 2-1)**, indicating that AuNRs do not aggregate with each other. This is also supported by the fact that the extinction spectra of the AuNR–DNA polyion complexes are almost identical to those of the AuNRs alone **(Figure 2-2F, L)**.

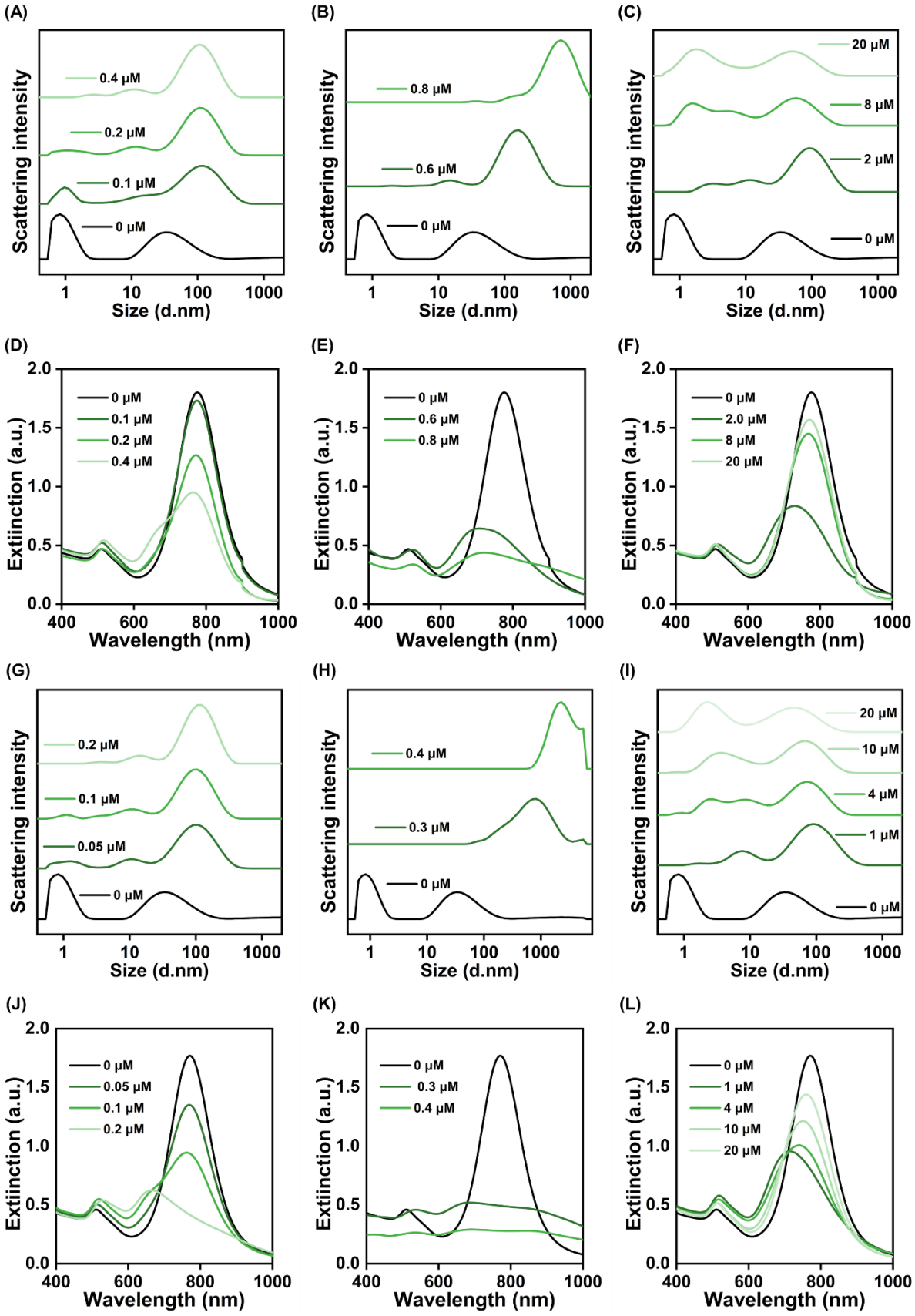

Figure 2-2 Characterization of the aggregation state of AuNR–DNA polyion complexes. (A–C and G–I) Typical DLS profiles of AuNR–ssDNA or AuNR–dsDNA polyion complexes prepared at low (0.4

μM for ssDNA (A) and 0.2 μM for dsDNA (G)), medium (0.8 μM for ssDNA (B) and 0.4 μM for dsDNA (H)) and high (20 μM for ssDNA (C) and 20 μM for dsDNA (I)) DNA concentrations. Arrows indicate the peaks resulting from the rotation motion of individual NRs. (D–F and J–L) Extinction spectra of AuNR–ssDNA or AuNR–dsDNA polyion complexes prepared at low (≤0.4 μM for ssDNA (D) and ≤0.2 μM for dsDNA (J)), medium (0.6–0.8 μM for ssDNA (E) and 0.3–0.4 μM for dsDNA (K)) and high (≤20 μM for ssDNA (F) and 20 μM for dsDNA (L)) DNA concentrations. For comparison, data for AuNRs alone are shown as dotted gray lines in all the figures.

Table 2-1 The size of AuNR–DNA polyion complexes measured by DLS

Type	DNA conc. (μM)	Size (nm)
AuNRs alone		37.8
AuNR–ssDNA	0.1	106
	0.2	106
	0.4	106
	0.6	164
	0.8	712
	2	91.3
	8	58.8
	20	50.7
AuNR–dsDNA	0.05	106
	0.1	106
	0.2	106
	0.3	825
	0.4	2300
	1	91.3
	4	68.1
	10	68.1
	20	43.8

Figure 2-3 The images of AuNRs solution with different DNA concentration. From left to right: no DNA (dispersed), low amount of DNA (assembled), medium amount of DNA (aggregated) and high amount of DNA (dispersed).

2.4.2 Plasmonic CD of AuNR–DNA polyion complexes

As described above, I have correlated the relative abundance of AuNRs and DNA with the aggregation state of their polyion complexes **(Figure 2-4A)**. Next, I measured the CD spectra of AuNR–DNA polyion complexes in the wavelength range from 400 nm to 1000 nm **(Figure 2-4B–G)**. Figures 2-4B and E show the CD spectra at the low ssDNA or dsDNA concentrations (≤0.4 μM for ssDNA and ≤0.2 μM for dsDNA). AuNRs alone are naturally optically silent, but when mixed with DNA, plasmonic CD signals were generated. For ssDNA, a peak at the longer wavelength (≈820 nm) and a dip at the shorter wavelength (≈660 nm) were observed (positive couplet). The peak/dip intensities increased/decreased to 104 mdeg/125 mdeg with increasing ssDNA concentration. Interestingly, AuNR–dsDNA polyion complexes exhibited CD signals with opposite sign, i.e., a dip at the longer wavelength (≈800 nm) and a peak at the shorter wavelength (≈650 nm) (negative couplet) with zero-crossing and peak/dip position almost unchanged. As in the case of AuNR–dsDNA polyion complexes, the dip/peak intensities decreased/increased to -49 mdeg/58 mdeg with increasing DNA concentration, respectively. Smaller inter-particle distance increased the strength of LSPR and its coupling significantly, leading to an enhanced CD response.[19] This suggests that the increased proportion of SBS aggregate is responsible for the increased plasmonic CD intensity.

At intermediate DNA concentrations (0.6–0.8 μM for ssDNA and 0.3–0.4 μM for dsDNA), the CD bands broadened and decreased in intensity compared to those at lower DNA concentrations **(Figure 2-4C and F)**. In addition, the offset between the L-LSPR peak position and the zero crossing became larger (Δλ≈20 nm). These were probably due to the inhomogeneous degree of optical activity among randomly aggregated AuNRs, in addition to the sedimentation of giant aggregates.

At high DNA concentrations (>0.8 μM M for ssDNA, >0.4 μM for dsDNA), the plasmonic CD of the AuNR–DNA polyion complex became weaker **(Figure 2-4D and G)**. In particular, no plasmonic CD could be detected for the AuNR–ssDNA polyion complex **(Figure 2-4D)**. This is agreed with the results reported by Link et al.[85] However, AuNR–dsDNA polyion

complexes exhibited bisignate plasmonic CD signals with a negative couplet even at higher DNA concentrations (>20 μM), and the CD band gradually red shifted with increasing dsDNA concentration **(Figure 2-4G)**. As mentioned above, when the dsDNA concentration is above 20 μM, excess dsDNA prevents AuNRs from aggregating with each other and enhances coupling effects between AuNRs, lowering the resonance energy and leading to a red shift.

It is also worth noting that when mixed dsDNA hybridized by ssDNA and its complementary DNA at room temperature and AuNRs to form poyion complexes, it showed different results. As shown in **Figure 2-5A**, with small amount of dsDNA, the CD intensity also increased with increasing dsDNA concentration, but the CD peak blue shifted. It is possible that the simultaneous presence of dsDNA and ssDNA to induce disordered AuNR assemblies, which leads to an increase in the surface plasmon frequency, thereby resulting in a blue-shift of the CD band.[99] With large amount of dsDNA, the CD also red shifted, but the CD intensity decreased with dsDNA concentration increasing **(Figure 2-5C)**. Based on the results of Figure 2-4D, it shows that no CD signal occurred. So, in this case, the simultaneous presence of dsDNA and ssDNA, the CD intensity was decreased also due to the remain ssDNA. Although the order and disorder AuNR–dsDNA polyion complexes show different CD intensity, the sign of CD are same, both negative CD. So, to keep the same buffer concentration (10 mM Tris-HCl), the dsDNA for all subsequent experiments were formed by hybridization at room temperature.

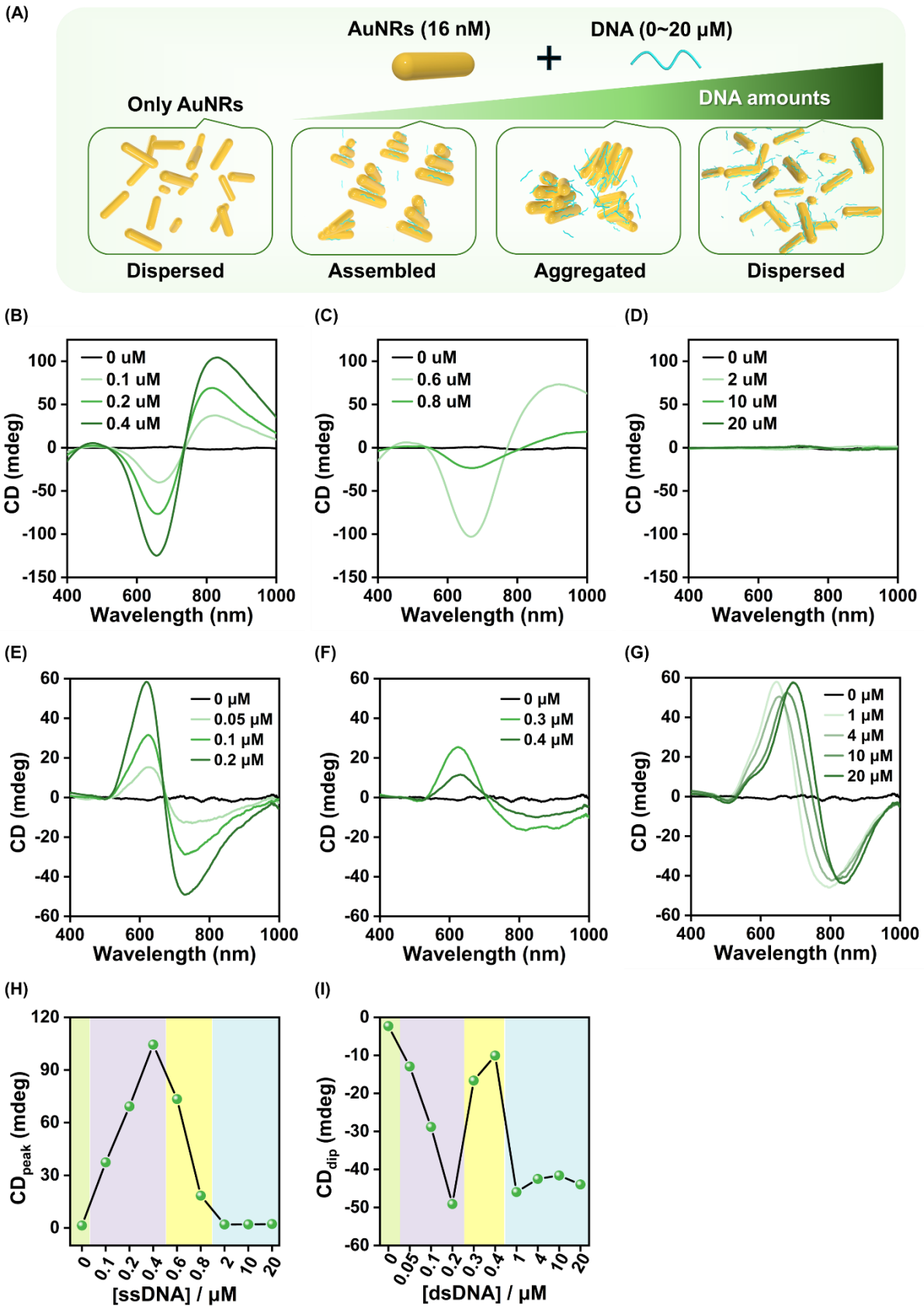

Figure 2-4 (A) Schematic illustration of AuNR assembly states at different DNA conditions. AuNRs form SBS aggregates at low DNA concentrations, random and giant aggregates at intermediate DNA concentrations, and almost no aggregates at high DNA concentrations. **(B–G)** CD spectra of AuNR–

ssDNA or AuNR–dsDNA polyion complexes prepared without DNA or at low (≤0.4 μM for ssDNA (B) and ≤0.2 μM for dsDNA (E)), medium (0.6–0.8 μM for ssDNA (C) and 0.3–0.4 μM for dsDNA (F)) and high (≤20 μM for ssDNA (D) and 20 μM for dsDNA (G)) DNA concentrations. (H, I) Plots of the CD peak intensities of the AuNR–ssDNA polyion complex (H) and the CD dip intensities of AuNR–dsDNA polyion complex (I) as a function of the DNA concentration. To facilitate dsDNA formation, the ssDNA and complementary DNA in buffer were denatured at 95°C for 5 min, hybridized at 65°C for 30 min, equilibrated to 37°C for 15 min and cooled down to room temperature for 30 min. Finally, the stock solution was used to form polyion complexes with AuNRs in 10 mM Tris-HCl buffer (pH 7.6) solution.

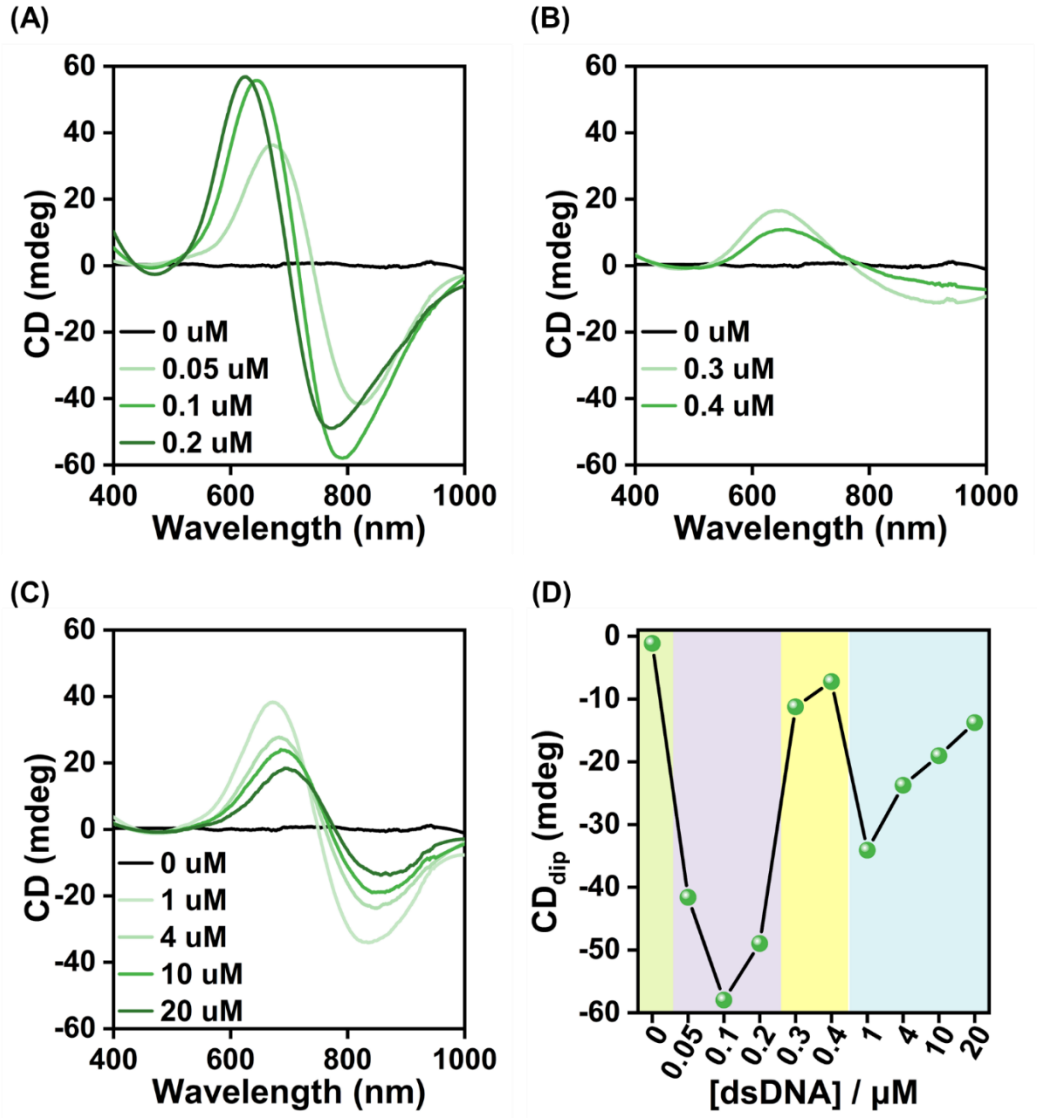

Figure 2-5 (A-C) The CD spectra of AuNR–dsDNA polyion complexes prepared without DNA or at low (≤0.2 μM), medium (0.3–0.4 μM) and high (≤20 μM) DNA concentrations. (D) Plots of the CD dip intensities of the AuNR–dsDNA polyion complex as a function of the DNA concentration. The dsDNA was hybridized by ssDNA and its complementary ssDNA first in 10 mM Tris-HCl buffer (pH 7.6) for 20 min frist. Then, it was mixed with AuNRs to form polyion complexes.

2.4.3 Base sequence dependencies of plasmonic CD in AuNR–DNA polyion complexes

I have shown that AuNRs become optically active when forming polyion complexes with DNA, but I point out here that the intensity and sign of their plasmonic CD were highly dependent on the DNA sequence used. In fact, the AuNR–ssDNA polyion complexes consisting of ssDNA2 (complementary strand of ssDNA1 used so far) showed plasmonic CD signals with much weaker intensity than those for ssDNA1, but a positive couplet **(Figure 2-6)**.

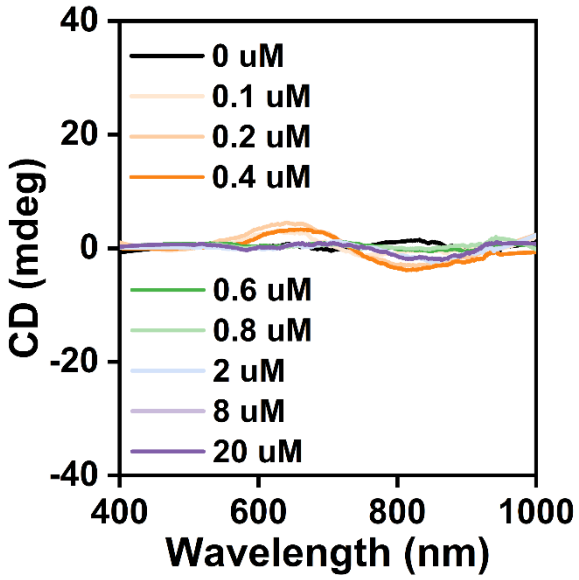

Figure 2-6 The CD spectra of AuNR–ssDNA2 polyion complexes.

To gain insight into the base sequence dependencies, I first measured the CD spectra of AuNR–DNA polyion complexes composed of 22 nt DNA homopolymers (that is, dA22, dC_{22}, dG_{22}, dT_{22}, $dA_{22}{\cdot}dT_{22}$, and $dG_{22}{\cdot}dC_{22}$), and then plotted either of the peak or the dip, which is located at a longer wavelength, against DNA concentrations **(Figure 2-7 and 2-8)**. In other words, the plots show positive values for the case of positive couplet CD and negative values for the case of negative couplet CD. Note that the value was set to 0 when no plasmonic CD was detected. As shown in **Figure 2-7** and **2-8**, the AuNR–dT_{22} polyion complexes were not optically active regardless of DNA concentration. The AuNR–dA_{22} and AuNR–dC_{22} polyion complexes exhibited positive couplet CD, but the AuNR–dG_{22}, AuNR–$dG_{22}{\cdot}dC_{22}$ and AuNR–$dA_{22}{\cdot}dT_{22}$ polyion complexes exhibited negative couplet CD. In terms of CD intensity,

AuNR–dA_{22}, AuNR–dG_{22} and AuNR–dG_{22}·dC_{22} polyion complexes reached maximum at low DNA concentrations (0.2 μM for dA_{22}, 0.6 μM for dG_{22} and 0.4 μM for dG_{22}·dC_{22}, whereas the AuNR–dC_{22} and AuNR–dG_{22}·dC_{22} polyion complexes showed the strongest signal intensity at relatively high DNA concentrations (2 μM for dC_{22} and 1 μM for dA_{22}·dT_{22}. It is also noteworthy that AuNR–dC_{22} polyion complexes were not optically active at low DNA concentrations (0.1–0.8 μM), but showed the strongest optical activity (≈350 mdeg at 828 nm) at a relatively high DNA concentration (2 μM) even compared to the other polyion complexes. From this value, the *g*-factor was calculated to be 0.02 which was as high as that of the AuNR–protein polyion complex system **(Figure 2-9)**.[42]

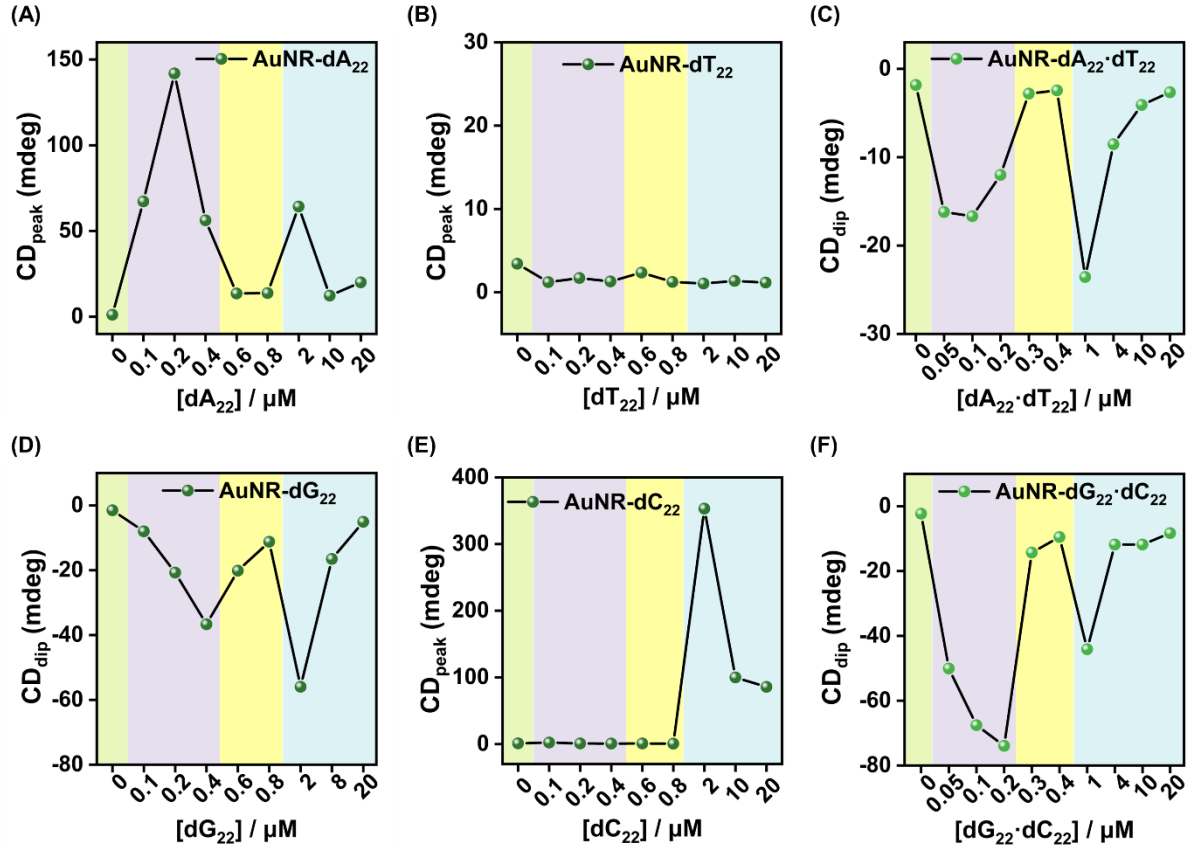

Figure 2-7 Changes in plasmonic CD peak or dip intensity of AuNR–DNA polyion complexes composed of homopolymer DNA at different DNA concentrations. (A) AuNR–dA_{22} polyion complexes, (B) AuNR–dT_{22} polyion complexes, (C) AuNR–dA_{22}·dT_{22} polyion complexes, (D) AuNR–dG_{22} polyion complexes, (E) AuNR–dC_{22} polyion complexes, (F) AuNR–dG_{22}·dC_{22} polyion complexes. The peak is plotted when the AuNR–DNA polyion complexes exhibit a positive couplet CD and the dip is plotted when they exhibit a negative couplet CD.

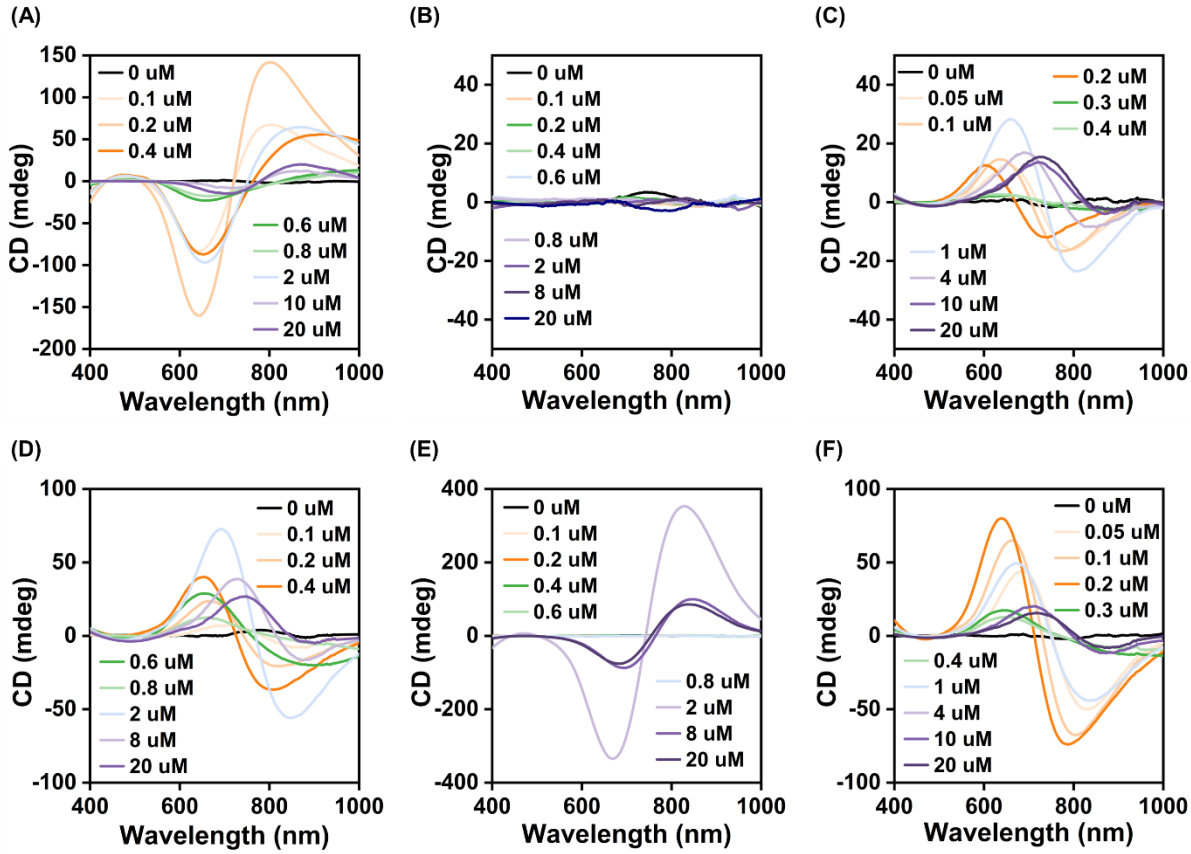

Figure 2-8 The CD spectra of AuNR–DNA polyion complexes composed of homopolymer DNA at different DNA concentrations. (A) AuNR–dA_{22} polyion complexes, (B) AuNR–dT_{22} polyion complexes, (C) AuNR–dA_{22}·dT_{22} polyion complexes, (D) AuNR–dG_{22} polyion complexes, (E) AuNR–dC_{22} polyion complexes, (F) AuNR–dG_{22}·dC_{22} polyion complexes.

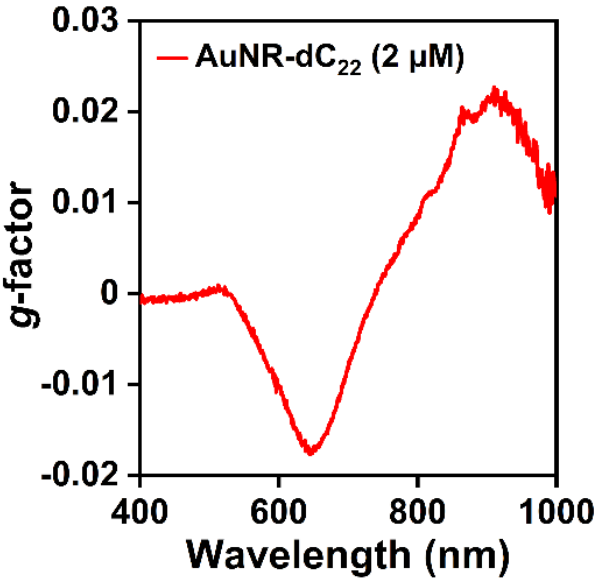

Figure 2-9 The *g*-factor of AuNR–dC_{22} polyion complexes (dC_{22}: 2 μM). If absorption and CD spectra are measured in the same optical cell and concentration, the *g*-factor was calculated as,

$$g\text{-factor} = \frac{\Delta\varepsilon}{\varepsilon} = \frac{\Delta A}{A} \approx \frac{CD(mdeg)}{32980 \cdot A}$$

$\Delta\varepsilon$ was molar circular dichroism, ε was molar absorption coefficient, ΔA was difference of absorbance of left and right circularly polarized lights and A was absorbance of sample. As CD measurements provide theta (mdeg) and the CD can be converted to the appropriate absorbance "units" (32980 mdeg = 1 absorbance "unit" for an optical path length of 1 mm which was employed in this experiment).[85]

ssDNA homopolymers other than dT_{22} have been reported to adopt unique chiral structures. For example, dG_{22} and dC_{22} fold into secondary structures such as G-quadruplex and i-motif by intra- and intermolecular base pairing of Hoogsteen-type. In addition, dA_{22} adopts a single-stranded helical structure due to strong base stacking interactions (base stacking interaction strength follows the order purine-purine > purine-pyrimidine > pyrimidine-pyrimidine). dT_{22}, on the other hand, is considered to have a random coil conformation because it does not form intra- and intermolecular base pairs and the stacking interaction is weak. Taking this into account, I hypothesized that such secondary structures of ssDNA may act as a plasmon chirality inducing motif similar to the helical structure of dsDNA.

If this hypothesis is correct, the plasmonic CD of AuNR–ssDNA polyion complexes should disappear due to reduced intramolecular base pairing and stacking interactions. To validate this, I prepared AuNR–DNA polyion complexes consisting of 22 nt ssDNA (A_XC_{22-X}, T_XG_{22-X}, A_XG_{22-X}, T_XC_{22-X}) of 12 different sequences (the subscript indicates the number of bases) (DNA sequences are listed in **Table 2-2**) and 22 bp dsDNA ($A_XC_{22-X}\cdot T_XG_{22-X}$, $A_XG_{22-X}\cdot T_XC_{22-X}$) formed by ssDNA. In this experiment, the X was 6, 11 or 16, and the DNA concentration was set to 0.2 μM. As shown in **Figure 2-10A–C**, the AuNR–dA_XC_{22-X} polyion complexes showed no plasmonic CD regardless of X. On the other hand, the AuNR–dT_XG_{22-X} polyion complexes showed plasmonic CD at X=6, but no plasmonic CD when X was 11 or 16. Similarly, as shown in **Figure 4D–F**, the AuNR–dA_XG_{22-X} polyion complexes showed plasmonic CD and the AuNR–dT_XC_{22-X} polyion complexes showed no plasmonic CD regardless of X. These results support our hypothesis.

It is also important to note here that all the AuNR–dsDNA polyion complexes prepared with these ssDNA showed plasmonic CD **(Figure 2-10)**. Therefore, even if none of the mutually complementary ssDNAs induced plasmonic CD (i.e., even in the combinations of

$C_{11}A_{11}$ and $T_{11}G_{11}$, $C_{16}A_6$ and $T_{16}G_6$, the dsDNA formed by their hybridization was able to render AuNRs optically active. This also supports our notion that the polymer conformation is important for the generation of plasmon CD.

Table 2-2 List of DNA copolymer sequences used to prepare AuNR–DNA polyion complexes.

No.	Type	Sequence (5'→3')
1	**A6C16**	**ACCCCCCCCACCACCAAACCCC**
2	A11C11	ACCAACCCAACCCCCAAAACAA
3	A16C6	AAAAAACACCCCAAAAAACAAA
4	G16T6	GGGGTTTGGTGGTGGGGGGGGT
5	G11T11	TTGTTTTGGGGGTTGGGTTGGT
6	G6T16	TTTGTTTTTTGGGGTGTTTTTT
7	A6G16	AGGGAGAGGAGGAGGGGAGGGG
8	A11TG11	GAGAGAAAGGGAGGGGAAAAAG
9	A16G6	GAGAGAAGAGAAAAAGAAAAAA
10	T6C16	CCCCTCCCCTCCTCCTCTCCCT

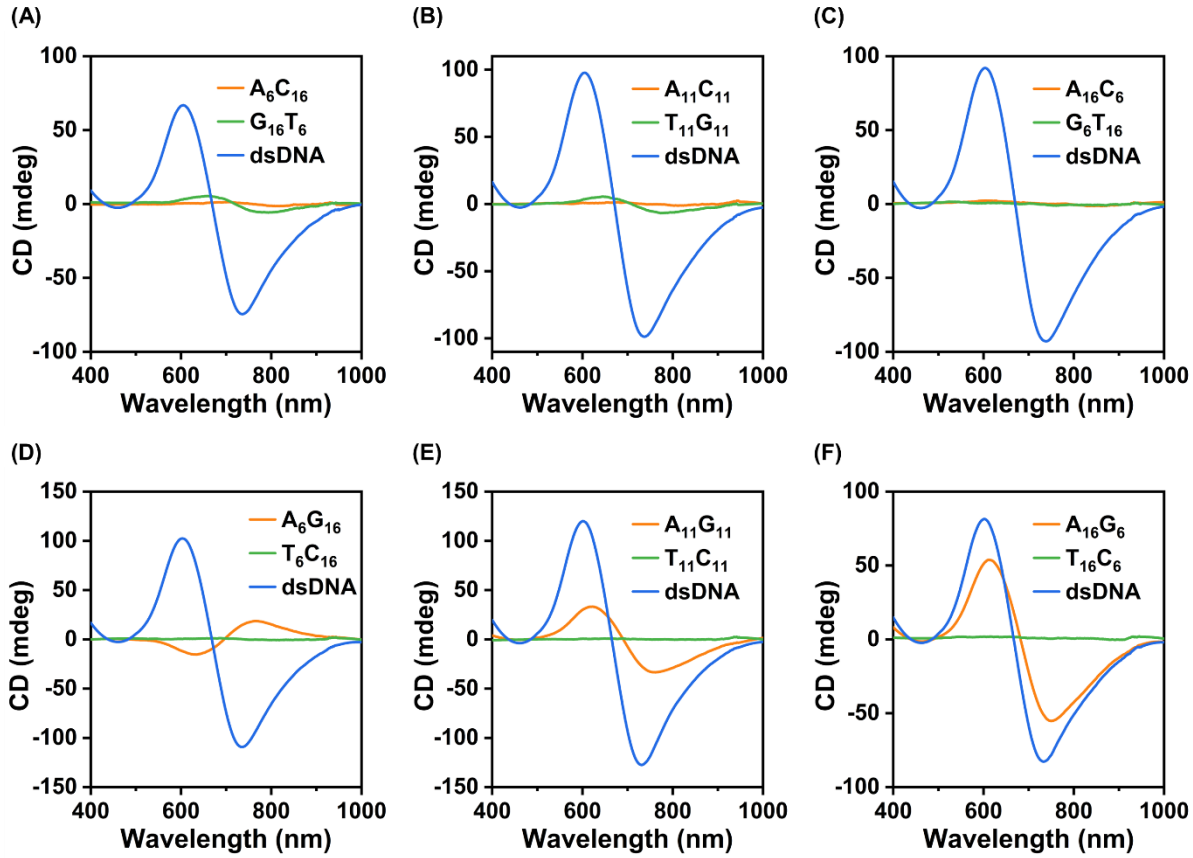

Figure 2-10 CD spectra of AuNR–ssDNA or AuNR–dsDNA polyion complexes prepared at a DNA concentration of 200 nM: (A) AuNR–A_6C_{16}, AuNR–$G_{16}T_6$ and AuNR–A_6C_{16}·$G_{16}T_6$, (B) AuNR–$A_{11}C_{11}$, AuNR–$G_{11}T_{11}$ and AuNR–$A_{11}C_{11}$·$G_{11}T_{11}$, (C) AuNR–$A_{16}C_6$, AuNR–G_6T_{16} and AuNR–$A_{16}C_6$·G_6T_{16}, (D) AuNR–A_6G_{16}, AuNR–$C_{16}T_6$ and AuNR–A_6G_{16}·$C_{16}T_6$, (B) AuNR–$A_{11}G_{11}$, AuNR–$C_{11}T_{11}$ and AuNR–$A_{11}G_{11}$·$C_{11}T_{11}$, (C) AuNR–$A_{16}G_6$, AuNR–C_6T_{16} and AuNR–$A_{16}G_6$·C_6T_{16} polyion cpmplxes.

2.4.4 Plasmonic CD of AuNR–L- or L-/D-DNA polyion complexes

To gain more insight into the plasmonic CD of AuNR–DNA polyion complexes, I used L-form (unnatural form) DNA. As expected from previous studies, the AuNR–L-DNA polyion complexes exhibited a CD spectrum with mirror-image symmetry with respect to the case using D-DNA **(Figure 2-11A)**. Almost no plasmonic CD was observed when the racemic mixtures were used **(Figure 2-11A)**, indicating that AuNR–L-DNA and AuNR–D-DNA may show the twists in opposite directions. To investigate the effect of duplex formation, I prepared AuNR–DNA polyion complexes using an equal mixture of L-form ssDNA-1 (L1) and L-form ssDNA-2 (L2). As shown in **(Figure 2-11B)**, the AuNR–DNA polyion complexes exhibited a positive couplet plasmonic CD, in contrast to the case using both D-form ssDNA (D-form ssDNA-1 (D1) and D-form ssDNA-2 (D2)). I further prepared AuNR–D-/L-DNA polyion complexes using enantiomeric combinations of ssDNA. Because D-DNA and L-DNA are chiral enantiomers, their sequences cannot complement each other to form a double-stranded structure. As shown in **Figure 2-11C**, the AuNR–D1/L2 polyion complexes exhibit plasmonic CD which is almost same as AuNR–D1 polyion complexes **(Figure 2-11D)**. The slight enhancement of the CD signal may be caused by the electrostatic interaction between L2 and AuNRs promoting side-by-side aggregation of AuNRs. Similarly, the AuNR–L1/D2 polyion complexes exhibit plasmonic CD which is almost same as AuNR–L1 polyion complexes. These results confirm that the chiral geometry in AuNR–DNA polyion complexes is the origin of the plasmonic chirality..

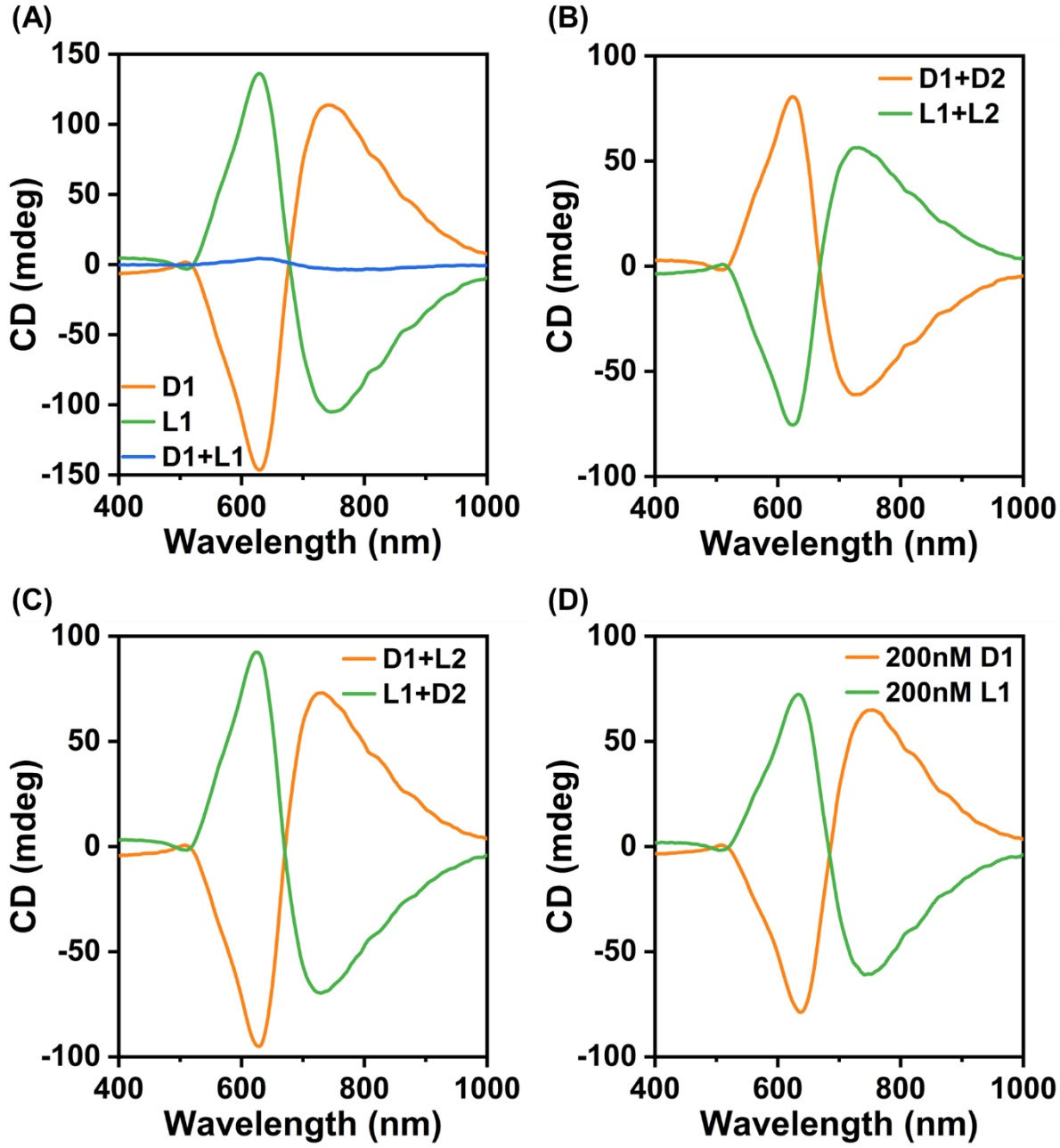

Figure 2-11 The CD spectra of AuNR–DNA polyion complexes. (A) the AuNR–D1 (D-ssDNA1: 400 nM), the AuNR–L1 (L-ssDNA1: 400 nM) and the AuNR–D1+L1 (mixture: 200 nM D-ssDNA1 and 200nM L-ssDNA1); (B) AuNR–D1+D2 (mixture: 200 nM D-ssDNA1and 200nM D-ssDNA2) and AuNR–L1+L2 (mixture: 200 nM L-ssDNA1and 200nM L-ssDNA2); (C) AuNR–D1+L2 (mixture: 200 nM D-ssDNA1and 200nM L-ssDNA2) and AuNR–L1+D2 (mixture: 200 nM L-ssDNA1and 200nM D-ssDNA2); (D) the AuNR–D1 (D-ssDNA1: 200 nM), the AuNR–L1 (L-ssDNA1: 200 nM).

2.4.5 Chiral geometric features of AuNR–DNA polyion complexes

To gain insight into this unusual chirality inversion phenomena, I performed Cryo-TEM observation of the AuNR–poly(dA22) polyion complexes. **Figure 2-12A-C** showd the 3D reconstruction images by Amira software and the **Figure 2-12D** showed the Cryo-TEM tomography reconstruction images by computer. It can be seen from Figures 2-12C and D that the reconstructed image has great similarity, so it could be reconstructed and characterized by Amira software. At the same time, it could also prove the the AuNRs were assembled with side-by-side manner. Next, I select the AuNRs assemblies with a gap less than 5 nm (22 base ssDNA: Width $\approx$ 1-2 nm, Amino-EG6-undecanethiol: Length $\approx$ 4.14 nm) to calculate their dihedral angles. Surprisedly, the statistical analysis of the dihedral angles (φ) for AuNRs from tomographic images by Amira software showed that most of the dihedral angles fall within the 0-10° range, indicating a strong preference for small twist angles, which is contributed to the overall chiral geometry of the assembly **(Figure 2-12E)**. Furthermore, the distribution of twist directions (88.6% positive and 11.4% negative) demonstrates a significant bias towards a right-handed twist in the AuNR assemblies **(Figure 2-12F)**. The overwhelming preference for a positive twist direction further supports the chiral nature of the AuNR–dA_{22} complexes, indicating that the assembly process favors the formation of right-handed helices. Simulation of the plasmon CD signals of these assemblies yielded CD spectra with signs consistent with the experimental results **(Figure 2-12G and H)**. These results supported that AuNR–dA_{22} complexes exhibit strong chiral characteristics, with a marked preference for right-handed twisting.

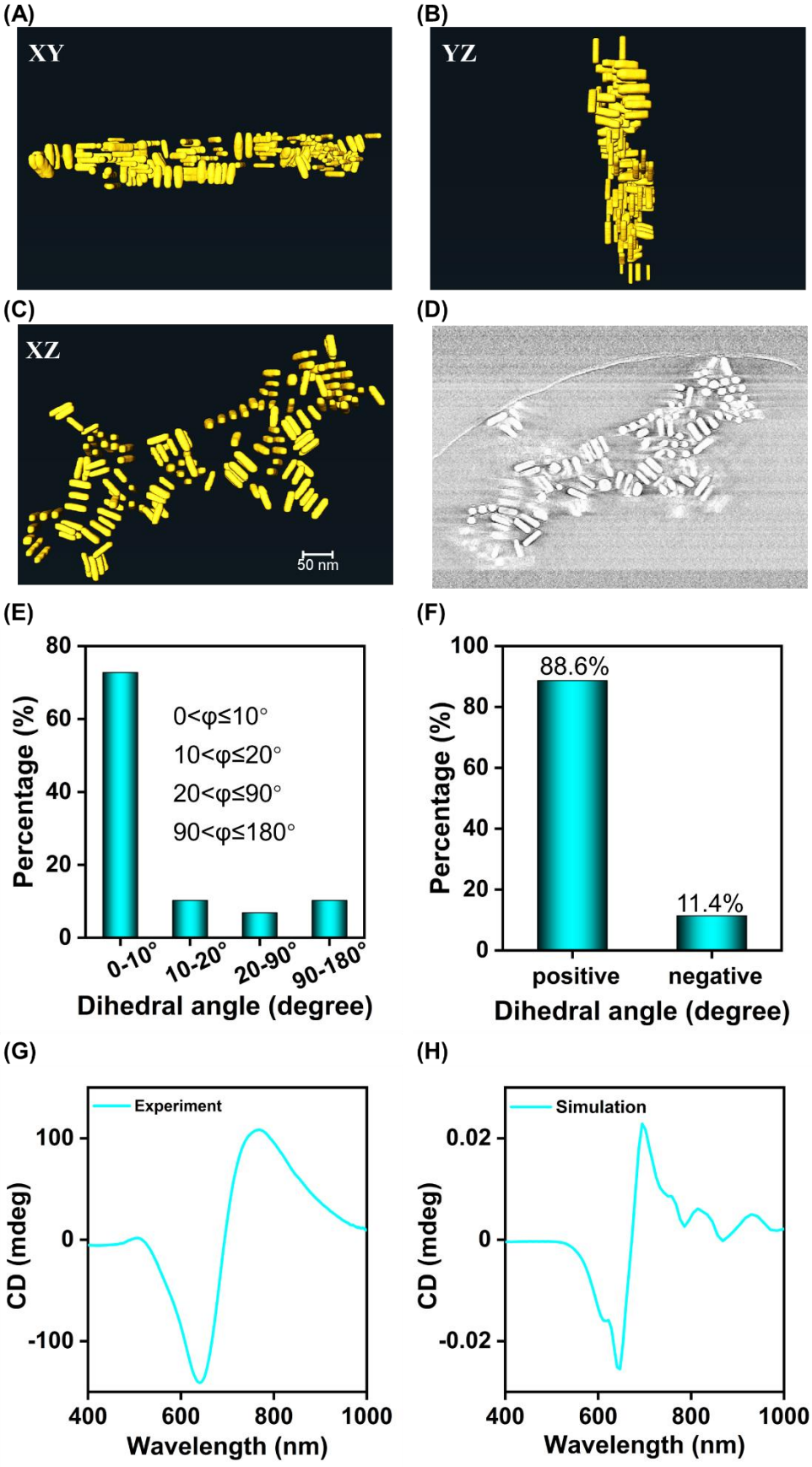

Figure 2-12 Chiral geometry of the AuNR–dA_{22} polyion complexes. (A-C) Amira software reconstructs

images: (A) XY view, (B) YZ view, (C) XZ view. The scale bar represents 50 nm. (D) Cryo-TEM tomography reconstruction images by computer. (E) Statistical analysis of the dihedral angles φ for AuNRs from cryo-TEM tomography images. (F) The percentage of twist direction of the AuNR assemblies (positive: right-handed; negative: left-handed). (G) Experimental CD spectra of AuNRs assemblies (poly(dA_{22}): 150 nM). (H) Simulated CD spectra of AuNRs assemblies by FDTD. (The model was imported from Amira software.

2.4.6 Plasmonic CD of AuNR–(Noncomplementary)DNA polyion complexes

To further understand the relationship between DNA and plasmonic CD in AuNR–DNA polyion complex, I investigated the plasmonic CD of polyion complexes formed by AuNRs and noncomplementary ssDNA. Based on the experimental results shown in **Figure 2-13**, it was suggested that the plasmonic CD intensity of AuNR–dA_{22} assemblies was enhanced more than five-fold with the addition of dG_{22} than dA_{22} alone and the plasmonic CD intensity of AuNR–dG_{22} assemblies was also enhanced with the addition of dT_{22} than dG_{22} alone. While the addition of dA_{22} with dC_{22} caused significant decrease in plasmonic CD intensity. And there was still no plasmonic CD when mixing dC_{22} with dT_{22}, because AuNR–dC_{22} and AuNR–dT_{22} polyion complex didn't show any plasmonic CD at that DNA concentration. These CD spectra reveal the chiral properties of different DNA sequence combinations in AuNR–DNA polyion complex. This suggests that interactions between specific DNA sequences can significantly alter their optical properties, paving the way for the application of AuNR–DNA polyion complex in chiral materials and chiral catalysis.

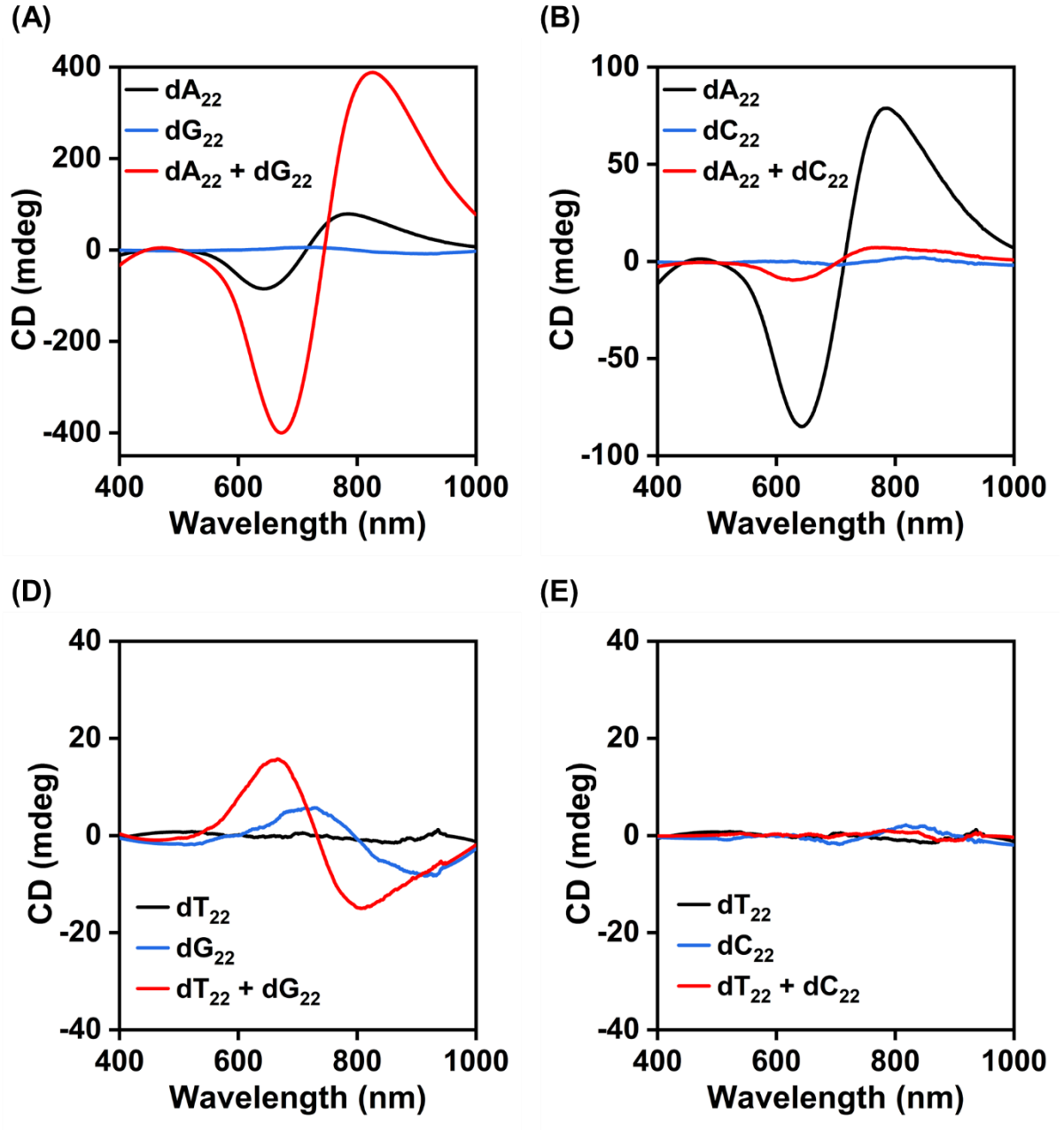

Figure 2-13 CD spectra and photographs of the AuNRs assemblies with DNA. (A) 100 nM dA_{22}, 100 nM dG_{22} and 100 nM dA_{22} with 100 nM dG_{22}. (B) 100 nM dA_{22}, 100 nM dC_{22} and 100 nM dA_{22} with 100 nM dC_{22}. (C) 100 nM dT_{22}, 100 nM dG_{22} and 100 nM dT_{22} with 100 nM dG_{22}. (D) 100 nM dT_{22}, 100 nM dC_{22} and 100 nM dT_{22} with 100 nM dC_{22}.

2.5 Conclusion

In conclusion, I investigated the plasmonic chirality in AuNR–DNA polyion complexes and elucidated the relationship between DNA structures and plasmonic CD. Specifically, I found that the intensity and sign of the plasmonic CD signals can be controlled by altering the DNA sequence or adjusting the ratio of DNA to AuNRs. This result supported the hypothesis that DNA with strong base pairing and stacking interactions can induce plasmonic CD in DNA-induced chiral AuNR assemblies, while DNA with weak base stacking interactions cannot. Furthermore, the chiral geometry was the origin of plasmonic CD in AuNR–DNA polyion complexes. The plasmonic CD in AuNR–DNA polyion complexes disappeared when L-DNA1 and D-DNA1 were added, while not disappeared when D-DNA1 and L-DNA2 were added. The observation by cryo-TEM also showed the twisted structure in AuNR–dA_{22} polyion complexes. This research advances the detailed understanding of DNA structure-plasmonic CD relationship in AuNR–DNA polyion complexes, Hence, I hope that this study will pave the way for deeper explorations into the origin of plasmonic CD and expanding the potential applications of such complexes, especially in chiral sensing.

Chapter 3

Plasmonic circular dichroism-based metal ion detection using gold nanorod–DNA complexes

3.1 Abstract

I report that complexes formed between gold nanorods (AuNRs) and metal-mediated DNA exhibit plasmonic circular dichroism (CD) signals up to ~400 times stronger than the molecular CD signal of DNA. This substantial enhancement enables the detection of metal ions, offering a promising approach to analytical applications in chiral biochemistry.

3.2 Introduction

DNA has several advantages that make it an excellent biosensing probe.[100-102] First, by designing the base sequence, DNA can recognize various target substance such as metal ions,[103] small molecules[104, 105] and proteins.[106] Second, DNA can undergo conformational changes upon recognition of a target substance.[107] By taking advantage of these features, a variety of methods have been developed for the detection of target substances.[100-102] For example, the analyte-triggered DNA conformational change can be converted into an optical or electrical signal by modification with fluorophores[108] or electroactive moieties.[109] Plasmonic nanoparticles, such as gold nanoparticles, are also a powerful tool for converting DNA conformational changes into an optical signal.[110] Due to localized surface plasmon resonance (LSPR), plasmonic nanoparticles exhibit a color change in accordance with the distance between the particles.[111] This color change can be triggered by probe DNA on the particle surface for detection of target substances.[112] In addition, as DNA is a chiral molecule, its conformational changes can be directly detected with a circular dichroism (CD) spectrometer,[82] although CD spectroscopy suffers from low detection sensitivity. For example, for a 20-base pair double-stranded (ds)DNA, a high sample concentration of ~2 μM is required to obtain a CD signal.[82] Thus, CD spectroscopy has not been widely used for DNA-based biosensors. Induced plasmonic chirality, a phenomenon in which an achiral plasmonic nanostructure becomes optically active in response to chiral molecules,[113, 114] may help overcome this shortcoming. It is known that plasmonic CD is induced by dipoledipole interactions between chiral adsorbates and plasmon nanostructures and/or by the chiral assembly of plasmonic nanoparticles.[114] One notable aspect of this phenomenon is that the intensity of the plasmonic CD is much higher than that of the

molecular CD.[13, 115-117] For example, Kneer et al. sandwiched a DNA origami sheet between two gold nanorods (AuNRs) and demonstrated the emergence of plasmonic CD signals ~300 times more intense than that of the DNA origami.[13] Chiral selfassemblies of AuNRs induced by helical polymers showed a strong CD response in the vis–NIR region.[46] Serum albumin and AuNR complexes provided strong plasmonic CD[42, 85, 114, 118] and chiral assemblies of AuNRs as revealed by cryo-transmission electron microscopy (TEM).[114] However, the relationship between the protein structure and plasmonic CD of AuNR–protein complexes remains unclear due to the complex protein structures.[85] Based on our previous studies of plasmonic AuNR–DNA complexes,[89-92] DNA can be utilized as an ideal molecule for the construction of nanoparticle-molecule complexes to induce plasmonic CD, owing to the clearer structural information. By leveraging these attributes, not only are the potential applications of such complexes expanded in terms of chiral sensing, but it also paves the way for deeper explorations into chiroptical mechanisms in nanoparticle-molecule complexes.

Although the molecular structure required to induce plasmonic chirality remains controversial, a common feature of many of these molecules is a helical structure.[13, 42, 46, 51, 85, 91, 113-115, 118, 119] It is well known that Hg^{2+}, which is highly toxic to the human body, mediates thymine mismatching and forms thymine–Hg^{2+}– thymine (T–Hg^{II} –T) complexes.[120, 121] Thus, single-stranded (ss)DNA can be hybridized to form dsDNA (helical structure) in the presence of Hg^{2+}. Additionally, thymine-rich ssDNA adopts a random coil structure (non-helical structure) due to weak base pair stacking interactions.[75] Based on this insight, in this study, I demonstrate that the plasmonic CD induced by AuNR–DNA complexes can be used for metal ion detection **(Scheme 3-1)**.

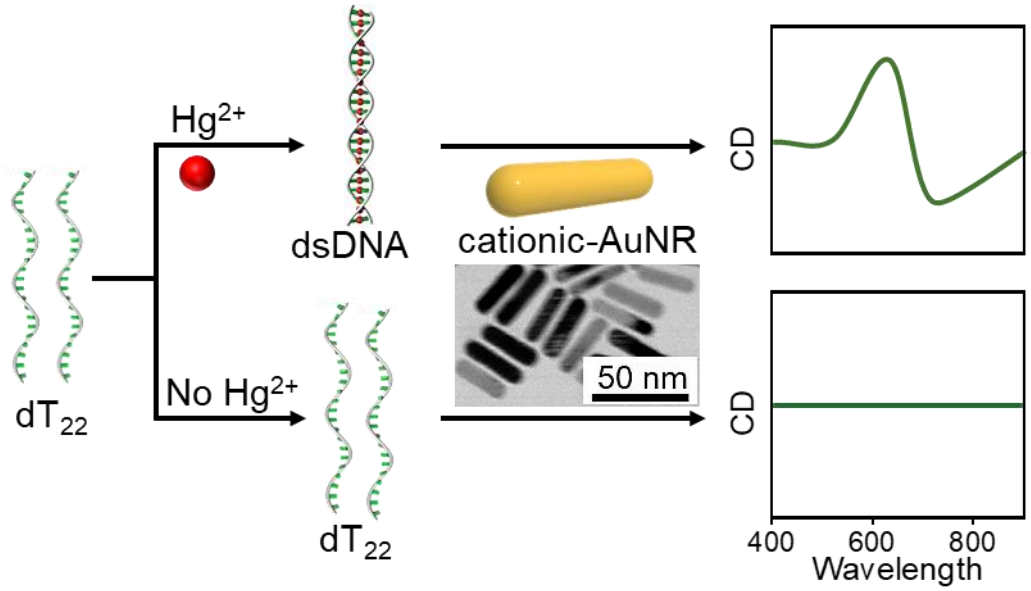

Scheme 3-1 Schematic illustration of this study. The AuNR–DNA complexes, showing plasmonic CD signals based on DNA conformational changes from random coil to helix, can be used for the detection of Hg^{2+}.

3.3 Experimental Section

3.3.1 Materials and Instruments

20-(11-Mercaptoundecanyloxy)-3, 6, 9, 12, 15, 18-hexaoxaeicosane-1-amine (cationic ligand) hydrochloride was purchased from Dojindo Laboratories (Japan). Oligodeoxynucleotides (ODNs) were purchased from Thermo Fisher Scientific Inc. (USA). SYBR Green I was purchased from Lonza (Rockland, MD, USA). Metal standard solutions (Hg^{2+} and Ag^{+}, Cr^{6+}, Cu^{2+}, Fe^{3+}, Zn^{2+}) were purchased from FUJIFILM Wako Pure Chemical Co., Ltd (Japan). Extinction spectra were measured with a V-770 UV-vis spectrometer (JASCO Corp., Japan). Dynamic light scattering (DLS) profiles were obtained with a Zetasizer Nano ZS system (Malvern Panalytical, UK). The fluorescence images were captured using the Printgraph CMOS I (ATTO Corporation, Japan). Circular dichroism (CD) measurements were conducted with a J-820 spectrometer (JASCO Corp., Japan). Scanning transmission electron microscopic (STEM) images were obtained using a STEM HD-2000 system (Hitachi High-Tech Manufacturing & Service Co., Ltd., Japan) with a 200 kV acceleration voltage.

3.3.2 Synthesis of gold nanorods (AuNRs)

AuNRs with a diameter of ~10 nm and a length of ~40 nm were synthesized according to the seed growth method.[98] (1) Preparation of seed solution: a gold seed solution was prepared in a 50 mL plastic tube by adding an ice-cold $NaBH_4$ solution (600 μL, 0.01 M) to a mixture of a $HAuCl_4 \cdot 3H_2O$ solution (250 μL, 0.01 M) and a CTAB solution (7.5 mL, 0.1 M) under gentle shaking. The seed solution was then kept in an incubator (30°C) for at least 2 h. (2) Growth reaction: growth solutions were prepared in 100 mL plastic tubes by sequentially adding $HAuCl_4 \cdot 3H2O$ solution (400 μL, 0.01 M), $AgNO_3$ solution (240 μL, 0.01 M) and an ascorbic solution (64 μL, 0.1 M) to a CTAB solution (40 mL, 0.1 M). The gold seed solutions (96 μL) were injected into the growth solutions (40 mL) while the growth solution was shaken gently. The growth solutions were then left undisturbed in an incubator (30°C) for at least 3 h. (3) Purification: the prepared AuNRs solutions were transferred to 1.5 mL plastic tubes and

divided into 1000 mL portions. The AuNRs were sedimented by centrifugation (18,000 g, 20 min, 30°C), and the supernatant (900 μL) was removed. The plastic tubes were then filled with Milli-Q water (900 μL) and vortexed. This centrifugal purification procedure was repeated twice so that all chemicals except for the AuNRs were diluted 100-fold.

3.3.3 Surface modification of AuNRs with cationic ligands

Methanol solutions of the cationic ligand(20-(11-Mercaptoundecanyloxy)-3, 6, 9, 12, 15, 18- hexaoxaeicosane-1-amine, hydrochloride) (10 mM) were prepared. The ligand solution (10 mM, 35 μL) was added to the purified AuNRs solution (1000 μL) in a 1.5 mL plastic tube. The AuNRs solution containing the ligands was vortexed and kept undisturbed at 42°C for at least 12 h. Then, the solution was centrifuged (18 000 g, 20 min, 30°C), the supernatant (900 μL) was removed, and Milli-Q water (900 μL) was added to the residue solution. This centrifugal purification was performed twice to remove free ligands from the AuNRs solution. Finally, the concentration of the ligand modified AuNRs was adjusted to the desired concentration by centrifugal concentration.

3.3.4 Preparation of AuNR–DNA polyion complexes

In a typical procedure, Tris-HCl buffer solution (20 μL, 100 mM, pH=7.6), Milli-Q water (53.6 μL), and Hg^{2+} solution (26.4 μL, 50 μM) were added to a 1.5 mL plastic tube. ssDNA was then added to this mixture and vortexed. Finally, cationic ligand-modified AuNRs (70 μL, 45.7 nM) were added and vortexed again to prepare AuNR–DNA complexes.

3.3.5 Fluorescence measurement of SYBR Green I (SG)

In a typical procedure, Tris-HCl buffer solution (20 μL, 100 mM, pH=7.6), Milli-Q water (119.6 μL), metal ion solution (Hg^{2+}, Ag^{+}, Cr^{6+}, Cu^{2+}, Fe^{3+} and Zn^{2+}) (26.4 μL, 50 μM), DNA (30 μL, 4 μM), and SG (4 μL, 100×) were mixed in a 1.5 mL plastic tube and vortexed. Then, each solution was transferred to a quartz cuvette with an optical path length of 1 mm. Finally, the fluorescence intensity of each solution was measured with a Printgraph CMOS I system.

The measurement conditions were as follows, filter: cyan, iris: 19, zoom: 0, focus: 3, and time: 4 sec.

3.3.6 Circular Dichroism (CD) measurement

Each of the samples was transferred to a quartz cuvette with an optical path length of 1 mm. The quartz cuvettes were set in a CD spectrometer, and the CD spectra were collected. The measurement conditions were as follow, scan speed: 200 nm/min, response: 1 msec, bandwidth: 15 nm, and scans: 2. All of the CD spectra were smoothed using a 50-point Savitzky-Golay algorithm.

3.4 Results and Discussion

3.4.1 The formation of dT_{22} helix by Hg^{2+}

First, I confirmed the structural changes in dT_{22} (sequence: 5'-TTTTTTTTTTTTTTTTTTTTTT-3') through recognition of Hg^{2+}. I used Tris-HCl solutions for all experiments in this study. I measured the fluorescence intensity of a mixture of dT_{22} (final concentration = 0.6 μM) and SYBR Green I (SG) containing Hg^{2+} and other metal ions (Ag^{+}, Cr^{6+}, Cu^{2+}, Fe^{3+}, and Zn^{2+}). Note that the concentration of metal ions was set to the minimum amount (6.6 μM) required for Hg^{2+} to mediate all of the thymine mismatches. SG stains dsDNA more efficiently than ssDNA;[122] therefore, by comparing fluorescence intensities, it is possible to confirm whether dT_{22} adopts a ss or ds conformation. As expected, the fluorescence intensity of SG with Hg^{2+} was significantly greater than that for other metal ions or blank samples without Hg^{2+} **(Figure 3-1)**. These results confirmed the ds formation of dT_{22} by Hg^{2+} even under our experimental conditions.

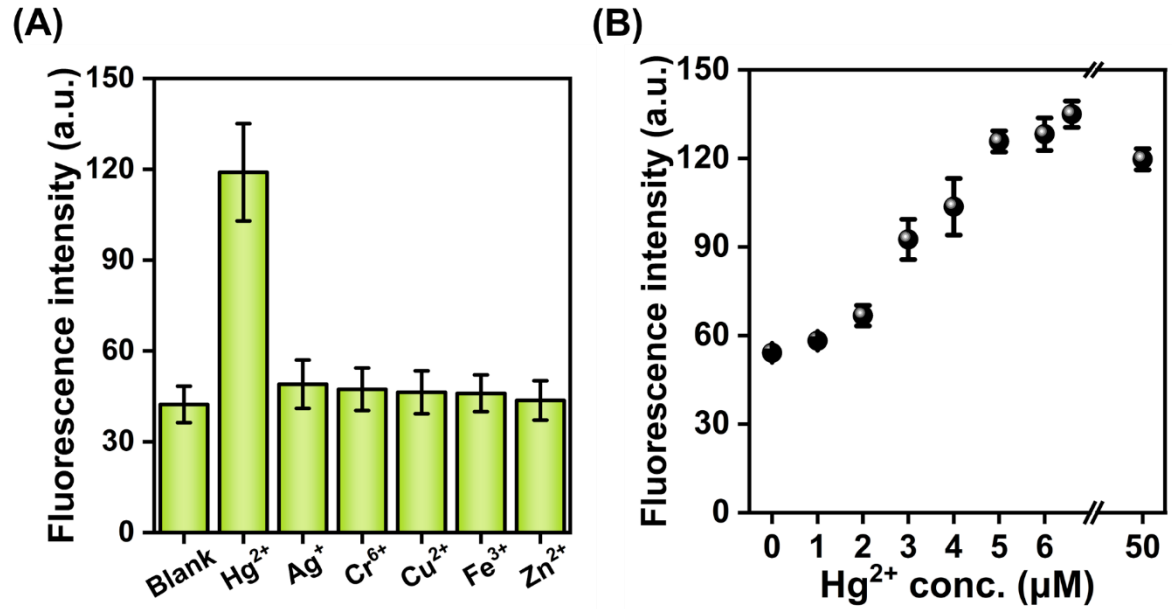

Figure 3-1 (A) The fluorescence intensity of a mixture of dT_{22} and SG containing Hg^{2+} and other metal ions (Ag^{+}, Cr^{6+}, Cu^{2+}, Fe^{3+}, and Zn^{2+}). (B) Plots of the fluorescence intensity versus Hg^{2+} concentration. Error bars represent standard deviation (n = 3).

3.4.2 The formation of AuNR–dT_{22} complexes

Next, I investigated the formation of DNA complexes with AuNRs via electrostatic interactions. I prepared cationic AuNRs (size: ~40 nm × ~10 nm, zeta potential: +13.8 mV, final concentration = 16 nM) by the surface exchange of cetyltrimethylammonium bromide (CTAB)-covered AuNRs with primary amine-terminated hexaethylene glycol thiol ligands, to make them both more stable and controllable. Then, the cationic AuNRs were added into the Tris-HCl buffer solution containing dT_{22} to form AuNR–DNA complexes. Dynamic light scattering (DLS) was used to characterize the complexes. As shown in **Figure 3-2A**, AuNR alone showed DLS peaks at ~1 nm and ~39 nm. The former results from rotational motion and the latter results from translational motion.[123] The mixture of AuNRs and dT_{22} showed a DLS peak at ~150 nm, indicating complex formation. The position of this peak was almost completely independent of the Hg^{2+} concentration. I then measured the extinction spectra of AuNR alone and the AuNR–dT_{22} complexes **(Figure 3-2B)**. AuNR alone showed a transverse (T)-LSPR peak at ~510 nm and a longitudinal (L)-LSPR peak at ~760 nm. In contrast, AuNR–dT_{22} complexes exhibited a T-LSPR peak around ~530 nm and a L-LSPR peak around ~660 nm, regardless of the presence or absence of Hg^{2+}. The shift in the L-LSPR peak to a shorter wavelength indicates that the AuNRs assembled in a side-by-side manner.[124, 125] This was also supported by scanning transmission electron microscopy (STEM) imaging **(Figure 3-2C, D)**. The above DLS and extinction spectra results demonstrated the successful formation of AuNR–DNA complexes.

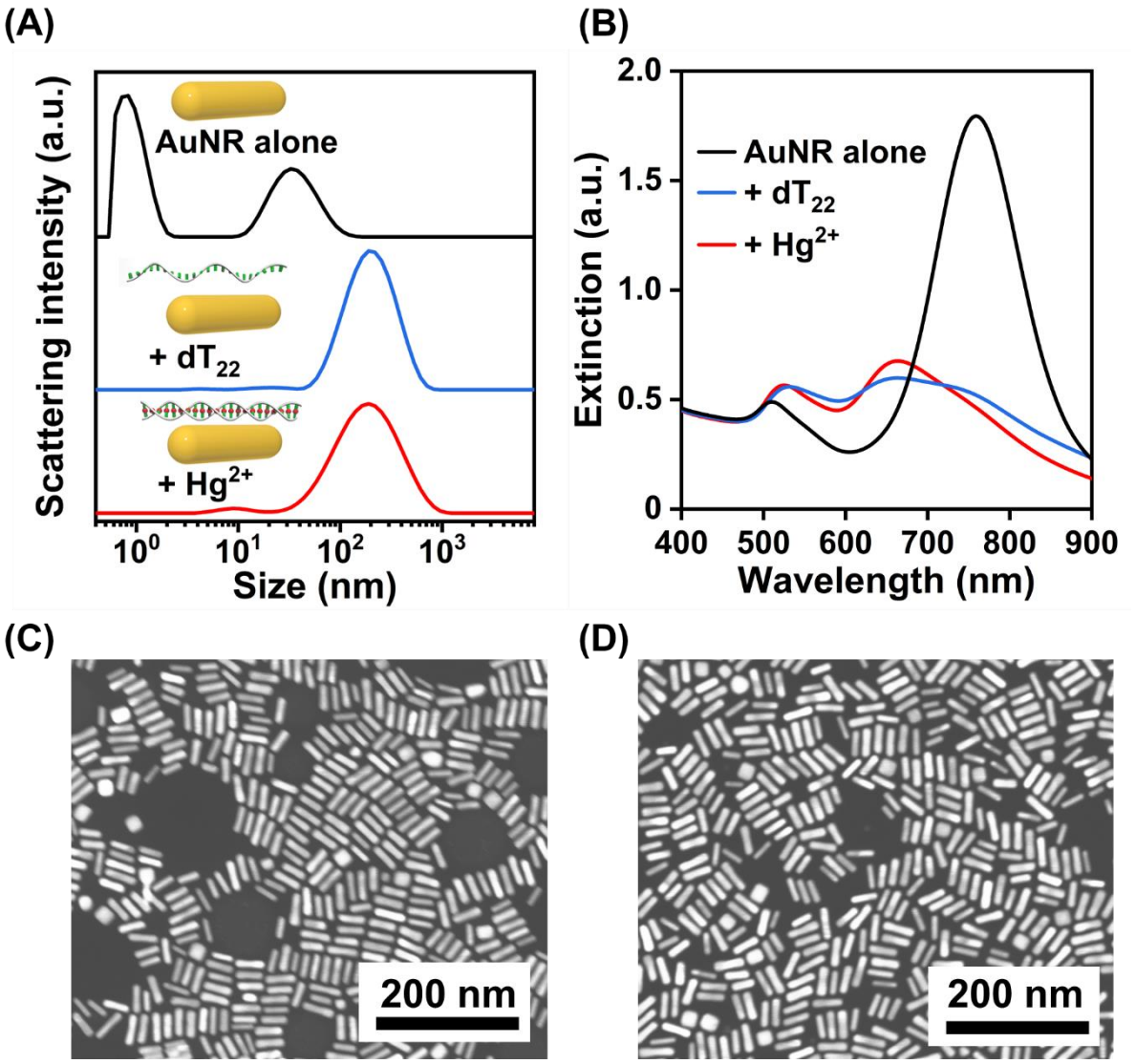

Figure 3-2 (A) DLS profiles of AuNR alone (black line) and AuNR–dT_{22} complexes prepared in the absence (blue line) or presence (red line) of Hg^{2+}. (B) Extinction spectra of AuNR alone (black line), and AuNR–dT_{22} complexes prepared in the absence (blue line) or presence (red line) of Hg^{2+}. (C, D) Typical STEM images of the AuNR–dT_{22} complexes prepared in the absence (C) and presence (D) of Hg^{2+}. (AuNRs: 16 nM; dT_{22}: 0.6 μM; Hg^{2+}: 6.6 μM).

3.4.3 The CD of AuNR–dT_{22} complex

Although the size and morphology of the AuNRs assemblies did not differ markedly (Figure 3-2), there was a clear difference between the optical activities of the AuNR–dT_{22} complexes with and without Hg^{2+}. **Figure 3-3A** shows their CD spectra. Note that all CD spectra shown in this work have been smoothed using the Savitzky–Golay method **(Figure 3-4)**.[123] In the absence of Hg^{2+}, neither AuNR alone nor the AuNR–dT_{22} complexes showed plasmonic CD in the visible region **(Figure 3-3A)**. In contrast, the AuNR–dT_{22} complexes with Hg^{2+} showed negative couplet CD with a dip at ~720 nm and a peak at ~620 nm. In the UV region, the AuNR–dT_{22} complexes with Hg^{2+} exhibit similar but distinct CD characteristics to those without AuNRs in the same region due to the large electromagnetic field near the Hg^{2+}-mediated DNA.[68] Indeed, similar results were observed in the AuNR–dsDNA complexes in which dsDNA was formed by dT_{22} and dA_{22} (sequence: 5'-AAAAAAAAAAAAAAAAAAAAA-3') **(Figure 3-5A)**.

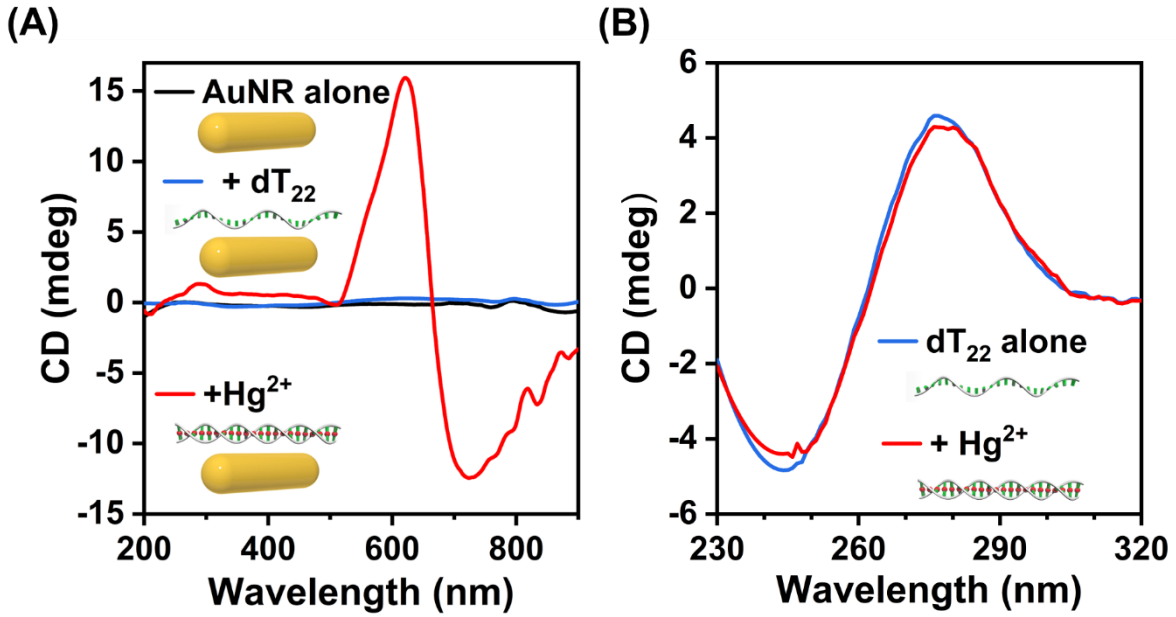

Figure 3-3 CD spectra for (A) 16 nM AuNR alone (black line), AuNR and 0.6 μM dT_{22} complexes (blue line), AuNR and dT_{22} complexes with 6.6 μM Hg^{2+} (red line), (B) 20 μM dT_{22} alone (blue line) and with 220 μM Hg^{2+} (red line).

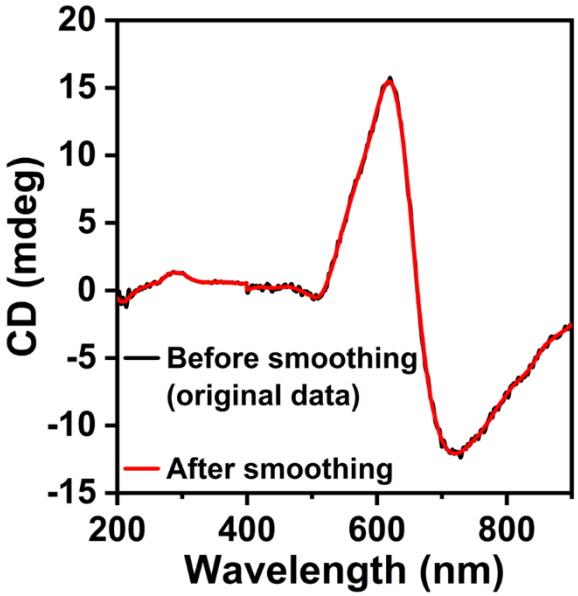

Figure 3-4 Typical CD spectra for AuNR–dT_{22} complexes, prepared in the presence of Hg^{2+}, before and after Savitzky–Golay smoothening.

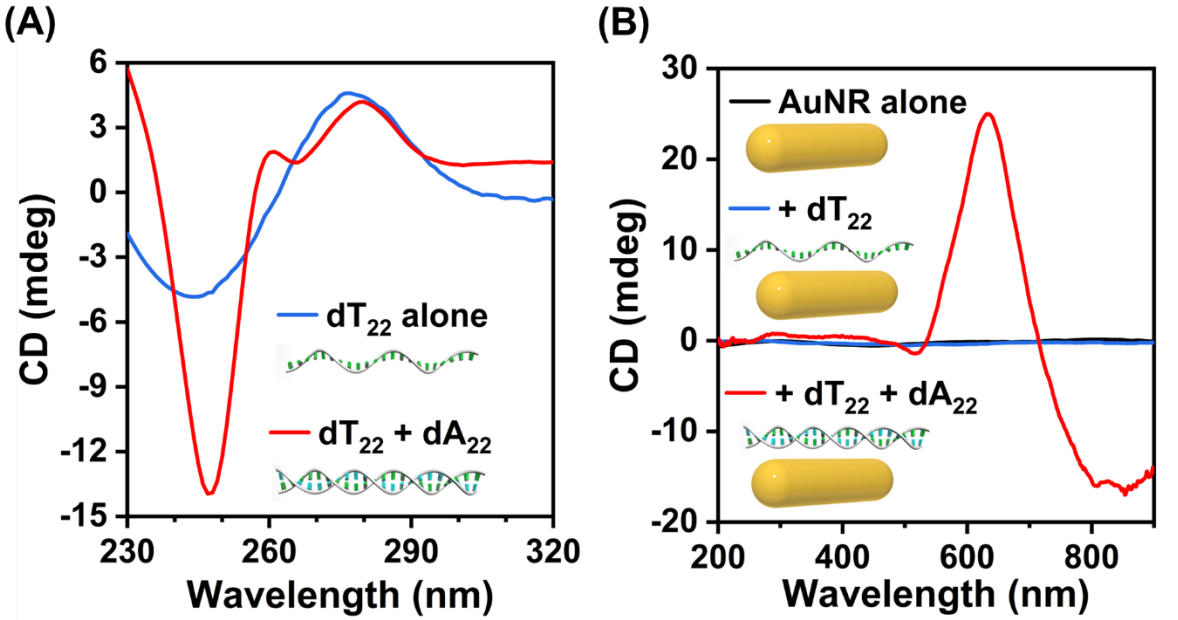

Figure 3-5 CD spectra for (A) AuNR alone (black line), AuNRs and 0.6 μM dT_{22} complexes (blue line), AuNRs and 0.3μM dT_{22} complexes with 0.3μM dA_{22} (red line), (B) 20 μM dT_{22} alone (blue line) and 10 μM dT_{22} with 10 μM dA_{22} (red line).

Here we emphasize three important characteristics. First, the plasmonic CD was much larger than the molecular CD of the DNA in the UV region (the plasmonic CD was detected even though the DNA was below the detection limit). To quantitatively

compare the plasmonic CD with the CD of the DNA, we used the following equation:[115, 117]

$$A_{CD} = \frac{\Delta CD_{(plasmon)}/c_{(DNA)}}{\Delta CD_{(DNA)}/c_{0(DNA)}}$$

where A_{CD} is the enhancement factor, $\Delta CD_{(plasmon)}$ is the difference between the peak and dip values of the plasmonic CD signal, $c_{(DNA)}$ is the concentration of DNA in the AuNR–DNA complexes solution, $\Delta CD_{(DNA)}$ is the difference between the peak and dip values of the molecular CD signal of DNA alone, and $c_{0(DNA)}$ is the concentration of the DNA alone. As a result, the A_{CD} from AuNR–dT_{22} complexes at a Hg^{2+} concentration of 6.6 μM was calculated to be 97, indicating a significant advantage in terms of detection. Second, a clear change in plasmonic CD in the visible region was observed even with a low Hg^{2+} concentration **(Figure 3-3A)**, although the molecular CD of dT_{22} was almost unchanged with Hg^{2+} **(Figure 3-3B)**. However, dsDNA formation with dA_{22} caused a clear change in molecular CD **(Figure 3-5B)**. Third, compared with SG fluoresce method **(Figure 3-1)**, no strong background signal was observed in this system **(Figure 3-3A)**. These results suggest that the AuNR–DNA complexes not only enhance the CD signal intensity of DNA but also recognize conformational changes in metal-mediated DNA, as a plasmonic CD signal, with greater sensitivity; thereby demonstrating their potential applications in metal ion detection

3.4.4 The performance of AuNR–dT_{22} complex in Hg^{2+} detection

In order to test the analytical performance with regard to metal ion detection using the AuNR–DNA complexes, the plasmonic chiroptical activities of the AuNR–dT_{22} complexes were recorded upon addition of Hg^{2+} at different concentrations **(Figure 3-6A)**. Even when the Hg^{2+} concentration was changed, the zero-crossing (~670 nm) and peak (~610 nm) positions remained nearly identical. In addition, as shown in **Figure 3-7**, the zero-crossing and the L-LSPR peak were well matched. **Figure 3-6B** plots the $\Delta CD_{(plasmon)}$ versus Hg^{2+} concentration, which shows that the plasmonic CD began to be detected around the Hg^{2+} concentration of 2 μM. This is consistent with the Hg^{2+} concentration at which dT_{22} began to form double strands **(Figure 3-1B)**. When the concentration of Hg^{2+} was over 6.6 μM, ΔCD reached its largest

value (~25 mdeg). The saturation may be explained by the fact that the ss dT_{22} was completely consumed in the presence of 6.6 μM of Hg^{2+}. It is also worth noting that the plasmonic CD signal in our system did not decrease, as in the fluorescence method, in the presence of high Hg^{2+} concentrations (Figure 3-1), indicating its good stability with regard to Hg^{2+} detection. I also tested the plasmonic CD responses to the other potential interfering compounds, including Ag^{+}, Cr^{6+}, Cu^{2+}, Fe^{3+}, and Zn^{2+}, under the same reaction conditions. Interestingly, except for Hg^{2+} with high reproducibility **(Figure 3-8)**, no obvious plasmonic CD signal was obtained in the presence of the other interfering ions (6.6 μM) in the sensing systems, indicating good selectivity toward Hg^{2+} **(Figure 3-6B)**. These results indicated that the AuNR–DNA complex system shows good analytical performance with regard to metal ions.

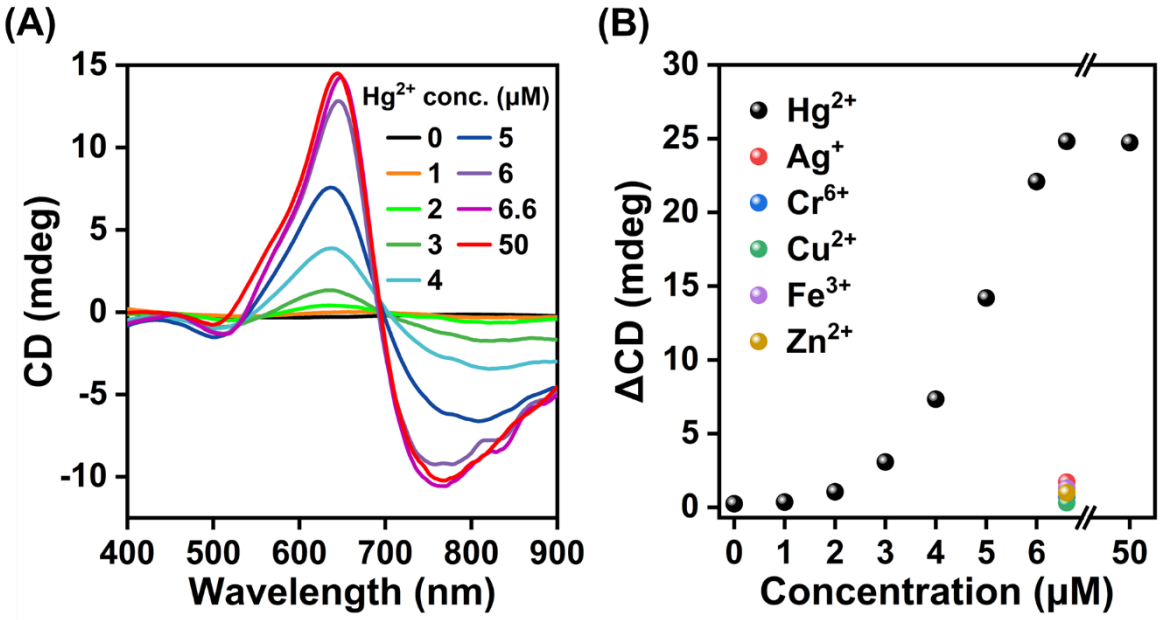

Figure 3-6 (A) CD spectra for AuNR–dT_{22} complexes prepared at different concentrations of Hg^{2+}. (B) Plots of ΔCD versus Hg^{2+} or other metal ion concentrations (6.6 μM).

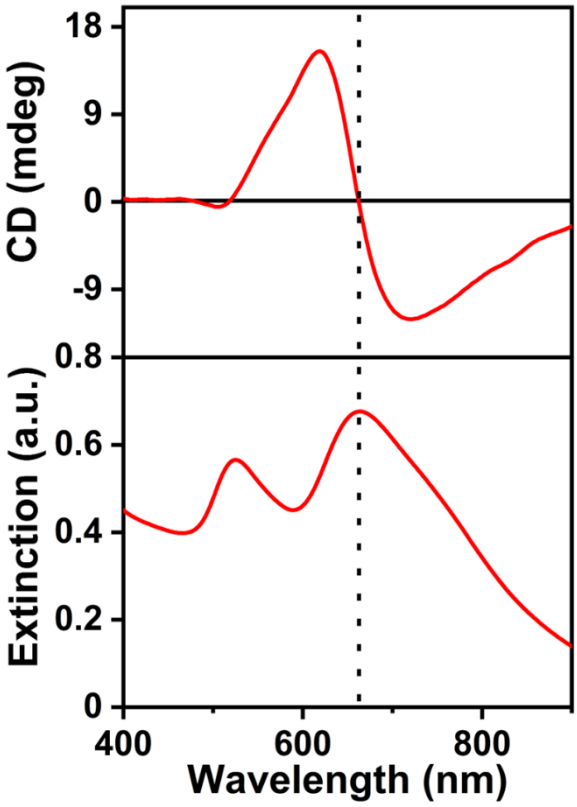

Figure 3-7 The CD and extinction spectra for AuNR–dT_{22} complexes with Hg^{2+} (6.6 μM).

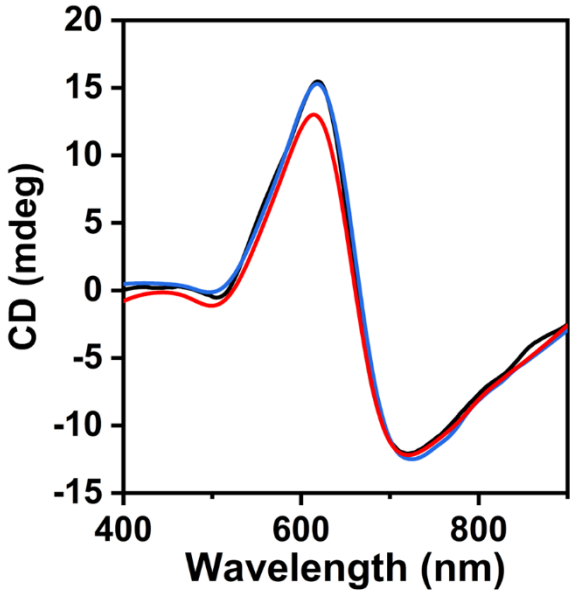

Figure 3-8 Under the same condition, experiments were conducted on three different samples of AuNR–dT_{22} complex with 6.6 μM Hg^{2+} to check the reproducibility. The mean ΔCD intensity is 26.9±1.4 (n=3).

3.4.5 The CD of AuNR–dC_{22} complex

The advantage of our detection method is that the ion of interest can be changed simply by changing the base sequence. To demonstrate this, I performed an experiment using Ag^+ as another model ion. For this experiment, a probe DNA with the sequence 5'-CCCCCCCCCCCCCCCCCCCCCC-3' (dC_{22}) was used **(Figure 3-9A)**. dC_{22} underwent a conformation change caused by Ag^+ as Ag^+ mediates cytosine mismatching and formed cytosine–Ag^+–cytosine (C–Ag^I–C) base pairs,[126] as confirmed by CD measurements **(Figure 3-9B)**. As shown in Figure 4A, the AuNR–dC_{22} complexes showed no plasmonic CD in the absence of Ag^+. However, in the presence of Ag^+, the AuNR–dC_{22} complexes exhibit negative couplet plasmonic CD. The A_{CD} from AuNR–dC_{22} complexes at Ag^+ concentration of 6.6 μM was calculated to be 400. It is noteworthy that the AuNR–dC_{22} complexes exhibit a marked plasmonic CD. Specifically, AuNR–dC_{22} complexes with Ag^+ (6.6 μM) show a higher value of *g*-factor (1.0×10^{-2}), which represents the dissymmetry, whereas the AuNR–dT_{22} complex with Hg^{2+} (6.6 μM) shows a lower value (0.09×10^{-2}) **(Figure 3-10)**. This value is comparable to that of the AuNR–protein complex system which has side-by-side AuNR chiral assemblies (1.9×10^{-2}).[42]

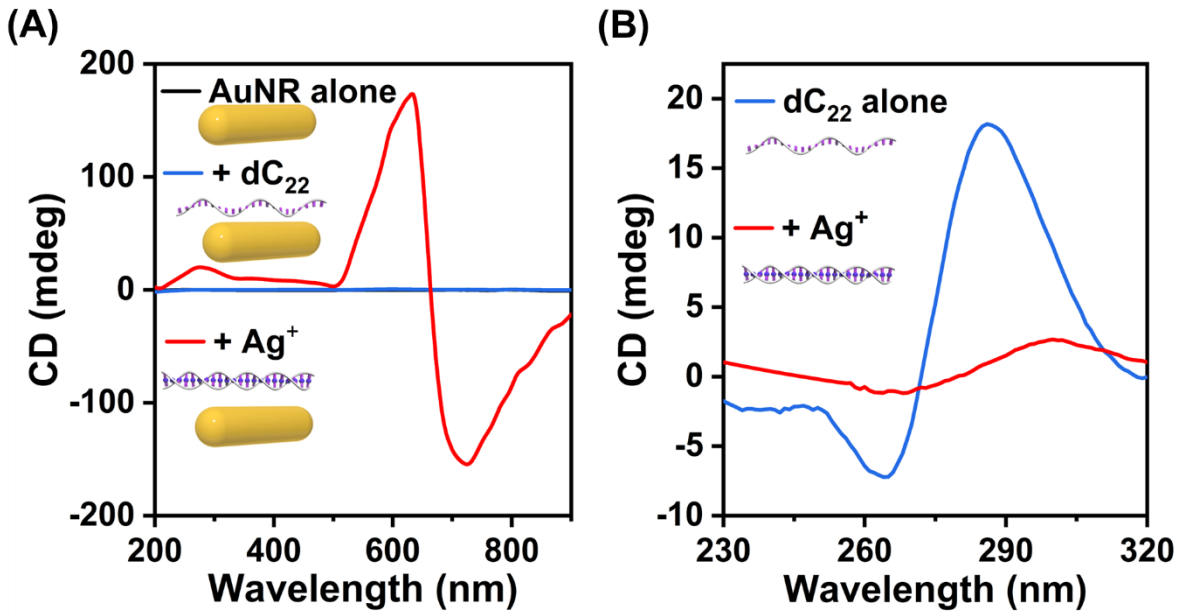

Figure 3-9 CD spectra for (A) 16 nM AuNR alone (black line), AuNR and 0.6 μM dC_{22} complexes (blue line), AuNR and dC_{22} complexes with 6.6 μM Ag^+ (red line), (B) 20 μM dC_{22} alone (blue line)

and with 220 μM Ag^+ (red line).

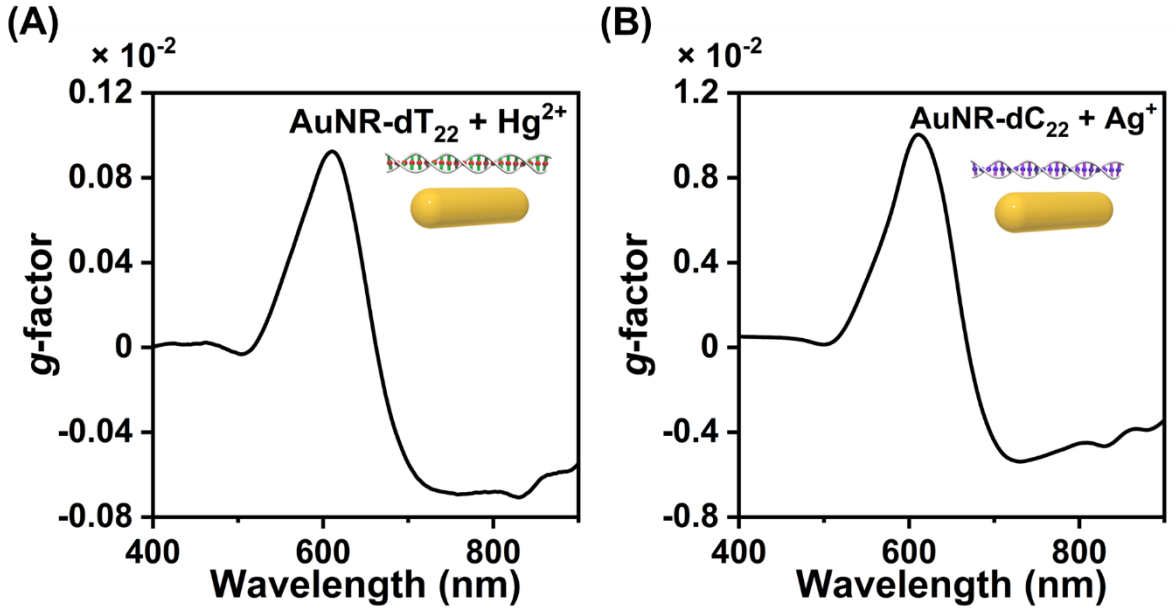

Figure S6 *g*-factor of (A) the AuNR–dT_{22} complexes prepared in the presence of Hg^{2+} (6.6 μM) and (B) the AuNR–dC_{22} complexes prepared in the presence of Ag^+ (6.6 μM). If absorption and CD spectra are measured in the same optical cell and concentration, the *g*-factor was calculated as,

$$g\text{-factor} = \frac{\Delta\varepsilon}{\varepsilon} = \frac{\Delta A}{A} \approx \frac{CD(mdeg)}{32980 \cdot A}$$

Δε was molar circular dichroism, ε was molar absorption coefficient, Δ*A* was difference of absorbance of left and right circularly polarized lights and *A* was absorbance of sample. As CD measurements provide theta (mdeg) and the CD can be converted to the appropriate absorbance "units" (32980 mdeg = 1 absorbance "unit" for an optical path length of 1 mm which was employed in this experiment).[85]

3.5 Conclusion

In summary, I have demonstrated that conformational changes in DNA can be observed by the induced plasmonic optical activity from AuNR–DNA complexes, which has afforded the ability to detect metal ions (Hg^{2+} and Ag^{+}) with no significant background signal. Importantly, the induced plasmonic CD in the visible region was much larger than the molecular CD of the DNA in the UV region. It is also noteworthy that clear changes in plasmonic CD could be caused even with metal-mediated DNAs that show little molecular CD change. I believe that this study will inspire further research on chiral plasmonic applications and facilitate exploration into the chiroptical mechanisms.

Chapter 4

Conclusion and Outlook

Conclusion

This study primarily investigates the plasmonic chirality generated by nanoparticle assemblies induced by chiral molecules. So far, while various molecule-induced chiral plasmonic nanoparticles (e.g., AuNR–protein complexes) have been reported, the relationship between molecular structure and plasmonic circular dichroism (CD) remains unclear. In the present work, I aimed to explore this relationship by utilizing DNA, with its well-defined structural characteristics, to induce chiral assemblies of AuNRs through electrostatic interactions. The results demonstrate that the plasmonic CD signals generated by the AuNR–DNA polyion complexes are highly dependent on the DNA structure and electrostatic interactions. Specifically, I found that the intensity and sign of the plasmonic CD signals can be controlled by altering the DNA sequence or adjusting the ratio of DNA to AuNRs. This result supports the hypothesis that DNA with strong base pairing and stacking interactions can induce plasmonic CD in DNA-induced chiral AuNR assemblies, while DNA with weak base stacking interactions cannot. Furthermore, leveraging this principle, the author applied the AuNR–DNA polyion complex in chiral sensing applications. For example, single-stranded(ss) dT_{22} (random coil) does not induce plasmonic CD in AuNR assemblies; however, upon the addition of Hg^{2+}, dT_{22} forms a helix, which then induces plasmonic CD in the AuNR assemblies, enabling the detection of Hg^{2+}.

In summary, this study is the first report on DNA sequence-dependent plasmonic chirality in AuNR–DNA polyion complexes. It provides insights into the relationship between molecular structure and plasmonic chirality and highlights the potential of using AuNR–DNA polyion complexes for sensitive detection and structural analysis of metal ions, DNA, and proteins, thereby paving the way for advancements in biosensing and nano-photonics.

Outlook

Building on the findings of this study, there are several avenues for future research and development. One promising direction is the exploration of different types of nanoparticles and their interactions with various biomolecules. By expanding the range of nanoparticle shapes, sizes, and compositions, it may be possible to achieve even greater control over the plasmonic CD response and enhance the sensitivity and specificity of detection systems.

Additionally, further investigations into the fundamental mechanisms underlying the plasmonic CD response are warranted. Firstly, while all AuNR–dsDNA consistently produces negative CD signals, AuNR–ssDNA can generate both negative and positive CD signals. This phenomenon that remains unexplained by current research. Secondly, the influence of the relationship between DNA sequence length and AuNR size on plasmonic CD signals needs further exploration. While the present study has examined the effect of DNA sequence length, a more comprehensive investigation into the impact of AuNR size is necessary. Finally, the mechanism underlying the stronger plasmonic CD signals observed in mixed non-complementary ssDNA induced AuNR assemblies also requires additional research. Advanced computational modeling and simulations, combined with experimental techniques could provide deeper insights into the factors influencing the plasmonic CD signals.

Moreover, the development of new strategies for enhancing the stability and reproducibility of plasmonic CD signals is essential. Addressing challenges related to the aggregation and sedimentation of nanoparticles, as well as the effects of varying solution conditions, will be key to ensuring reliable and consistent performance of plasmonic CD-based assays. Employing surface modifications and functionalization techniques to improve nanoparticle stability and biocompatibility could further enhance the practical applicability of these systems.

Finally, exploring the potential of plasmonic CD for studying dynamic biological

processes represents an exciting frontier. Real-time monitoring of biomolecular interactions, conformational changes, and cellular events using plasmonic CD could provide valuable insights into complex biological systems. This could have far-reaching implications for fields such as molecular biology, pharmacology, and synthetic biology, where understanding the dynamics of biomolecular interactions is crucial.

In a word, the plasmonic CD response of AuNR–DNA polyion complexes offers a versatile and powerful tool for biosensing and structural analysis. Continued research and innovation in this area hold the promise of advancing our understanding of chirality origin and developing new technologies for biomedical and environmental applications.

References

(1) Mateos-Timoneda, M. A.; Crego-Calama, M.; Reinhoudt, D. N. Supramolecular chirality of self-assembled systems in solution. *Chem Soc Rev* **2004**, *33* (6), 363-372. DOI: 10.1039/b305550g.

(2) Liu, M. H.; Zhang, L.; Wang, T. Y. Supramolecular Chirality in Self-Assembled Systems. *Chem Rev* **2015**, *115* (15), 7304-7397. DOI: 10.1021/cr500671p.

(3) Winogradoff, D.; Li, P. Y.; Joshi, H.; Quednau, L.; Maffeo, C.; Aksimentiev, A. Chiral Systems Made from DNA. *Adv Sci* **2021**, *8* (5). DOI: ARTN 200311310.1002/advs.202003113.

(4) Green, M. M.; Jain, V. Homochirality in Life: Two Equal Runners, One Tripped. *Origins Life Evol B* **2010**, *40* (1), 111-118. DOI: 10.1007/s11084-009-9180-7.

(5) Trost, B. M.; Brindle, C. S. The direct catalytic asymmetric aldol reaction. *Chem Soc Rev* **2010**, *39* (5), 1600-1632. DOI: 10.1039/b923537j.

(6) Zhu, G. D.; Okamura, W. H. Synthesis of Vitamin-D (Calciferol). *Chem Rev* **1995**, *95* (6), 1877-1952. DOI: DOI 10.1021/cr00038a007.

(7) Soukoulis, C. M.; Kafesaki, M.; Economou, E. N. Negative-index materials: New frontiers in optics. *Adv Mater* **2006**, *18* (15), 1941-1952. DOI: 10.1002/adma.200600106.

(8) Woody, R. W. Circular-Dichroism. *Method Enzymol* **1995**, *246*, 34-71. DOI: 10.1016/0076-6879(95)46006-3.

(9) Kelly, S. M.; Jess, T. J.; Price, N. C. How to study proteins by circular dichroism. *Bba-Proteins Proteom* **2005**, *1751* (2), 119-139. DOI: 10.1016/j.bbapap.2005.06.005.

(10) Liu, N.; Liedl, T. DNA-Assembled Advanced Plasmonic Architectures. *Chem Rev* **2018**, *118* (6), 3032-3053. DOI: 10.1021/acs.chemrev.7b00225.

(11) Zhao, Y.; Askarpour, A. N.; Sun, L. Y.; Shi, J. W.; Li, X. Q.; Alù, A. Chirality detection of enantiomers using twisted optical metamaterials. *Nat Commun* **2017**, *8*, 14180. DOI: 10.1038/ncomms14180.

(12) Warning, L. A.; Miandashti, A. R.; McCarthy, L. A.; Zhang, Q. F.; Landes, C. F.; Link, S. Nanophotonic Approaches for Chirality Sensing. *Acs Nano* **2021**, *15* (10), 15538-15566. DOI: 10.1021/acsnano.1c04992.

(13) Kneer, L. M.; Roller, E. M.; Besteiro, L. V.; Schreiber, R.; Govorov, A. O.; Liedl, T. Circular Dichroism of Chiral Molecules in DNA-Assembled Plasmonic Hotspots. *Acs Nano* **2018**, *12* (9), 9110-9115. DOI: 10.1021/acsnano.8b03146.

(14) Cortie, M. B. The weird world of nanoscale gold. *Gold Bull* **2004**, *37* (1-2), 12-19. DOI: 10.1007/Bf03215512.

(15) Anker, J. N.; Hall, W. P.; Lyandres, O.; Shah, N. C.; Zhao, J.; Van Duyne, R. P. Biosensing with plasmonic nanosensors. *Nat Mater* **2008**, *7* (6), 442-453. DOI: 10.1038/nmat2162.

(16) Cecconello, A.; Besteiro, L. V.; Govorov, A. O.; Willner, I. Chiroplasmonic DNA-based nanostructures. *Nat Rev Mater* **2017**, *2* (9), 17039. DOI: 10.1038/natrevmats.2017.39.

(17) Zheng, J. P.; Cheng, X. Z.; Zhang, H.; Bai, X. P.; Ai, R. Q.; Shao, L.; Wang,

J. F. Gold Nanorods: The Most Versatile Plasmonic Nanoparticles. *Chem Rev* **2021**, *121* (21), 13342-13453. DOI: 10.1021/acs.chemrev.1c00422.

(18) Shen, X. B.; Zhan, P. F.; Kuzyk, A.; Liu, Q.; Asenjo-Garcia, A.; Zhang, H.; de Abajo, F. J. G.; Govorov, A.; Ding, B. Q.; Liu, N. 3D plasmonic chiral colloids. *Nanoscale* **2014**, *6* (4), 2077-2081. DOI: 10.1039/c3nr06006c.

(19) Lv, J. W.; Gao, X. Q.; Han, B.; Zhu, Y. F.; Hou, K.; Tang, Z. Y. Self-assembled inorganic chiral superstructures. *Nat Rev Chem* **2022**, *6* (2), 125-145. DOI: 10.1038/s41570-021-00350-w.

(20) Meng, D. J.; Chen, Y. D.; Ji, Y. L.; Shi, X. H.; Wang, H.; Wu, X. C. Temperature Effect of Plasmonic Circular Dichroism in Dynamic Oligomers of AuNR@Ag Nanorods Driven by Cysteine: The Role of Surface Atom Migration. *Adv Opt Mater* **2021**, *9* (2), 2001274. DOI: 10.1002/adom.202001274.

(21) Cao, J.; Sun, T.; Grattan, K. T. V. Gold nanorod-based localized surface plasmon resonance biosensors: A review. *Sensor Actuat B-Chem* **2014**, *195*, 332-351. DOI: 10.1016/j.snb.2014.01.056.

(22) Govorov, A. O.; Gun'ko, Y. K.; Slocik, J. M.; Gérard, V. A.; Fan, Z. Y.; Naik, R. R. Chiral nanoparticle assemblies: circular dichroism, plasmonic interactions, and exciton effects. *J Mater Chem* **2011**, *21* (42), 16806-16818. DOI: 10.1039/c1jm12345a.

(23) Zhang, H.; Govorov, A. O. Giant circular dichroism of a molecule in a region of strong plasmon resonances between two neighboring gold nanocrystals. *Phys Rev B* **2013**, *87* (7), 075410. DOI: 10.1103/PhysRevB.87.075410.

(24) Layani, M. E.; Ben Moshe, A.; Varenik, M.; Regev, O.; Zhang, H.; Govorov, A. O.; Markovich, G. Chiroptical Activity in Silver Cholate Nanostructures Induced by the Formation of Nanoparticle Assemblies. *J Phys Chem C* **2013**, *117* (43), 22240-22244. DOI: 10.1021/jp400993j.

(25) Guerrero-Martínez, A.; Auguié, B.; Alonso-Gómez, J. L.; Dzolic, Z.; Gómez-Graña, S.; Zinic, M.; Cid, M. M.; Liz-Marzán, L. M. Intense Optical Activity from Three-Dimensional Chiral Ordering of Plasmonic Nanoantennas. *Angew Chem Int Edit* **2011**, *50* (24), 5499-5503. DOI: 10.1002/anie.201007536.

(26) Kuzyk, A.; Schreiber, R.; Fan, Z. Y.; Pardatscher, G.; Roller, E. M.; Högele, A.; Simmel, F. C.; Govorov, A. O.; Liedl, T. DNA-based self-assembly of chiral plasmonic nanostructures with tailored optical response. *Nature* **2012**, *483* (7389), 311-314. DOI: 10.1038/nature10889.

(27) Sun, W.; Boulais, E.; Hakobyan, Y.; Wang, W. L.; Guan, A.; Bathe, M.; Yin, P. Casting inorganic structures with DNA molds. *Science* **2014**, *346* (6210), 1258361. DOI: 10.1126/science.1258361.

(28) Shemer, G.; Krichevski, O.; Markovich, G.; Molotsky, T.; Lubitz, I.; Kotlyar, A. B. Chirality of silver nanoparticles synthesized on DNA. *J Am Chem Soc* **2006**, *128* (34), 11006-11007. DOI: 10.1021/ja063702i.

(29) Fan, Z. Y.; Govorov, A. O. Chiral Nanocrystals: Plasmonic Spectra and Circular Dichroism. *Nano Lett* **2012**, *12* (6), 3283-3289. DOI: 10.1021/nl3013715.

(30) Lee, H. E.; Ahn, H. Y.; Mun, J.; Lee, Y. Y.; Kim, M.; Cho, N. H.; Chang, K.;

Kim, W. S.; Rho, J.; Nam, K. T. Amino-acid- and peptide-directed synthesis of chiral plasmonic gold nanoparticles. *Nature* **2018**, *556* (7701), 360-365. DOI: 10.1038/s41586-018-0034-1.

(31) Govorov, A. O. Plasmon-Induced Circular Dichroism of a Chiral Molecule in the Vicinity of Metal Nanocrystals. Application to Various Geometries. *J Phys Chem C* **2011**, *115* (16), 7914-7923. DOI: 10.1021/jp1121432.

(32) Fan, Z. Y.; Govorov, A. O. Plasmonic Circular Dichroism of Chiral Metal Nanoparticle Assemblies. *Nano Lett* **2010**, *10* (7), 2580-2587. DOI: 10.1021/nl101231b.

(33) Drezet, A.; Genet, C.; Laluet, J. Y.; Ebbesen, T. W. Optical chirality without optical activity: How surface plasmons give a twist to light. *Opt Express* **2008**, *16* (17), 12559-12570. DOI: 10.1364/Oe.16.012559.

(34) Soukoulis, C. M.; Wegener, M. Past achievements and future challenges in the development of three-dimensional photonic metamaterials. *Nat Photonics* **2011**, *5* (9), 523-530. DOI: 10.1038/Nphoton.2011.154.

(35) Deubel, M.; Von Freymann, G.; Wegener, M.; Pereira, S.; Busch, K.; Soukoulis, C. M. Direct laser writing of three-dimensional photonic-crystal templates for telecommunications. *Nat Mater* **2004**, *3* (7), 444-447. DOI: 10.1038/nmat1155.

(36) Hendry, E.; Carpy, T.; Johnston, J.; Popland, M.; Mikhaylovskiy, R. V.; Lapthorn, A. J.; Kelly, S. M.; Barron, L. D.; Gadegaard, N.; Kadodwala, M. Ultrasensitive detection and characterization of biomolecules using superchiral fields. *Nat Nanotechnol* **2010**, *5* (11), 783-787. DOI: 10.1038/Nnano.2010.209.

(37) Maniappan, S.; Dutta, C.; Solís, D. M.; Taboada, J. M.; Kumar, J. Surfactant Directed Synthesis of Intrinsically Chiral Plasmonic Nanostructures and Precise Tuning of their Optical Activity through Controlled Self-Assembly. *Angew Chem Int Edit* **2023**, *62* (21). DOI: 10.1002/anie.202300461.

(38) Lee, H. E.; Kim, R. M.; Ahn, H. Y.; Lee, Y. Y.; Byun, G. H.; Im, S. W.; Mun, J.; Rho, J.; Nam, K. T. Cysteine-encoded chirality evolution in plasmonic rhombic dodecahedral gold nanoparticles. *Nat Commun* **2020**, *11* (1). DOI: 10.1038/s41467-019-14117-x.

(39) Cho, N. H.; Kim, Y. B.; Lee, Y. Y.; Im, S. W.; Kim, R. M.; Kim, J. W.; Namgung, S. D.; Lee, H. E.; Kim, H.; Han, J. H.; et al. Adenine oligomer directed synthesis of chiral gold nanoparticles. *Nat Commun* **2022**, *13* (1), 3831. DOI: 10.1038/S41467-022-31513-y.

(40) Ma, W.; Kuang, H.; Xu, L. G.; Ding, L.; Xu, C. L.; Wang, L. B.; Kotov, N. A. Attomolar DNA detection with chiral nanorod assemblies. *Nat Commun* **2013**, *4*, 2689. DOI: 10.1038/ncomms3689.

(41) Mastroianni, A. J.; Claridge, S. A.; Alivisatos, A. P. Pyramidal and Chiral Groupings of Gold Nanocrystals Assembled Using DNA Scaffolds. *J Am Chem Soc* **2009**, *131* (24), 8455-8459. DOI: 10.1021/ja808570g.

(42) Shinmori, H.; Mochizuki, C. Strong chiroptical activity from achiral gold nanorods assembled with proteins. *Chem Commun* **2017**, *53* (49), 6569-6572. DOI: 10.1039/c7cc03089d.

(43) Lu, J.; Xue, Y.; Bernardino, K.; Zhang, N. N.; Gomes, W. R.; Ramesar, N. S.; Liu, S. H.; Hu, Z.; Sun, T. M.; de Moura, A. F.; et al. Enhanced optical asymmetry in supramolecular chiroplasmonic assemblies with long-range order. *Science* **2021**, *371* (6536), 1368-1374. DOI: 10.1126/science.abd8576.

(44) Wang, L.; Urbas, A. M.; Li, Q. Nature-Inspired Emerging Chiral Liquid Crystal Nanostructures: From Molecular Self-Assembly to DNA Mesophase and Nanocolloids. *Adv Mater* **2020**, *32* (41), 1801335. DOI: 10.1002/adma.201801335.

(45) Querejeta-Fernández, A.; Chauve, G.; Methot, M.; Bouchard, J.; Kumacheva, E. Chiral Plasmonic Films Formed by Gold Nanorods and Cellulose Nanocrystals. *J Am Chem Soc* **2014**, *136* (12), 4788-4793. DOI: 10.1021/ja501642p.

(46) Cheng, G. Q.; Xu, D.; Lu, Z. Y.; Liu, K. Chiral Self-Assembly of Nanoparticles Induced by Polymers Synthesized

Reversible Addition-Fragmentation Chain Transfer Polymerization. *Acs Nano* **2019**, *13* (2), 1479-1489. DOI: 10.1021/acsnano.8b07151.

(47) Liu, J. G.; Yin, F.; Hu, J.; Ju, Y. Fabrication and Applications of Supramolecular Chiral Assemblies. *Chinese J Org Chem* **2021**, *41* (3), 1031-1052. DOI: 10.6023/cjoc202008011.

(48) Liu, W. L.; Han, H.; Wang, J. Q. Recent Advances in the 3D Chiral Plasmonic Nanomaterials. *Small* **2024**, *20* (8). DOI: 10.1002/smll.202305725.

(49) Rodier, M.; Keijzer, C.; Milner, J.; Karimullah, A. S.; Roszak, A. W.; Barron, L. D.; Gadegaard, N.; Lapthorn, A. J.; Kadodwala, M. Biomacromolecular charge chirality detected using chiral plasmonic nanostructures. *Nanoscale Horiz* **2020**, *5* (2), 336-344. DOI: 10.1039/c9nh00525k.

(50) Guselnikova, O.; Elashnikov, R.; Svorcik, V.; Kartau, M.; Gilroy, C.; Gadegaard, N.; Kadodwala, M.; Karimullah, A. S.; Lyutakov, O. Coupling of plasmonic hot spots with shurikens for superchiral SERS-based enantiomer recognition. *Nanoscale Horiz* **2023**, *8* (4), 499-508. DOI: 10.1039/d3nh00008g.

(51) Zhu, Y. Y.; Xu, L. G.; Ma, W.; Xu, Z.; Kuang, H.; Wang, L. B.; Xu, C. L. A one-step homogeneous plasmonic circular dichroism detection of aqueous mercury ions using nucleic acid functionalized gold nanorods. *Chem Commun* **2012**, *48* (97), 11889-11891. DOI: 10.1039/c2cc36559f.

(52) Yan, W. J.; Wang, Y. L.; Zhuang, H.; Zhang, J. H. DNA-engineered chiroplasmonic heteropyramids for ultrasensitive detection of mercury ion. *Biosens Bioelectron* **2015**, *68*, 516-520. DOI: 10.1016/j.bios.2015.01.028.

(53) Xu, L. G.; Gao, Y. F.; Kuang, H.; Liz-Marzán, L. M.; Xu, C. L. MicroRNA-Directed Intracellular Self-Assembly of Chiral Nanorod Dimers. *Angew Chem Int Edit* **2018**, *57* (33), 10544-10548. DOI: 10.1002/anie.201805640.

(54) Zhu, F.; Li, X. Y.; Li, Y. C.; Yan, M.; Liu, S. Q. Enantioselective Circular Dichroism Sensing of Cysteine and Glutathione with Gold Nanorods. *Analytical Chemistry* **2015**, *87* (1), 357-361. DOI: 10.1021/ac504017f.

(55) Gao, F.; Sun, M.; Ma, W.; Wu, X.; Liu, L.; Kuang, H.; Xu, C. A Singlet Oxygen Generating Agent by Chirality-dependent Plasmonic Shell-Satellite

Nanoassembly. *Adv Mater* **2017**, *29* (18), 1606864. DOI: 10.1002/adma.201606864.

(56) Qu, A. H.; Sun, M. Z.; Kim, J. Y.; Xu, L. G.; Hao, C. L.; Ma, W.; Wu, X. L.; Liu, X. G.; Kuang, H.; Kotov, N. A.; et al. Stimulation of neural stem cell differentiation by circularly polarized light transduced by chiral nanoassemblies. *Nat Biomed Eng* **2021**, *5* (1), 103-113. DOI: 10.1038/s41551-020-00634-4.

(57) Hao, C. L.; Xu, L. G.; Ma, W.; Wu, X. L.; Wang, L. B.; Kuang, H.; Xu, C. L. Unusual Circularly Polarized Photocatalytic Activity in Nanogapped Gold-Silver Chiroplasmonic Nanostructures. *Adv Funct Mater* **2015**, *25* (36), 5816-5822. DOI: 10.1002/adfm.201502429.

(58) Zhan, P. F.; Wang, Z. G.; Li, N.; Ding, B. Q. Engineering Gold Nanoparticles with DNA Ligands for Selective Catalytic Oxidation of Chiral Substrates. *Acs Catal* **2015**, *5* (3), 1489-1498. DOI: 10.1021/cs5015805.

(59) Wang, L.-Y.; Smith, K. W.; Dominguez-Medina, S.; Moody, N.; Olson, J. M.; Zhang, H.; Chang, W.-S.; Kotov, N.; Link, S. Circular Differential Scattering of Single Chiral Self-Assembled Gold Nanorod Dimers. *ACS Photonics* **2015**, *2* (11), 1602-1610. DOI: 10.1021/acsphotonics.5b00395.

(60) Shen, X. B.; Asenjo-Garcia, A.; Liu, Q.; Jiang, Q.; de Abajo, F. J. G.; Liu, N.; Ding, B. Q. Three-Dimensional Plasmonic Chiral Tetramers Assembled by DNA Origami. *Nano Lett* **2013**, *13* (5), 2128-2133. DOI: 10.1021/nl400538y.

(61) Tian, Y.; Wang, T.; Liu, W. Y.; Xin, H. L.; Li, H. L.; Ke, Y. G.; Shih, W. M.; Gang, O. Prescribed nanoparticle cluster architectures and low-dimensional arrays built using octahedral DNA origami frames. *Nat Nanotechnol* **2015**, *10* (7), 637-644. DOI: 10.1038/Nnano.2015.105.

(62) Urban, M. J.; Dutta, P. K.; Wang, P. F.; Duan, X. Y.; Shen, X. B.; Ding, B. Q.; Ke, Y. G.; Liu, N. Plasmonic Toroidal Metamolecules Assembled by DNA Origami. *J Am Chem Soc* **2016**, *138* (17), 5495-5498. DOI: 10.1021/jacs.6b00958.

(63) Shen, X. B.; Song, C.; Wang, J. Y.; Shi, D. W.; Wang, Z. G.; Liu, N.; Ding, B. Q. Rolling Up Gold Nanoparticle-Dressed DNA Origami into Three-Dimensional Plasmonic Chiral Nanostructures. *J Am Chem Soc* **2012**, *134* (1), 146-149. DOI: 10.1021/ja209861x.

(64) Shen, C. Q.; Lan, X.; Zhu, C. G.; Zhang, W.; Wang, L. Y.; Wang, Q. B. Spiral Patterning of Au Nanoparticles on Au Nanorod Surface to Form Chiral AuNR@AuNP Helical Superstructures Templated by DNA Origami. *Adv Mater* **2017**, *29* (16), 1606533. DOI: 10.1002/adma.201606533.

(65) Lan, X.; Chen, Z.; Dai, G. L.; Lu, X. X.; Ni, W. H.; Wang, Q. B. Bifacial DNA Origami-Directed Discrete, Three-Dimensional, Anisotropic Plasmonic Nanoarchitectures with Tailored Optical Chirality. *J Am Chem Soc* **2013**, *135* (31), 11441-11444. DOI: 10.1021/ja404354c.

(66) Lan, X.; Lu, X. X.; Shen, C. Q.; Ke, Y. G.; Ni, W. H.; Wang, Q. B. Au Nanorod Helical Superstructures with Designed Chirality. *J Am Chem Soc* **2015**, *137* (1), 457-462. DOI: 10.1021/ja511333q.

(67) Lan, X.; Su, Z. M.; Zhou, Y. D.; Meyer, T.; Ke, Y. G.; Wang, Q. B.; Chiu, W.;

Liu, N.; Zou, S. L.; Yan, H.; et al. Programmable Supra-Assembly of a DNA Surface Adapter for Tunable Chiral Directional Self-Assembly of Gold Nanorods. *Angew Chem Int Edit* **2017**, *56* (46), 14632-14636. DOI: 10.1002/anie.201709775.

(68) Zhu, Z. N.; Liu, W. J.; Li, Z. T.; Han, B.; Zhou, Y. L.; Gao, Y.; Tang, Z. Y. Manipulation of Collective Optical Activity in One-Dimensional Plasmonic Assembly. *Acs Nano* **2012**, *6* (3), 2326-2332. DOI: 10.1021/nn2044802.

(69) Song, C. Y.; Blaber, M. G.; Zhao, G. P.; Zhang, P. J.; Fry, H. C.; Schatz, G. C.; Rosi, N. L. Tailorable Plasmonic Circular Dichroism Properties of Helical Nanoparticle Superstructures. *Nano Lett* **2013**, *13* (7), 3256-3261. DOI: 10.1021/nl4013776.

(70) Kumar, J.; Eraña, H.; López-Martínez, E.; Claes, N.; Martín, V. F.; Solís, D. M.; Bals, S.; Cortajarena, A. L.; Castilla, J.; Liz-Marzán, L. M. Detection of amyloid fibrils in Parkinson's disease using plasmonic chirality. *P Natl Acad Sci USA* **2018**, *115* (13), 3225-3230. DOI: 10.1073/pnas.1721690115.

(71) Yan, J.; Chen, Y. D.; Hou, S.; Chen, J. Q.; Meng, D. J.; Zhang, H.; Fan, H. Z.; Ji, Y. L.; Wu, X. C. Fabricating chiroptical starfruit-like Au nanoparticles interface modulation of chiral thiols. *Nanoscale* **2017**, *9* (31), 11093-11102. DOI: 10.1039/c7nr03712k.

(72) Núñez-Martínez, M.; Arias, S.; Quiñoá, E.; Riguera, R.; Freire, F. Dynamic Chiral PPA-AgNP Nanocomposites: Aligned Silver Nanoparticles Decorating Helical Polymers. *Chem Mater* **2021**, *33* (12), 4805-4812. DOI: 10.1021/acs.chemmater.1c00805.

(73) Jung, S. H.; Jeon, J.; Kim, H.; Jaworski, J.; Jung, J. H. Chiral Arrangement of Achiral Au Nanoparticles by Supramolecular Assembly of Helical Nanofiber Templates (vol 136, pg 6446, 2014). *J Am Chem Soc* **2014**, *136* (29), 10542-10542. DOI: 10.1021/ja505485a.

(74) Xie, J. J.; Che, S. A. Chirality of Anisotropic Metal Nanowires with a Distinct Multihelix. *Chem-Eur J* **2012**, *18* (50), 15954-15959. DOI: 10.1002/chem.201203017.

(75) Saenger, W. *Principles of nucleic acid structure*; Springer Science & Business Media, 2013.

(76) Yakovchuk, P.; Protozanova, E.; Frank-Kamenetskii, M. D. Base-stacking and base-pairing contributions into thermal stability of the DNA double helix (vol 34, pg 564, 2006). *Nucleic Acids Res* **2006**, *34* (2), 564-574. DOI: 10.1093/nar/gkj523.

(77) Hagen, T.; Laski, A.; Brümmer, A.; Pruska, A.; Schlösser, V.; Cléry, A.; Allain, F. H. T.; Zenobi, R.; Bergmann, S.; Hall, J. Inosine Substitutions in RNA Activate Latent G-Quadruplexes. *J Am Chem Soc* **2021**, *143* (37), 15120-15130. DOI: 10.1021/jacs.1c05214.

(78) Karabiyik, H.; Sevinçek, R.; Karabiyik, H. π-Cooperativity effect on the base stacking interactions in DNA: is there a novel stabilization factor coupled with base pairing H-bonds? *Phys Chem Chem Phys* **2014**, *16* (29), 15527-15538. DOI: 10.1039/c4cp00997e.

(79) Sasabe, J.; Suzuki, M. Distinctive Roles of D-Amino Acids in the Homochiral

World: Chirality of Amino Acids Modulates Mammalian Physiology and Pathology. *Keijo J Med* **2019**, *68* (1), 1-16. DOI: 10.2302/kjm.2018-0001-IR.

(80) Brooks, W. H.; Guida, W. C.; Daniel, K. G. The Significance of Chirality in Drug Design and Development. *Curr Top Med Chem* **2011**, *11* (7), 760-770. DOI: 10.2174/156802611795165098.

(81) Fasman, G. D. *Circular dichroism and the conformational analysis of biomolecules*; Springer Science & Business Media, 2013.

(82) Kypr, J.; Kejnovská, I.; Renciuk, D.; Vorlícková, M. Circular dichroism and conformational polymorphism of DNA. *Nucleic Acids Res* **2009**, *37* (6), 1713-1725. DOI: 10.1093/nar/gkp026.

(83) Petryayeva, E.; Krull, U. J. Localized surface plasmon resonance: Nanostructures, bioassays and biosensing-A review. *Anal Chim Acta* **2011**, *706* (1), 8-24. DOI: 10.1016/j.aca.2011.08.020.

(84) Lin, D. W.; Xing, Q. G.; Wang, Y. F.; Qi, W.; Su, R. X.; He, Z. M. Supramolecular Chiral Self-Assembly of Peptides and Its Applications. *Prog Chem* **2019**, *31* (12), 1623-1636. DOI: 10.7536/Pc190446.

(85) Warning, L. A.; Miandashti, A. R.; Misiura, A.; Landes, C. F.; Link, S. Naturally Occurring Proteins Direct Chiral Nanorod Aggregation. *J Phys Chem C* **2022**, *126* (5), 2656-2668. DOI: 10.1021/acs.jpcc.1c09644.

(86) Qiu, H. B.; Che, S. N. Chiral mesoporous silica: Chiral construction and imprinting cooperative self-assembly of amphiphiles and silica precursors. *Chem Soc Rev* **2011**, *40* (3), 1259-1268. DOI: 10.1039/c0cs00002g.

(87) Cho, N. H.; Kim, H.; Kim, J. W.; Lim, Y. C.; Kim, R. M.; Lee, Y. H.; Nam, K. T. Perspective Chiral inorganic nanomaterials for biomedical applications. *Chem-Us* **2024**, *10* (4), 1052-1070. DOI: 10.1016/j.chempr.2023.12.016.

(88) Wang, Z. Y.; Zhang, N. N.; Li, J. C.; Lu, J.; Zhao, L.; Fang, X. D.; Liu, K. Serum albumin guided plasmonic nanoassemblies with opposite chiralities. *Soft Matter* **2021**, *17* (26), 6298-6304. DOI: 10.1039/d1sm00784j.

(89) Nakamura, S.; Mitomo, H.; Aizawa, M.; Tani, T.; Matsuo, Y.; Niikura, K.; Pike, A.; Naya, M.; Shishido, A.; Ijiro, K. DNA Brush-Directed Vertical Alignment of Extensive Gold Nanorod Arrays with Controlled Density. *Acs Omega* **2017**, *2* (5), 2208-2213. DOI: 10.1021/acsomega.7b00303.

(90) Nakamura, S.; Mitomo, H.; Sekizawa, Y.; Higuchi, T.; Matsuo, Y.; Jinnai, H.; Ijiro, K. Strategy for Finely Aligned Gold Nanorod Arrays Using Polymer Brushes as a Template. *Langmuir* **2020**, *36* (13), 3590-3599. DOI: 10.1021/acs.langmuir.9b03835.

(91) Nakamura, S.; Mitomo, H.; Yonamine, Y.; Ijiro, K. Salt-triggered Active Plasmonic Systems Based on the Assembly/Disassembly of Gold Nanorods in a DNA Brush Layer on a Solid Substrate. *Chem Lett* **2020**, *49* (7), 749-752. DOI: 10.1246/cl.200185.

(92) Nakamura, S.; Mitomo, H.; Suzuki, S.; Torii, Y.; Sekizawa, Y.; Yonamine, Y.; Ijiro, K. Self-assembly of Gold Nanorods into a Highly Ordered Sheet via Electrostatic Interactions with Double-stranded DNA. *Chem Lett* **2022**, *51* (5), 529-532. DOI:

10.1246/cl.220069.

(93) Lin, C.; Ke, Y.; Li, Z.; Wang, J. H.; Liu, Y.; Yan, H. Mirror image DNA nanostructures for chiral supramolecular assemblies. *Nano Lett* **2009**, *9* (1), 433-436. DOI: 10.1021/nl803328v.

(94) Akiyama, Y.; Wang, G.; Shiraishi, S.; Kanayama, N.; Takarada, T.; Maeda, M. Rapid naked-eye discrimination of cytochrome P450 genetic polymorphism through non-crosslinking aggregation of dna-functionalized gold nanoparticles. *ChemistryOpen* **2016**, *5* (6), 508-512. DOI: 10.1002/open.201600110.

(95) Wang, L.; Wang, G.; Shi, Y.; Zhang, L.; An, R.; Takarada, T.; Maeda, M.; Liang, X. Accelerated non-crosslinking assembly of DNA-functionalized nanoparticles in alcoholic solvents: For application in the identification of clear liquors. *Analyst* **2020**, *145* (9), 3229-3235. DOI: 10.1039/D0AN00029A.

(96) Nishikawa, M.; Rattanakiat, S.; Takakura, Y. DNA-based nano-sized systems for pharmaceutical and biomedical applications. *Advanced drug delivery reviews* **2010**, *62* (6), 626-632. DOI: 10.1016/j.addr.2010.03.006.

(97) Shi, Y.; Chen, Q.; Liu, Y.; Wang, G. Capability of Au nano-rhombic dodecahedra in a label-free colorimetric assay: application in the determination of S^{2-} and Hg^{2+}. *Analyst* **2022**, *147* (15), 3578-3584. DOI: 10.1039/D2AN00852A.

(98) Sau, T. K.; Murphy, C. J. Seeded high yield synthesis of short Au nanorods in aqueous solution. *Langmuir* **2004**, *20* (15), 6414-6420. DOI: 10.1021/la049463z.

(99) Kumar, J.; López-Martínez, E.; Cortajarena, A. L.; Solís, D. M.; Taboada, J. M.; Díez-Buitrago, B.; Pavlov, V.; Liz-Marzán, L. M. Charge-Induced Shifts in Chiral Surface Plasmon Modes in Gold Nanorod Assemblies. *Particle & Particle Systems Characterization* **2019**, *36* (5), 1800368. DOI: 10.1002/ppsc.201800368.

(100) Tjong, V.; Tang, L.; Zauscher, S.; Chilkoti, A. "Smart" DNA interfaces. *Chem Soc Rev* **2014**, *43* (5), 1612-1626. DOI: 10.1039/c3cs60331h.

(101) Meng, H. M.; Liu, H.; Kuai, H. L.; Peng, R. Z.; Mo, L. T.; Zhang, X. B. Aptamer-integrated DNA nanostructures for biosensing, bioimaging and cancer therapy. *Chem Soc Rev* **2016**, *45* (9), 2583-2602. DOI: 10.1039/c5cs00645g.

(102) Yoo, H.; Jo, H.; Oh, S. S. Detection and beyond: challenges and advances in aptamer-based biosensors. *Mater Adv* **2020**, *1* (8), 2663-2687. DOI: 10.1039/d0ma00639d.

(103) Rajendran, M.; Ellington, A. D. Selection of fluorescent aptamer beacons that light up in the presence of zinc. *Anal Bioanal Chem* **2008**, *390* (4), 1067-1075. DOI: 10.1007/s00216-007-1735-8.

(104) Ellington, A. D.; Szostak, J. W. Selection in vitro of single-stranded DNA molecules that fold into specific ligand-binding structures. *Nature* **1992**, *355* (6363), 850-852.

(105) Huizenga, D. E.; Szostak, J. W. A DNA Aptamer That Binds Adenosine and Atp. *Biochemistry-Us* **1995**, *34* (2), 656-665. DOI: DOI 10.1021/bi00002a033.

(106) Bock, L. C.; Griffin, L. C.; Latham, J. A.; Vermaas, E. H.; Toole, J. J. Selection of Single-Stranded-DNA Molecules That Bind and Inhibit Human Thrombin.

Nature **1992**, *355* (6360), 564-566. DOI: DOI 10.1038/355564a0.

(107) Nutiu, R.; Li, Y. F. In vitro selection of structure-switching signaling aptamers. *Angew Chem Int Edit* **2005**, *44* (7), 1061-1065. DOI: 10.1002/anie.200461848.

(108) Tyagi, S.; Kramer, F. R. Molecular beacons: probes that fluoresce upon hybridization. *Nature biotechnology* **1996**, *14* (3), 303-308. DOI: 10.1038/nbt0396-303.

(109) Fan, C.; Plaxco, K. W.; Heeger, A. J. Electrochemical interrogation of conformational changes as a reagentless method for the sequence-specific detection of DNA. *Proceedings of the National Academy of Sciences* **2003**, *100* (16), 9134-9137. DOI: 10.1073/pnas.1633515100.

(110) Saha, K.; Agasti, S. S.; Kim, C.; Li, X. N.; Rotello, V. M. Gold Nanoparticles in Chemical and Biological Sensing. *Chem Rev* **2012**, *112* (5), 2739-2779. DOI: 10.1021/cr2001178.

(111) Ghosh, S. K.; Pal, T. Interparticle coupling effect on the surface plasmon resonance of gold nanoparticles: From theory to applications. *Chem Rev* **2007**, *107* (11), 4797-4862. DOI: 10.1021/cr0680282.

(112) Wang, L.; He, Z.; Chen, Q.; Wang, G.; Liang, X.; Takarada, T.; Maeda, M. Refreshing DNA-based nanoprobes by alcohol for heavy metal detection: Toward sustainable sensing nanomaterials. *ACS Sustainable Chemistry & Engineering* **2023**, *11* (9), 3611-3620. DOI: 10.1021/acssuschemeng.2c05833.

(113) Maoz, B. M.; Chaikin, Y.; Tesler, A. B.; Bar Elli, O.; Fan, Z. Y.; Govorov, A. O.; Markovich, G. Amplification of Chiroptical Activity of Chiral Biomolecules by Surface Plasmons. *Nano Lett* **2013**, *13* (3), 1203-1209. DOI: 10.1021/nl304638a.

(114) Zhang, Q. F.; Hernandez, T.; Smith, K. W.; Jebeli, S. A. H.; Dai, A. X.; Warning, L.; Baiyasi, R.; McCarthy, L. A.; Guo, H.; Chen, D. H.; et al. Unraveling the origin of chirality from plasmonic nanoparticle-protein complexes. *Science* **2019**, *365* (6460), 1475-1478. DOI: 10.1126/science.aax5415.

(115) Lu, F.; Tian, Y.; Liu, M.; Su, D.; Zhang, H.; Govorov, A. O.; Gang, O. Discrete Nanocubes as Plasmonic Reporters of Molecular Chirality. *Nano Lett* **2013**, *13* (7), 3145-3151. DOI: 10.1021/nl401107g.

(116) Wang, R. Y.; Wang, P.; Liu, Y. N.; Zhao, W. J.; Zhai, D. W.; Hong, X. H.; Ji, Y. L.; Wu, X. C.; Wang, F.; Zhang, D.; et al. Experimental Observation of Giant Chiroptical Amplification of Small Chiral Molecules by Gold Nanosphere Clusters. *J Phys Chem C* **2014**, *118* (18), 9690-9695. DOI: 10.1021/jp5025813.

(117) Wang, W. H.; Wu, F. X.; Zhang, Y. Q.; Wei, W. L.; Niu, W. X.; Xu, G. B. Boosting chiral amplification in plasmon-coupled circular dichroism using discrete silver nanorods as amplifiers. *Chem Commun* **2021**, *57* (60), 7390-7393. DOI: 10.1039/d1cc01891d.

(118) Hou, S.; Zhang, H.; Yan, J.; Ji, Y. L.; Wen, T.; Liu, W. Q.; Hu, Z. J.; Wu, X. C. Plasmonic circular dichroism in side-by-side oligomers of gold nanorods: the influence of chiral molecule location and interparticle distance. *Phys Chem Chem Phys* **2015**, *17* (12), 8187-8193. DOI: 10.1039/c4cp06029f.

(119) Ma, W.; Kuang, H.; Wang, L. B.; Xu, L. G.; Chang, W. S.; Zhang, H. N.; Sun, M. Z.; Zhu, Y. Y.; Zhao, Y.; Liu, L. Q.; et al. Chiral plasmonics of self-assembled nanorod dimers. *Sci Rep-Uk* **2013**, *3*, 1934. DOI: 10.1038/srep01934.

(120) Miyake, Y.; Togashi, H.; Tashiro, M.; Yamaguchi, H.; Oda, S.; Kudo, M.; Tanaka, Y.; Kondo, Y.; Sawa, R.; Fujimoto, T.; et al. Mercury-mediated formation of thymine-Hg-thymine base pairs in DNA duplexes. *J Am Chem Soc* **2006**, *128* (7), 2172-2173. DOI: 10.1021/ja056354d.

(121) Benda, L.; Straka, M.; Sychrovsky, V.; Bour, P.; Tanaka, Y. Detection of mercury–TpT dinucleotide binding by Raman spectra: A computational study. *J Phys Chem A* **2012**, *116* (32), 8313-8320. DOI: 10.1021/jp3045077.

(122) Zipper, H.; Brunner, H.; Bernhagen, J.; Vitzthum, F. Investigations on DNA intercalation and surface binding by SYBR Green I, its structure determination and methodological implications. *Nucleic Acids Res* **2004**, *32* (12), e103-e103.

(123) Savitzky, A.; Golay, M. J. E. Smoothing + Differentiation of Data by Simplified Least Squares Procedures. *Analytical Chemistry* **1964**, *36* (8), 1627-1639. DOI: 10.1021/ac60214a047.

(124) Gluodenis, M.; Foss, C. A. The effect of mutual orientation on the spectra of metal nanoparticle rod-rod and rod-sphere pairs. *J Phys Chem B* **2002**, *106* (37), 9484-9489. DOI: 10.1021/jp014245p.

(125) Yang, J.; Sekizawa, Y.; Shi, X.; Ijiro, K.; Mitomo, H. Assembly/disassembly control of gold nanorods with uniform orientation on anionic polymer brush substrates. *Bull Chem Soc Jpn* **2024**, *97* (7). DOI: 10.1093/bulcsj/uoae073.

(126) Ono, A.; Cao, S.; Togashi, H.; Tashiro, M.; Fujimoto, T.; Machinami, T.; Oda, S.; Miyake, Y.; Okamoto, I.; Tanaka, Y. Specific interactions between silver (I) ions and cytosine–cytosine pairs in DNA duplexes. *Chem Commun* **2008**, (39), 4825-4827. DOI: 10.1039/B808686A.

Acknowledgement

The present dissertation is the collection of the studies, which have been accomplished at the Division of Soft Matter, Graduate School of Life Sciences, The University of Hokkaido and Molecular Device Laboratory under the direction of Professor Kuniharu Ijiro and Associate Prof. Hideyuki Mitomo from November 2021 to September 2024. I would like to express my deep appreciation and respect to them for their continuous guidance, encouragement and heartwarming support throughout my work.

I would like to express my great gratitude to Assistant Prof. Satoshi Nakamura (Institute for the Promotion of General Graduate Education, Yamagata University) for his continuous guidance, assistance and encouragement throughout the duration of this project. I am also immensely grateful to and Assistant Prof. Yusuke Yonamine (Research Institute for Electronic Science, Hokkaido University) for his careful reviewing and helpful suggestions on the manuscript. Additionally, I would like to express my sincere gratitude to Prof. Guoqing Wang (MOE Key Laboratory of Evolution and Marine Biodiversity and Institute of Evolution and Marine Biodiversity, Ocean University of China) for his concern during the past three years.

Furthermore, I would like to thank to the members of the Molecular Devices Laboratory, Postdoc. Takehiro Yachi, Postdoc. Han Lin, Ms. Chie Takeuchi, Ms. Aki Okuhara, Ms. Melda Taspika, Ms. Jingyan Yang, Ms. Wenting Wei, Ms. Zhiyu He, Mr. Yingqi Mu, Mr. Tianxu Gao, Mr. Dongyu Zhang, Mr. Haoran Zhang, Mr. Abdul Kaiyum, Ms. Honoka Watanabe, Mr. Tomoki Ikemizu, Ms. Mio Nakamura, Ms. Hono Ogihara and Ms. Erika Kurimoto for their great help in my work and daily life.

In addition, I am greatly indebted to the scholarships of the Japanese Government-Financed scholarship under the International Graduate Program: Training Program for Global Leaders in Life Science (IGP) supported by The Ministry of Education, Culture, Sports, Science and Technology, Japan (MEXT).

Finally, I would like to express my devoted appreciation to my family for their sacrificial help, affectionate encouragement and loving care.